

University of Kentucky

UKnowledge

Theses and Dissertations--Chemical and
Materials Engineering

Chemical and Materials Engineering

2023

SURFACE PROPERTIES, WORK FUNCTION, AND THERMIONIC ELECTRON EMISSION CHARACTERIZATION OF MATERIALS FOR NEXT- GENERATION DISPENSER CATHODES

Antonio Mantica

University of Kentucky, amma347@uky.edu

Author ORCID Identifier:

<https://orcid.org/0000-0001-6964-6625>

Digital Object Identifier: <https://doi.org/10.13023/etd.2023.283>

[Right click to open a feedback form in a new tab to let us know how this document benefits you.](#)

Recommended Citation

Mantica, Antonio, "SURFACE PROPERTIES, WORK FUNCTION, AND THERMIONIC ELECTRON EMISSION CHARACTERIZATION OF MATERIALS FOR NEXT-GENERATION DISPENSER CATHODES" (2023). *Theses and Dissertations--Chemical and Materials Engineering*. 151.

https://uknowledge.uky.edu/cme_etds/151

This Doctoral Dissertation is brought to you for free and open access by the Chemical and Materials Engineering at UKnowledge. It has been accepted for inclusion in Theses and Dissertations--Chemical and Materials Engineering by an authorized administrator of UKnowledge. For more information, please contact UKnowledge@lsv.uky.edu.

STUDENT AGREEMENT:

I represent that my thesis or dissertation and abstract are my original work. Proper attribution has been given to all outside sources. I understand that I am solely responsible for obtaining any needed copyright permissions. I have obtained needed written permission statement(s) from the owner(s) of each third-party copyrighted matter to be included in my work, allowing electronic distribution (if such use is not permitted by the fair use doctrine) which will be submitted to UKnowledge as Additional File.

I hereby grant to The University of Kentucky and its agents the irrevocable, non-exclusive, and royalty-free license to archive and make accessible my work in whole or in part in all forms of media, now or hereafter known. I agree that the document mentioned above may be made available immediately for worldwide access unless an embargo applies.

I retain all other ownership rights to the copyright of my work. I also retain the right to use in future works (such as articles or books) all or part of my work. I understand that I am free to register the copyright to my work.

REVIEW, APPROVAL AND ACCEPTANCE

The document mentioned above has been reviewed and accepted by the student's advisor, on behalf of the advisory committee, and by the Director of Graduate Studies (DGS), on behalf of the program; we verify that this is the final, approved version of the student's thesis including all changes required by the advisory committee. The undersigned agree to abide by the statements above.

Antonio Mantica, Student

Dr. Thomas John Balk, Major Professor

Dr. Fuqian Yang, Director of Graduate Studies

SURFACE PROPERTIES, WORK FUNCTION, AND THERMIONIC ELECTRON
EMISSION CHARACTERIZATION OF MATERIALS FOR NEXT-GENERATION
DISPENSER CATHODES

DISSERTATION

A dissertation submitted in partial fulfillment of the
requirements for the degree of Doctor of Philosophy in the
College of Engineering
at the University of Kentucky

By
Antonio Miguel Mántica
Lexington, Kentucky
Director: Dr. Thomas John Balk, Professor of Engineering
Lexington, Kentucky
2023

Copyright © Antonio Miguel Mántica 2023
<https://orcid.org/0000-0001-6964-6625>

ABSTRACT OF DISSERTATION

SURFACE PROPERTIES, WORK FUNCTION, AND THERMIONIC ELECTRON EMISSION CHARACTERIZATION OF MATERIALS FOR NEXT-GENERATION DISPENSER CATHODES

A dispenser cathode's ability to thermionically emit electrons is highly dependent on its material properties, especially those of the surface. Understanding the relationship between surface properties and electron emission, therefore, is vital to reach the next generation of the many vacuum electron devices (VEDs) that rely on the physics of electron emission. In the past century, many techniques have been developed to characterize material surfaces and quantify thermionic emission. These techniques are based on a wide range of different physical phenomena, including measuring photoemission via the photoelectric effect, measuring the electrostatic potential between metals in electrical contact, and current collection via positively biased anodes in a diode configuration. They do not necessarily have one-to-one correlation with each other and they are often incapable of studying cathodes in their operational conditions of high temperatures and in a vacuum. An investigation into the correlation between surface properties and electron emission in such an environment is needed to move the field forward. As such, the Cathode Characterization Chamber (CCC) has been assembled at the University of Kentucky to function as one testing space to utilize many diverse surface and emissions characterization techniques simultaneously. In this work, multiple methods of improved implementations of the aforementioned techniques are described, including lesser-known applications such as measurement of contact potential difference at high temperatures and the collection of electron emission using a Kelvin probe in an Ultra-High Vacuum (UHV). Additionally, an investigation into dispenser cathode design using this knowledge is described here, wherein a multi-element alloy cathode coating is explored as a candidate for improved emission performance when compared to current standard cathode coatings. A key parameter for evaluating thermionic emission performance that will receive significant attention throughout here is the work function. And the full testing capabilities of the CCC are shown to be a valuable toolset for evaluating the work function under many environmental conditions that would not be possible without this unique system. Ultimately, the results show a path toward multiple improved implementations of cathode characterization and the use of those methods to propose improved cathode design.

KEYWORDS: thermionic emission, emissions testing, dispenser cathode, surface characterization, vacuum electron device, ultra-high vacuum

Antonio Miguel Mántica

(Name of Student)

04/28/23

Date

SURFACE PROPERTIES, WORK FUNCTION, AND THERMIONIC ELECTRON
EMISSION CHARACTERIZATION OF MATERIALS FOR NEXT-GENERATION
DISPENSER CATHODES

By
Antonio Miguel Mántica

Dr. Thomas John Balk

Director of Dissertation

Dr. Fuqian Yang

Director of Graduate Studies

04/28/2023

Date

DEDICATION

To all of those in my life who have helped me get here.

ACKNOWLEDGMENTS

To begin at the start of my journey, I must open with a thank you to my parents, Julie and Alejandro, who always encouraged me to follow my interests and who taught me that there is no greater virtue than love. Thank you to my sister, Nicolette, who has shown me that life is a song, which, even if not sung well, must be sung with passion. And thank you to all my confidants from those early days – Alex Thompson, Thomas Richardson, Jacob Benton – without you, I would probably still be a lifeguard at the local pool only working summers.

It suffices to say that I never would have made it here without having fallen in love with the study of physics – a fire whose spark is completely owed to the mentorship of Dr. Michael Rulison. To discuss the nature of the universe with you is to have sat beneath the olive grove at Plato's *Akademia*. My sincerest thanks are also extended to the team of scholars, who, during some of the most formative years of my life, mentored me and inspired in me a passion for learning: Dr. John Cramer, who taught me that sometimes science is more art than science; Dr. Devon Belcher, who taught me that even a squirrel can teach you everything about the world; Dr. Robert Hornback, who taught me the beauty of language and to celebrate humor, always; Dr. John Nardo, that mathematics are language; Matt Huff, that character develops when you take risks; Dr. Stephen Herschler, that humans are beautiful, complicated things; Dr. Brian Patterson, that machines are complicated, beautiful things; and Dr. Justin Wise, that the body and the mind are separate yet connected. And to Allen O'Reilly, I will never forget your words "If I give you a hard time, it's because I love you."

I could write thank yous to Dr. Zachary Vealey that would be longer than this dissertation. I likely have in the form of letters and poems and short stories and texts. But please know, Zac, when I say that I wouldn't be here if it weren't you, I mean *here* here.

Thank you to the camaraderie that at times literally carried me through my years in Athens. The charlatans, mountebanks, and zanies without sense or dignity. Dr. Eric Suter, Dr. Gregory Simchick, Brandon Campbell, Dr. Lauren Esserman, Dr. Learnmore Shenje, Shun Uechi, Annika Bergmann. Thank you to Dr. M. Howard Lee for inspiring me to appreciate life's simplicities. And to Dr. Loris Magnani, a lighthouse of inspiration in a sea of discontent.

To those who have been there throughout these final steps, it's been a joy. The whole team that has been there for me since my first day here: Alyssa Stubbers, Kerry Baker, Huanhuan Bai, Tibra Das Gupta, Dr. Mujan Seif, Annaliza Torres. Thank you to Dr. Thomas Cochell, who patiently held my hand as I transitioned from "physicist" to "materials engineer," and to Dr. Michael Detisch, whose days of conversation and support have been the bedrock of my success at UK.

My most heart-felt gratitude goes out to the members of my committee. Thank you to Dr. Hastings for your willingness to provide a listening ear and offer up assistance. Thank you to Dr. Rottmann for your ceaseless encouragement and for showing me that you can be a parent to a newborn and do this at the same time. Thank you to Dr. Beck for teaching me to always say "I hypothesize" instead of "I think," and for your limitless and contagious excitement for materials science. And thank you to Dr. Balk. Your mentorship has been invaluablely stalwart and has always been a benchmark for me to aspire to. Thank

you for taking me under your wing at a time of great uncertainty in my life, and for counseling me as I grew to become a materials scientist.

And to the one who has seen every high and every low and remained at my side to encourage and bolster me at every step, to my ineffably, beautifully, ardently incredible wife, Dr. Kathleen Bedard, thank you. You who has remained with me despite and in spite of my many failings. All of my successes are yours, Kate, and every word of this was typed under a photograph of you and our sweet, happy Helen. For as long as space endures, for as long as living beings remain, for as long as all abides, I love you.

TABLE OF CONTENTS

ACKNOWLEDGMENTS	iii
LIST OF TABLES	ix
LIST OF FIGURES	x
LIST OF EQUATIONS	xvi
LIST OF ACRONYMS	xvii
CHAPTER 1. Introduction.....	1
1.1 <i>Introduction to Dissertation</i>	1
1.2 <i>Overview of Dissertation</i>	2
CHAPTER 2. Background.....	4
2.1 <i>Historical Perspectives and Scientific Background</i>	4
2.1.1 Work function.	5
2.1.2 Vacuum Electronic Devices.....	6
2.1.3 Dispenser Cathodes.....	7
2.1.4 Thermionic Emission.	8
2.2 <i>Motivations for Research into Next-Generation Cathodes</i>	9
2.3 <i>Goals of Research</i>	10
CHAPTER 3. Materials and Methods	11
3.1 <i>Cathode Materials</i>	11
3.2 <i>Cathode Thin Films</i>	13
3.3 <i>Kelvin Probe Method</i>	14
CHAPTER 4. Cathode Characterization Chamber.....	18
4.1 <i>Passive Measurement Techniques</i>	19
4.1.1 Ultra-High Vacuum	20
4.1.2 Residual Gas Analysis	20
4.1.3 Heating Stage and Pyrometry	21
4.2 <i>Active Measurement Techniques</i>	24
4.2.1 Ambient Photoemission Spectroscopy	24
4.2.1.1 The Need for Additional Techniques.....	28
4.2.2 Kelvin Probe and Contact Potential Difference.....	30

4.2.2.1	Traditional application of Kelvin probe to measure CPD	30
4.2.2.1.1	A Caveat to the KP Method	32
4.2.2.2	High-Temperature CPD by non-traditional application of Kelvin probe 36	
4.2.3	Close-Spaced Diode Assembly	38
4.2.3.1	Thermionic Emission	38
4.2.3.2	Parameters of the Richardson-Dushman Equation	40
4.3	<i>Other Accessories</i>	44
4.3.1	Ion Polishing	44
4.3.2	Surface Photovoltage Spectroscopy	44
4.3.2.1	SPS Justification	45
4.3.2.2	SPS Applications	45
CHAPTER 5.	High-Temperature CPD and Work Function	47
5.1	<i>Application of the High-Temperature CPD Technique</i>	47
5.2	<i>Results and Discussion</i>	49
5.2.1	Work Function of the Kelvin Probe	49
5.2.2	Work Function and KP Temperature	50
5.2.3	Work Function and Sample Temperature	54
5.3	<i>Work Function and Other Material Properties</i>	56
5.4	<i>Conclusions</i>	59
CHAPTER 6.	Thermionic Emission Collection and Work Function	61
6.1	<i>The Richardson-Dushman Equation</i>	61
6.2	<i>Collecting Current Density with KP</i>	62
6.3	<i>KP Parameters and Current Density</i>	63
6.4	<i>Work Function, Thermionic Emission, and R-D Analysis</i>	69
CHAPTER 7.	Materials Characterization of Cathode Surfaces	76
7.1	<i>SEM</i>	76
7.2	<i>EDS</i>	79
7.3	<i>XRF</i>	81
7.4	<i>Results and Discussion</i>	81
CHAPTER 8.	CSD and the KP Emission Method	82
8.1	<i>CSD in the CCC</i>	82
8.1.1	On CSD Testing and Temperature	83
8.2	<i>Work Function from CSD</i>	84

8.2.1	Knee Temperature and Activation Schedule	85
8.2.2	Emission Decay and Recovery	87
8.3	<i>Work Function from KP Method</i>	89
8.4	<i>Work Function from High-Temperature CPD</i>	91
8.5	<i>Conclusion</i>	93
CHAPTER 9.	Alloy Development for Enhanced M-type Cathodes.....	95
9.1	<i>Processing and Design</i>	95
9.1.1	Cathode Coatings.....	96
9.2	<i>Sample Design</i>	96
9.2.1	XRF.....	97
9.3	<i>KP and Cathode Coating</i>	99
9.4	<i>Results and Discussion</i>	101
9.4.1	Correlation with Previous Work and Next Steps.....	102
CHAPTER 10.	Conclusion.....	103
10.1	<i>Summary and Conclusions</i>	103
10.2	<i>Future Work</i>	106
APPENDIX	109
REFERENCES	112
VITA	118

LIST OF TABLES

TABLE 1. WORK FUNCTION OF THE STAINLESS-STEEL KP TIP	50
TABLE 2. WORK FUNCTION AND RICHARDSON CONSTANT FROM FIGURE 29	72
TABLE 3. WORK FUNCTION AND RICHARDSON CONSTANT FROM FIGURE 30	74

LIST OF FIGURES

FIGURE 1. A TYPICAL DISPENSER CATHODE DESIGN WITH POROUS MATRIX ON TOP OF A HEATING ELEMENT (LEFT) AND THE IMPREGNATED BODY (RIGHT).	12
FIGURE 2. A RED-HOT GLOWING CATHODE MOUNTED ON THE HEATING ASSEMBLY OF THE CCC VIEWED IN PROFILE.	12
FIGURE 3. THE SURFACE OF A SCANDATE CATHODE AS SEEN IN A SCANNING ELECTRON MICROSCOPE AS RECEIVED FROM THE MANUFACTURER AND PRIOR TO ANY ACTIVATION STUDIES.	13
FIGURE 4. DIAGRAM SHOWING THE GEOMETRY OF THE REFRACTORY METAL M-TYPE CATHODE THIN FILM COATING STUDY. THE DEPOSITION TARGETS WERE IN A CROSSED X PATTERN OVER THE SAMPLE.....	14
FIGURE 5. DIAGRAM SHOWING THE DIFFERENT IN FERMI LEVELS BETWEEN A KELVIN PROBE TIP AND A SAMPLE UNDER INSPECTION.	16
FIGURE 6. A DIAGRAM OF A SAMPLE AND KELVIN PROBE TIP IN ELECTRICAL CONTACT WITH ONE ANOTHER, SHOWING THEIR FERMI LEVELS HAVE EQUALIZED, AND ALSO HIGHLIGHTING THE MAGNITUDE OF CPD.	17
FIGURE 7. THE CATHODE CHARACTERIZATION CHAMBER. A PHOTOGRAPH OF THE CCC ASSEMBLED AT THE UNIVERSITY OF KENTUCKY, WHICH SHOWS ITS MANY DIFFERENT MODULES AND FEATURES.....	18
FIGURE 8. SCHEMATIC OF THE CATHODE CHARACTERIZATION CHAMBER. A DIAGRAM WHICH SHOWS A FEW KEY FEATURES OF THE CCC OF INTEREST TO THIS DISSERTATION, INCLUDING THE KELVIN PROBE, XYZ STAGE, AND A NUMBER OF OTHER USEFUL CATHODE CHARACTERIZATION TOOLS.	19
FIGURE 9. VIEW OF A HOT CATHODE IN THE CCC AS SEEN FROM AN UPPER VIEWPORT UNDERGOING KELVIN PROBE ANALYSIS. THE KELVIN PROBE TIP CAN BE SEEN ABOVE THE HOT, GLOWING SURFACE OF THE CATHODE, WHICH IS MOUNTED IN THE HEATING STAGE BUILT BY 3M TECHNICAL CERAMICS.	22

FIGURE 10. HOT CATHODE IN THE CCC AS VIEWED BY OPTICAL PYROMETRY. THE TOP ROW SHOWS THE CATHODE AT ROOM TEMPERATURE. THE BOTTOM ROW SHOWS THE CATHODE AT AN ELEVATED TEMPERATURE OF ABOUT 150 °C. THE LEFT COLUMN SHOWS THE SAME WHEN THE KELVIN PROBE TIP WAS 20 MM AWAY AND THE RIGHT COLUMN SHOWS THE KP AT 0.2 MM AWAY FROM THE EMITTING SURFACE. 23

FIGURE 11. THE CONSEQUENCES OF APS AT HIGH TEMPERATURES. (A) SHOWS APS PHOTOEMISSION DATA COLLECTED FROM A W PELLETT FOR A RANGE OF HEATER STAGE VOLTAGES (CORRESPONDING PROPORTIONALLY WITH STAGE TEMPERATURE). (B) SHOWS THE RESPECTIVE WORK FUNCTIONS FROM APPLYING THE FOWLER ANALYSIS TO THE SAME. ... 29

FIGURE 12. AMBIENT KELVIN PROBE SYSTEM. THE KELVIN PROBE RESTS ABOVE A SAMPLE STAGE. ON THE LEFT IS A CAMERA FOR MONITORING SAMPLES WHILE UNDER INSPECTION. 33

FIGURE 13. SAMPLE USED IN “WALK ACROSS” STUDY. THE SAMPLE WAS MADE TO HAVE A HIGH WF MATERIAL ADJACENT TO A LOW WF MATERIAL. IN THIS CASE, W (~4.34 eV) AND TA (~4.08 eV) WERE CHOSEN. 34

FIGURE 14. THE “WALK ACROSS” STUDY. THE KP TIP RECORDED A CPD MEASUREMENT ON THE PURELY W SIDE OF THE SAMPLE, AND THEN MOVED ACROSS THE FACE OF THE SAMPLE TOWARD THE TA SIDE, RECORDING CPD AND WF AT EACH STEP. 35

FIGURE 15. RESULTS OF “WALK ACROSS” STUDY. THE WF AT THE MIDPOINT OF THE TWO MATERIALS WAS EXTREMELY CLOSE TO THE NUMERICAL AVERAGE OF THE TWO ON THEIR OWN, PROVIDING THE ASSURANCE THAT INDEED THE KP TIP CAN ONLY “SEE” AN AVERAGE OF THE MATERIAL BENEATH IT. 36

FIGURE 16. KELVIN PROBE SIGNAL VS. KELVIN PROBE BIAS. (A) A ROOM TEMPERATURE CPD MEASUREMENT ON AN M-TYPE CATHODE; THE CPD “NULL-POINT” WAS 1193.0 mV. (B) THE SAME FOR THE CATHODE AT 600 °C; THE CPD EXTRAPOLATED HERE WAS 5026.0 mV. (C) SAME FOR THE CATHODE AT 1000 °C. NOTE: SIGNAL IS RECEIVED BY THE KELVIN PROBE AS A CURRENT, WHICH IS PASSED THROUGH AN ANALOG-TO-DIGITAL CONVERTER AND MEASURED BY THE SYSTEM SOFTWARE IN VOLTS. 37

FIGURE 17. CURRENT DENSITY PREDICTED BY THE RICHARDSON-DUSHMAN EQUATION FOR A GIVEN MATERIAL WITH A WORK FUNCTION OF 2.0 eV. SHOWING DIFFERENT PREDICTED EMISSION CURVES WITH DIFFERENT ASSUMED VALUES FOR THE RICHARDSON CONSTANT. 41

FIGURE 18. CURRENT DENSITY PREDICTED BY THE RICHARDSON-DUSHMAN EQUATION FOR A GIVEN MATERIAL WITH $A = 120 \text{ A/cm}^2\text{K}^2$, SHOWING DIFFERENT PREDICTIONS FOR THE SAME MATERIAL WITH DIFFERENT ASSUMED WORK FUNCTIONS..... 42

FIGURE 19. CURRENT DENSITY PREDICTED BY THE RICHARDSON-DUSHMAN EQUATION FOR DIFFERENT CRYSTALLOGRAPHIC ORIENTATIONS OF TUNGSTEN AT 1600 °C..... 43

FIGURE 20. SAMPLE AND KP TIP TEMPERATURE. SHOWS THE RELATIONSHIP BETWEEN SAMPLE SURFACE TEMPERATURE AND KELVIN PROBE TIP TEMPERATURE, FOR WHEN THE TIP WAS STATIONED ROUGHLY 10 MM AWAY FROM THE SURFACE. 52

FIGURE 21. WORK FUNCTION OF THE STAINLESS STEEL KELVIN PROBE TIP OVER THE PERIOD OF 1 YEAR. THE TIP WF WAS CALIBRATED TO A REFERENCE SAMPLE OF AU (111) CRYSTALLOGRAPHIC GOLD. THE RED DASHED LINE REPRESENTS THE AVERAGE OF THE KP WF VALUES, 4.71 eV. THE GREY LINE IS A LITERATURE REFERENCE VALUE OF AN ACCEPTABLE WF FOR STAINLESS STEEL AND THE BLUE LINE IS A REFERENCE VALUE FOR A WF OF BARIUM. 53

FIGURE 22. WORK FUNCTION AND TEMPERATURE FROM THE ASYMMETRIC BIAS TECHNIQUE. DATA FOR A W PELLET AND TWO M-TYPE CATHODES ARE SHOWN. THE TWO M-TYPE CATHODES WERE IDENTICAL IN BODY MATRIX BUT HAD DIFFERENT BAO:CAO:AL₂O₃ IMPREGNANT RATIOS, IN PARTICULAR 4:1:1 AND 6:1:2, RESPECTIVELY 55

FIGURE 23. YOUNG’S MODULUS VS. WORK FUNCTION. WORK FUNCTION MEASURED ON BULK SAMPLES USING AMBIENT KELVIN PROBE SYSTEM AND YOUNG’S MODULUS FROM ONLINE REFERENCE. THE RED DASHED LINE SHOWS THE PREDICTION FROM HUA AND LI, 2011..... 57

FIGURE 24. PLANE-STRAIN FRACTURE TOUGHNESS VS. WORK FUNCTION. WORK FUNCTION VALUES WERE MEASURED ON BULK MATERIAL SAMPLES AND VALUES OF FRACTURE TOUGHNESS WERE TAKEN FROM AN ONLINE DATABASE. 58

FIGURE 25. MODULATED KP BIAS, FIXED SPACING. CURRENT DENSITY COLLECTED BY THE KELVIN PROBE FROM A FIXED DISTANCE OF 2 CM AWAY FROM THE EMITTING SURFACE FOR AN M-TYPE CATHODE WITH 6:1:2 IMPREGNANT (OPEN RED), AND AN M-TYPE CATHODE WITH 4:1:1 IMPREGNANT (CLOSED BLACK). THE SHAPES CORRESPOND TO THE TIP BIASES OF +1 V (CIRCLE), +5 V (TRIANGLE), AND +10 V (SQUARE). 65

FIGURE 26. FIXED KP BIAS, MODULATED SPACING. CURRENT DENSITY COLLECTED BY THE KELVIN PROBE AT A FIXED BIAS OF +1 V FOR A POROUS TUNGSTEN PELLETT (OPEN RED) AND AN M-TYPE CATHODE WITH 4:1:1 IMPREGNANT (CLOSED BLACK). MEASUREMENTS AT TIP-TO-SAMPLE DISTANCES OF 0.5 CM (SQUARE), 1 CM (TRIANGLE) AND 2 CM (CIRCLE). 66

FIGURE 27. W PELLETT, MODULATED KP BIAS AND SPACING. CURRENT DENSITY COLLECTED BY KELVIN PROBE FROM A POROUS TUNGSTEN PELLETT, WITH PROBE BIAS OF +1 V (CLOSED BLACK) AND +10 V (OPEN RED); TIP-TO-SAMPLE SPACINGS OF 0.5 CM (CIRCLE), 1 CM (TRIANGLE), AND 2 CM (SQUARE). 68

FIGURE 28. R-D ANALYSIS, W PELLETT. EMISSION DATA COLLECTED FROM A TUNGSTEN PELLETT WITH A KELVIN PROBE TIP BIAS OF +10 V AND A TIP-TO-SAMPLE SPACING OF 0.5 CM. THESE DATA WERE PRESENTED PREVIOUSLY, BUT HERE THE RELEVANT ELEMENTS OF RICHARDSON-DUSHMAN ANALYSIS ARE HIGHLIGHTED AS AN EXAMPLE OF HOW WORK FUNCTION AND RICHARDSON CONSTANT CAN BE DERIVED FROM THE DATA. 70

FIGURE 29. REGIONS OF INTEREST FOR R-D ANALYSIS, MODULATED SPACING. EFFECTS OF VARYING THE TIP-TO-SAMPLE DISTANCE FOR AN M-TYPE CATHODE WITH 4:1:1 IMPREGNANT MATERIAL, AS BEFORE, BUT NOW WITH THE ADDITION OF LINES HIGHLIGHTING DISTINCT LINEAR REGIONS FROM WHICH TO EXTRAPOLATE WORK FUNCTION AND RICHARDSON CONSTANT. THE RESPECTIVE VALUES FOR THESE PARAMETERS ARE SHOWN IN THE TABLE BELOW. 72

FIGURE 30. REGIONS OF INTEREST FOR R-D ANALYSIS, MODULATED BIAS. KELVIN PROBE DATA FOR AN M-TYPE CATHODE WITH 4:1:1 IMPREGNANT MATERIAL, WHERE TIP BIAS HAS BEEN VARIED AS BEFORE, BUT NOW WITH THE ADDITION OF LINES HIGHLIGHTING DISTINCT LINEAR REGIONS FROM WHICH TO EXTRAPOLATE WORK FUNCTION AND RICHARDSON CONSTANT. THE RESPECTIVE VALUES FOR THESE PARAMETERS ARE SHOWN IN THE TABLE BELOW. 74

FIGURE 31. SEM OF AN M-TYPE CATHODE BEFORE AND AFTER ACTIVATION. (A-C) SEM MICROGRAPHS OF AN AS-RECEIVED M-TYPE CATHODE WITH 4:1:1 IMPREGNANT, BEFORE ANY HEATING. (D-F) MICROGRAPHS OF THE SAME M-TYPE CATHODE AFTER THE FULL SET OF HEATING EXPERIMENTS DESCRIBED IN THIS PAPER WERE CARRIED OUT. SCALE BARS: (A) 40 μM, (B) 5 μM, (C) 500 NM, (D) 40 μM, (E) 5 μM, (F) 500 NM. COMPLEMENTARY EDS ANALYSIS FOR THIS SAME SAMPLE IS SHOWN IN FIGURE 18. 77

FIGURE 32. SCANDATE CATHODE SURFACE (A) AS RECEIVED FROM THE MANUFACTURER AND PRIOR TO HEATING, (B) AFTER UNDERGOING THE ACTIVATION HEATING SCHEDULE OUTLINED BY THE MANUFACTURER. 78

FIGURE 33. EDS OF AN M-TYPE CATHODE POST-ACTIVATION. SPECIFICALLY, THE ANALYSIS OF THE TENDRILS GROWING OUT OF THE PORES ON THE SAME M-TYPE CATHODE SURFACE SHOWN IN FIGURE 17. (A) SEM IMAGE WITH SCALE BAR OF 2.5 μM , (B) COMPOSITE EDS ELEMENTAL MAP, (C) TUNGSTEN (W), (D) OSMIUM (OS), (E) BARIUM (BA), (F) OXYGEN (O). 80

FIGURE 34. CUSTOM UHV CSD ASSEMBLY. BUILT BY eBEAM INCORPORATED. THE ~ 2 MM DIAMETER CATHODE FACE CAN BE SEEN, AS THE ANODE PLATE IS SWIVELED DOWNWARD IN AN OPEN POSITION..... 82

FIGURE 35. CURRENT DENSITY FROM CSD TESTING, COLLECTED ON A DISPENSER CATHODE USING THE CUSTOM CSD ASSEMBLY BUILT BY eBEAM, INCORPORATED. 84

FIGURE 36. CSD ACTIVITY CURVES FOR A SCANDATE CATHODE, SHOWING DIFFERENT TRIALS WHERE DIFFERENT HEATING SCHEDULES WERE USED. COLLECTED USING THE eBEAM INCORPORATED CUSTOM CSD ASSEMBLY, USING A PULSED ANODE BIAS OF +700 V..... 86

FIGURE 37. CSD TEST RESULTS FOLLOWING A 100 HOUR TEST AND SUBSEQUENT ATTEMPT AT RECOVERY. COLLECTED USING THE eBEAM INCORPORATED CUSTOM CSD ASSEMBLY, USING A PULSED ANODE BIAS OF +700 V..... 88

FIGURE 38. CURRENT DENSITY VS TEMPERATURE FOR THE SAME CATHODE AS PREVIOUS, BUT FROM THE KP METHOD INTRODUCED IN THIS DISSERTATION..... 90

FIGURE 39. RESULTS FROM APPLYING THE HIGH-TEMPERATURE, ASYMMETRIC BIAS CPD METHOD TO THE SAME CATHODE AS PREVIOUS. 92

FIGURE 40. XRF RESULTS FOR THE SAMPLE MADE TO IDENTIFY M-TYPE CATHODE COATING CANDIDATES. SHOWING QUANTITIES OF W, RE, IR, OS, AND RU..... 98

FIGURE 41. CPD MEASUREMENT ARRAY OVERLAYED ON AN IMAGE OF THE M-TYPE CATHODE COATING CANDIDATE SAMPLE, SHOWING THE LOCATIONS OF POINTS WHERE CPD WAS MEASURED. 100

FIGURE 42. INTERPOLATED WF HEAT MAP FROM THE WFs OBTAINED BY MEASURING CPD ACROSS THE FACE OF THE M-TYPE CATHODE COATING CANDIDATE SAMPLE. THE CODE USED TO GENERATE THIS PLOT IS GIVEN IN THE APPENDIX. 101

FIGURE 43. CURRENT DENSITY FROM THE KP EMISSIONS COLLECTION METHOD FOR A 3D PRINTED CATHODE AND A SCANDATE CATHODE WITH THE SAME IMPREGNANT RATIOS. A W PELLETT IS ALSO SHOWN FOR COMPARISON..... 107

FIGURE 44. ASYMMETRIC CPD METHOD RESULTS FOR A 3D PRINTED AND SCANDATE CATHODE WITH THE SAME IMPREGNANT RATIO. A W PELLETT IS INCLUDED FOR COMPARISON. 108

LIST OF EQUATIONS

(EQUATION 1) FOWLER MODEL FOR PHOTOEMISSION	25
(EQUATION 2) PHOTOELECTRIC EFFECT ENERGY	26
(EQUATION 3) MODEL FOR RESISTIVE HEATING.....	27
(EQUATION 4)WORK FUNCTION AND CONTACT POTENTIAL DIFFERENCE	30
(EQUATION 5) RICHARDSON-DUSHMAN EQUATION.....	39
(EQUATION 6) WORK FUNCTION AND YOUNG’S MODULUS.....	57
(EQUATION 7) MODIFIED RICHARDSON-DUSHMAN EQUATION.....	64

LIST OF ACRONYMS

- A-KPS - Ambient Kelvin Probe System
- APS – Ambient Photoemission Spectroscopy
- C_B – Brightness Temperature in Degrees Celsius
- CCC – Cathode Characterization Chamber
- CPD – Contact Potential Difference
- CSD – Close-Spaced Diode
- EDS – Energy Dispersive X-Ray Spectroscopy
- KP – Kelvin Probe
- PE(S) – Photoemission (Spectroscopy)
- R-D – Richardson-Dushman
- RGA – Residual Gas Analysis / Analyzer
- SCL – Space-Charge Limited
- SEM – Scanning Electron Microscopy / Microscope
- SPS – Surface Photovoltage Spectroscopy
- SPV – Surface Photovoltage
- TL – Temperature-Limited
- TSP – Titanium Sublimation Pump
- UHV – Ultra-High Vacuum
- UV – Ultraviolet
- XRF – X-Ray Florescence

CHAPTER 1. INTRODUCTION

1.1 *Introduction to Dissertation*

This dissertation covers a body of research performed with the goals of developing better testing methods for modern dispenser cathodes and then using the knowledge obtained from those testing methods to predict material properties for next-generation dispenser cathode designs. This is because cathode performance is inherently limited by material properties, and so only through understanding the relationship between properties and performance will the technology that relies on them be improved. This dissertation will make use of well-established materials characterization and cathode evaluation techniques, but it will also introduce new methods of these techniques that make it possible to evaluate samples of interest within the unique operating environment of dispenser cathodes. Or more specifically, at extremely high temperatures within extremely low pressure environments.

In terms of evaluating dispenser cathodes, there are three primary parameters that this dissertation will focus on as criteria of interest: the state of the emitting surface face, the cathode's work function, and the quantity of thermionic electron emission released by the cathode. Each parameter will receive focus in its own turn as the dissertation describes how existing techniques helped or did not help in terms of evaluating cathodes in this unique environment. But it will also describe how these methods were employed to push collection abilities into desirable ranges not available under standard applications. Data will be shown for a wide array of types of samples, all relevant to dispenser cathodes and thermionic emission. Afterward, the results of these studies will be correlated with one

another in order to form a picture of, and ultimately propose a path toward a new design for future cathodes.

1.2 *Overview of Dissertation*

The opening chapters of this dissertation present a historical and scientific overview of the major milestones in the field, covering from the discovery of thermionic emission through the development of the dispenser cathode, and finishing with the state of modern cathodes today and include a discussion on the motivations to develop next-generation designs.

The dissertation will then move on to introduce the various relevant materials studied throughout, as well as provide a brief introduction to the Kelvin probe method, on which significant portions of these studies rely. It will then introduce the primary apparatus constructed for the evaluation of cathodes assembled at the University of Kentucky, the *Cathode Characterization Chamber*, or the CCC. Much more on the CCC will be given in the relevant chapter, but this singular testing chamber has shown itself to be a powerful wheelhouse for cathode testing and represents a serious addition to the field of cathode studies. The subsequent chapters of this dissertation will then illustrate how specific techniques have been implemented, and more importantly improved, while using the CCC to study dispenser cathodes. Namely, these techniques include high-temperature contact potential difference measurements, using the Kelvin probe as an emission current collector, and integrating close-spaced diode testing all into one testing space.

Coinciding with the above is a chapter that will highlight some of the additional materials characterization techniques carried out on cathode materials, external to the CCC.

And lastly, the closing chapters of this dissertation will look forward to how these techniques and the understandings gleaned from them can pave the way toward next-generation cathode design by describing an experiment that was carried out to identify candidate coatings for dispenser cathodes.

CHAPTER 2. BACKGROUND

2.1 *Historical Perspectives and Scientific Background*

The history of thermionic emission is a story of discovery, loss, and rediscovery. The phenomenon was first reported in 1853 by French physicist Edmond Becquerel, 38 years before the electron was named.^{1,2} Over the following half century, thermionic emission studies grew as scientists noticed that glowing hot metals discharged into the air when negatively charged but not when positively charged,³ and as the nineteenth century drew to a close, scientists had already begun to develop cathode/anode ray tubes.^{4,5}

The biggest breakthrough in the science of thermionic emission, however, would occur in 1883, when Thomas Edison filed a patent for an “electrical indicator” – the first U.S. patent for an electronic device.^{6,7} This device relied on passing a current through a carbon filament, sealed within an evacuated glass bulb, such that when a positively charged foil was also placed inside of the bulb, current was induced on the foil when increased voltage was applied to the filament. Although the name “the Edison effect” has not stuck, this device was only the first of many that relied on thermionic emission from dispensing cathode and a collecting anode, within a vacuum chamber.

But before diving any further, some physical background and definitions must be outlined. It will be necessary to understand the techniques and fundamental science behind how the investigations of this dissertation will be conducted in order to fully understand their findings. Some historical perspectives and necessary terms are also presented here.

2.1.1 Work function.

To begin, it will be vital to arrive at a mutual understanding of what is really meant by the phrase “work function.” The first of Albert Einstein’s four *Annus mirabilis* papers proposed discrete energy quanta, explaining why electrons were observed emitting from metals instantaneously and not in a gradually increasing fashion.⁸ In a later paper, Einstein refers to the energy barrier of emission as “the potential of this quantity of negative electricity relative to the body.”⁹ In more modern terms, this potential is usually called the work function. Although, experimentally speaking, it may be more succinctly defined as the potential of an electrical conductor such that an electron photo-excited from the surface has just enough energy to be detected by a nearby grounded collector.¹⁰

The energy needed to remove an electron sufficiently far away from a surface, i.e. such that it is not reabsorbed back into the material, can also be interpreted as the energy required to remove an electron from the material to a point of zero kinetic and potential energy away from the surface (or at what is called the vacuum energy level).¹¹ In this interpretation, the “work function” can be thought of as the difference between this vacuum energy level and the material’s Fermi level, or the thermodynamic work necessary to add an electron to the body of a material (more on this later). This is sort of a reverse interpretation of the previous definition for “work function.” As an analogy for the more visual thinkers, perhaps unhelpful otherwise, instead of thinking of the work function as the amount of work it takes to pick an apple from a tree and place it in a basket, this view interprets work function as the difference in the potential energy the apple has in the basket from the work that it took to grow the apple in the first place.

It may be tempting to think that work function is analogous to the ionization energy of an atom, but these are very different energies. The ionization energy refers to the amount of energy required to release a *bound* electron in an atom, and not the free electrons present in the “sea of electrons” of metals (even though this model too has recently faced calls for reevaluation¹²). These free electrons require much less energy to be released from their bodies than the ionization energy. In tungsten, for example, the ionization energy is nearly double the energy of the work function.¹³

An important note to bear in mind here regarding the upcoming sections on CPD measurement, is that when metals with dissimilar work functions are brought into thermal and electrical contact with one another, their Fermi levels will equalize via electron transfer from the lower work function material into the higher work function material.³⁰ This will be discussed in more detail a bit later, but this has important ramifications for the ability to measure the work function of two dissimilar metals in electrical contact with one another moving forward.

2.1.2 Vacuum Electronic Devices.

As previously stated, scores of scientific instruments and displays used today rely on vacuum electronic sources, which make use of low work function materials with high melting temperatures in the role of cathodes. The reason why it is desirable for the electron sources to be *in vacuo* is because when the surfaces of solid materials are exposed to air, the work function is fundamentally altered by the adsorption of environmental gas atoms and molecules; although this exposure can in fact sometimes increase, not decrease, the work function, depending on the situation. Interestingly, in the case of dissimilar material

surfaces on substrates, the adsorption of alkali atoms on surfaces has been often observed to shift the work function above the Fermi level of the substrate metal surface.¹⁴ Further advantages of being *in vacuo* are that in a controlled vacuum environment, the electrons are free to emit without significant concern of collision of other particles. And if there is a positively charged anode nearby, they will be summarily drawn toward the positive source. All of these reasons make the presence of the vacuum welcome and desirable for these applications.

2.1.3 Dispenser Cathodes.

At the forefront of modern cathode development are scandate cathodes, which combine scandium (Sc) and tungsten (W) to create cathodes able to produce “20 times the emission of conventional all-tungsten cathodes at the same temperature” and are able to produce current densities of $J \gg 10 \text{ A/cm}^2$ at operating temperatures of $T < 1000 \text{ }^\circ\text{C}$.^{15,57} A typical work function of an operating cathode of this type may be lower than 1.5 eV.¹⁶ A low work function also highlights the importance of lower operating temperatures, as this means emitter material evaporation is minimized and a longer operation lifetime for the cathode in question can be achieved. General scandate cathode lifetimes have been shown to be between 1,000 and over 10,000 hours depending on operating conditions and environment.^{17,18}

It is important to emphasize here, nevertheless, that the role that scandium actually plays in scandate cathodes is at this time not fully understood.¹⁹ There is even evidence to suggest that Sc is not the direct work function reducing agent, but instead a cleaning agent of W-oxides on the tungsten surface.⁵⁷ Understanding the roles that scandium composition,

Sc-containing alloys, or any other elements present, play in determining work function of a cathode is of vital importance to this work. This lack of understanding partly accounts for why the M-type cathode, which will be explored in greater detail in this dissertation later on, remains the most commonly used cathode across industrial applications today.

2.1.4 Thermionic Emission.

Broadly speaking, field emission can be understood as the quantum mechanical tunneling of electrons out of a solid, passing through the work function potential barrier.^{14, 20} Thermionic emission, a type of field emission, is the emission of electrons from a surface due to heating. The phenomenon that was long thought to describe electron emission as a result of heating was the space charge effect, or the idea that electrons literally boiled off the surface of the metal and surrounded the surface in a cloud of gas-like free electrons. This stems from the admittedly understandable idea that more heat means more boiling, and it gave rise to the idea that these thermal electrons, dubbed thermions, were distinct from the previously known field electrons – despite the fact that field electron emission had already been shown to be independent of temperature.²¹ More recently, however, it has become accepted that the real explanation is that the potential barrier height (work function) of the thermionic emitting material decreases with applied heating, allowing the electrons to escape more easily and that thermal electrons and field electrons are both just electrons.²² The name thermionic emission, unfortunately, has stuck.

2.2 *Motivations for Research into Next-Generation Cathodes*

As people and the machines that they use become increasingly connected throughout the earth and beyond, reliable long-distance communication becomes more necessary. Dispenser cathodes have been reliably used to amplify radio signals as a means to achieve communication across such distances.²³ The understanding and improvement of these electron sources, therefore, and the vacuum devices they are a part of, is necessary to keep up with the ever-expanding world. Thus, there is an important question that must be addressed: what are the exact physical processes that make a dispenser cathode desirable for these applications? The answer is not trivial. But to understand the phenomena that govern electron emission from cathodes, this research will choose to focus on the cathode material's surface and how the state of the surface affects the cathode's work function, or the energy required for the material to emit electrons. This will be discussed in greater detail later on, but before that it will be worthwhile to discuss the primary goals that this question has inspired for this research.

This research is highly motivated by the prospect of developing next-generation cathodes. As mentioned, the M-type cathode has remained the industry standard since its development in the 1960s. They are desirable for their relatively high current densities of emission ($> 10 \text{ A/cm}^2$) at moderate operating temperatures ($\sim 1100 \text{ }^\circ\text{C}$) and can be operated for tens of thousands of hours.⁵⁶ If the next generation seeks to improve upon these features, they will need to be able to output larger currents for the same temperatures, or equivalent currents at lower operating temperatures. Either case could mean longer lifetimes of applications for the many devices that make use of thermionic emitters.

2.3 *Goals of Research*

The first goal of this research is to understand, on both a theoretical and experimental level, the relationship between surface and work function. By knowing how surface properties influence an electron's ability to emit from a body, cathode operation and how cathodes can be used for humanity's benefit will be better understood. This goal will be considered achieved if the cathode characterization techniques pioneered by the CCC help lead to new cathode design. The second goal, which necessarily follows from the first, is therefore to develop techniques, or improve existing techniques, in order to evaluate cathodes in new ways and new regimes. Many of the leading techniques for cathode characterization are unable to evaluate work function in its activated state. In this dissertation, however, efforts are shown which pave the way for "live" cathode testing. This goal will be considered achieved when the techniques have revealed themselves to characterize cathodes in regimes never before reported on. The third and final goal, then, is to then use the acquired knowledge and understanding to propose an optimized cathode design or coating. Or at the least, propose a cathode design that has higher emission rates and/or lower operating temperatures than those which are widely in use today. This goal will be considered achieved when a cathode design has been proposed and subsequently evaluated and shown to outperform standard models under identical testing conditions.

CHAPTER 3. MATERIALS AND METHODS

3.1 *Cathode Materials*

Throughout the studies presented in this dissertation, a number of different cathode materials and samples will be studied. The first of which, to start off simply, is the pure tungsten (W) pellet. A porous tungsten (or tungsten-scandium) matrix comprises the body of all the cathodes studied in this work, so naturally it was deemed important to examine what the behaviors of a bare, uncoated and unimpregnated W pellet were. All instances of “W pellet” or other synonyms in this work refer to a standard pellet of 70% porosity and 3 mm diameter manufactured by 3M. All cathodes reported on here had pure W bodies unless otherwise noted to be a scandate cathode.

As stated previously, the industry standard cathode is the M-type cathode. Two M-type cathodes in particular are discussed in this dissertation, which were both 80% W pellets, coated with a thin film of Osmium-Ruthenium, and impregnated with different ratios of barium, calcium, and aluminum oxides ($\text{BaO}:\text{CaO}:\text{Al}_2\text{O}_3$), in the respective ratios of 4:1:1: and 6:1:2 (also manufactured by 3M). Barium here is the key ingredient, as its diffusion through the W pores to the surface creates a Ba-O dipole and is hypothesized to be the mechanism by which M-type cathodes can drop in work function by more than 2.0 eV when heated.⁵⁷

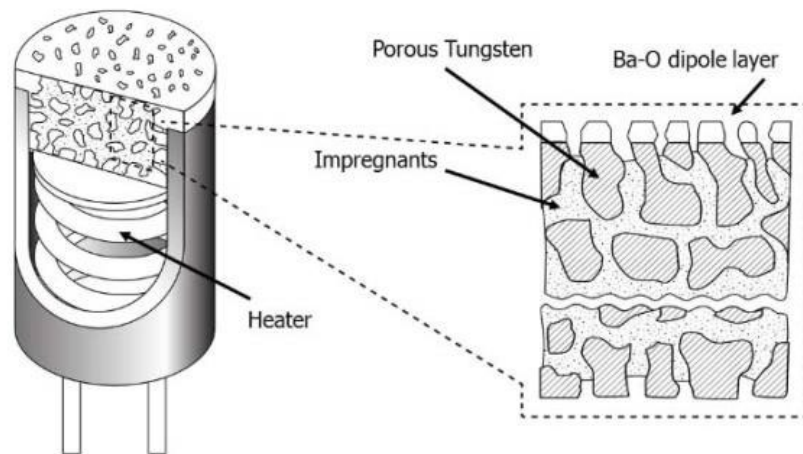


Figure 1. A typical dispenser cathode design with porous matrix on top of a heating element (left) and the impregnated body (right).²⁴



Figure 2. A red-hot glowing cathode mounted on the heating assembly of the CCC viewed in profile.

Scandate cathodes are also reported on in this dissertation. Scandate cathodes either contain scandium in the impregnant or in the tungsten matrix, the term is used interchangeably for either case. Using the cathode analysis techniques introduced in this dissertation, several different Sc-containing cathodes are examined.

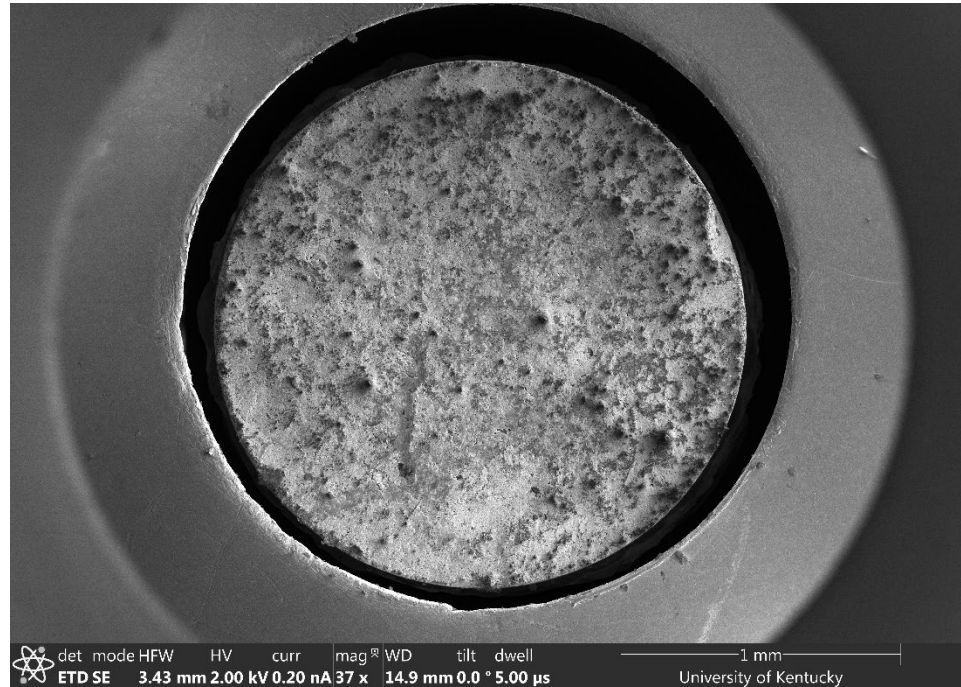


Figure 3. The surface of a scandate cathode as seen in a scanning electron microscope as received from the manufacturer and prior to any activation studies.

3.2 Cathode Thin Films

The discovery of a thin film (on the order of 100 nm) of a refractory metal on the surface of a dispenser cathode leading to improved emission was the birth of the M-type cathode.²⁵ Extensive studies have been done to find ways to lower the work function of

dispenser cathodes, but the M-type remains the best available today. An alloy of Osmium-Ruthenium is the leading coating of choice. This dissertation, however, implements a study where a W-Os-Ru alloy with small amounts of rhenium (Re) and iridium (Ir) is considered. The study sample was created using a magnetron sputtering system to deposit the metals onto a substrate surface, and then the work functions across the face of the sample were assessed.

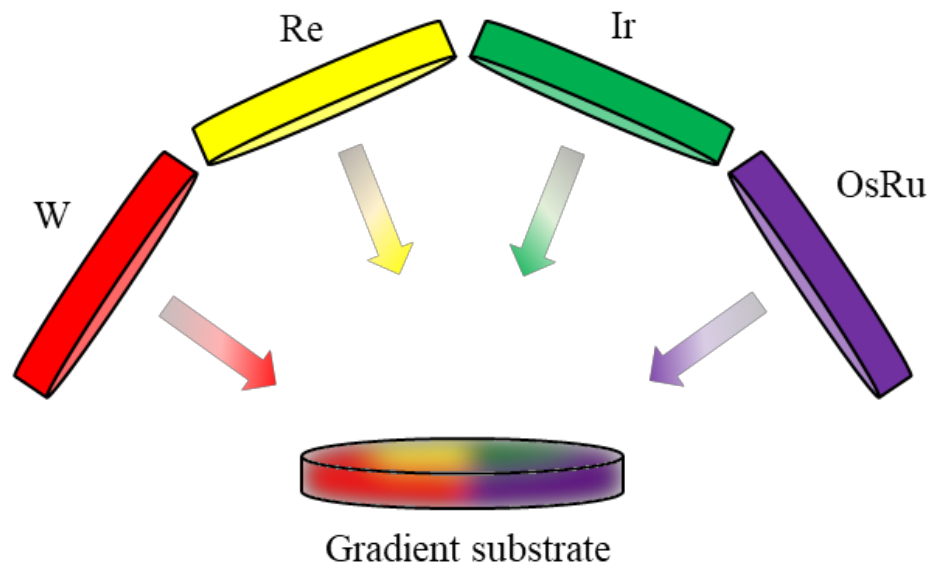


Figure 4. Diagram showing the geometry of the refractory metal M-type cathode thin film coating study. The deposition targets were in a crossed X pattern over the sample.

3.3 Kelvin Probe Method

A significant portion of the work in this dissertation relies on the use and understanding of the Kelvin probe. Toward that end, the time is appropriate here to

introduce the standard methods and applications of a Kelvin probe, and why it is so important for this work.

The Kelvin probe is a contactless device by which the contact potential difference (CPD) can be measured between a metallic tip and a sample under inspection first proposed by Lord Kelvin in 1898.²⁶ And CPD, as shall be shown a bit later on, is intimately tied to work function, the material property that this dissertation is largely concerned with. The Kelvin probe is able to measure CPD by being placed into a parallel plate capacitor configuration with the sample, such that they are in electrical contact with one another. Recall, as was mentioned earlier, that prior to coming into electrical contact the two materials are assumed to have different Fermi levels, or the amount of thermodynamic work to add an electron to the metal.^a In fact, one way of defining the work function is as the difference between a material's Fermi level and the energy that it would take to move a surface electron to a point far away enough from the surface where it could have 0 kinetic and 0 potential energy²⁷, a point called the vacuum energy.^b

^a Author's note: "Fermi level" and "Fermi energy" are often used interchangeably. "Fermi energy" more accurately refers to the theoretical maximum kinetic energy of electrons at absolute zero, a concept useful in the solid-state physics of extremely low temperature materials. "Fermi level" will be used in the context of work and electron liberation here.

^b Author's note: this is, again, a potentially misleading term because it relies on a theoretical vacuum surrounding the thermionic emitter with the same potential everywhere. In reality, the vacuum is contained within a metallic chamber of a material with its own work function. In other words, all points in the surrounding vacuum do not necessarily have the same electrostatic potential.

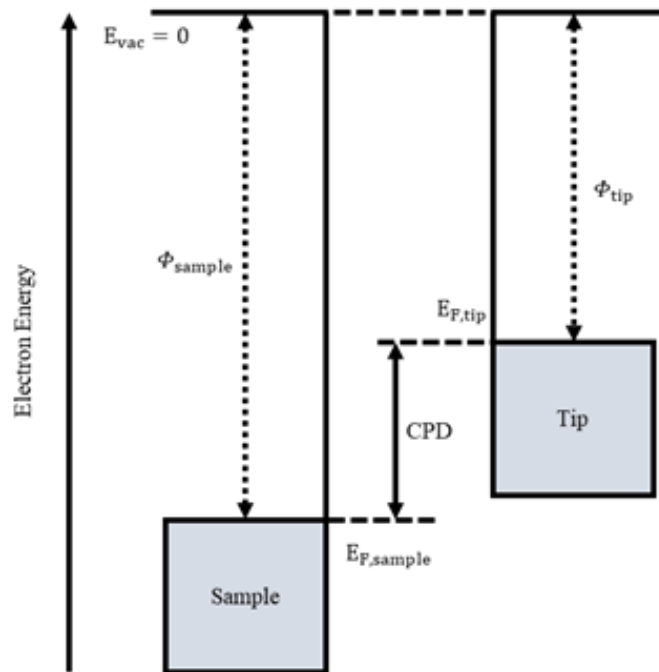


Figure 5. Diagram showing the different in Fermi levels between a Kelvin probe tip and a sample under inspection.³⁷

When two materials with different Fermi levels are brought into electrical contact with each other, however, electrons will naturally transfer from the lower work function material to the higher work function material, and their Fermi levels will equalize. This will also result in the low WF material becoming positively charged and the higher WF material becoming negatively charged, relatively speaking. And so in the Kelvin probe method, an external backing bias, or backing potential, is applied to the probe. This is also useful because, as will be illustrated in the next chapter, the backing bias that equals out the charge “seen” by the tip is necessary to measure the CPD.

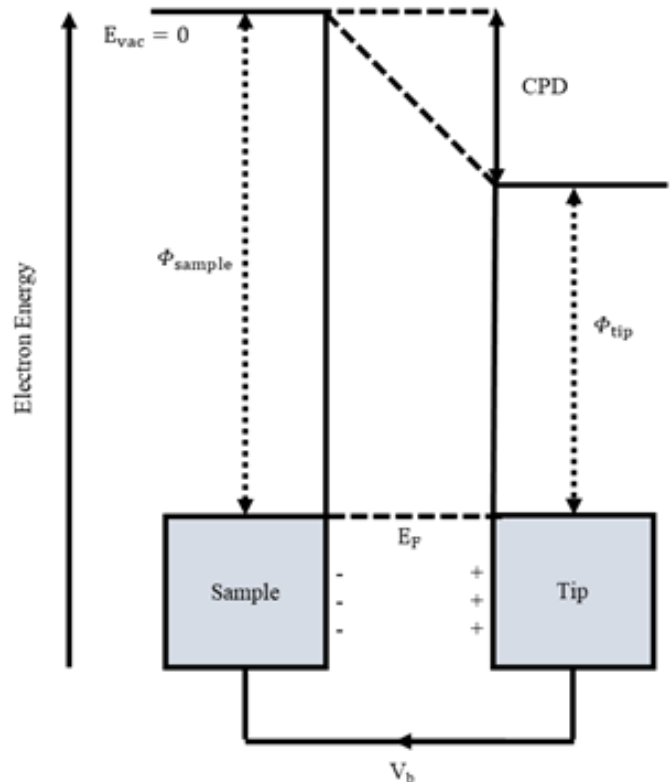


Figure 6. A diagram of a sample and Kelvin probe tip in electrical contact with one another, showing their Fermi levels have equalized, and also highlighting the magnitude of CPD.³⁷

This graphically illustrates what will be fleshed out mathematically and experimentally later: that the measured CPD is equivalent to the difference in work function between the two metals involved. Namely, the KP tip and the sample under inspection.

CHAPTER 4. CATHODE CHARACTERIZATION CHAMBER

The Cathode Characterization Chamber, or CCC (or more rarely the C^3), is a testing apparatus that has been assembled at the University of Kentucky with the singular goal of having one testing chamber capable of studying cathodes using a wide variety of characterization techniques simultaneously. It features many state-of-the-art testing modules and is capable of evaluating the performance of the most modern high performance cathodes. Its capabilities will be outlined in the following sections, starting first with the features that are ongoing, passively measuring, for all experiments, and then moving on to its specific, direct measurement techniques and other accessories.

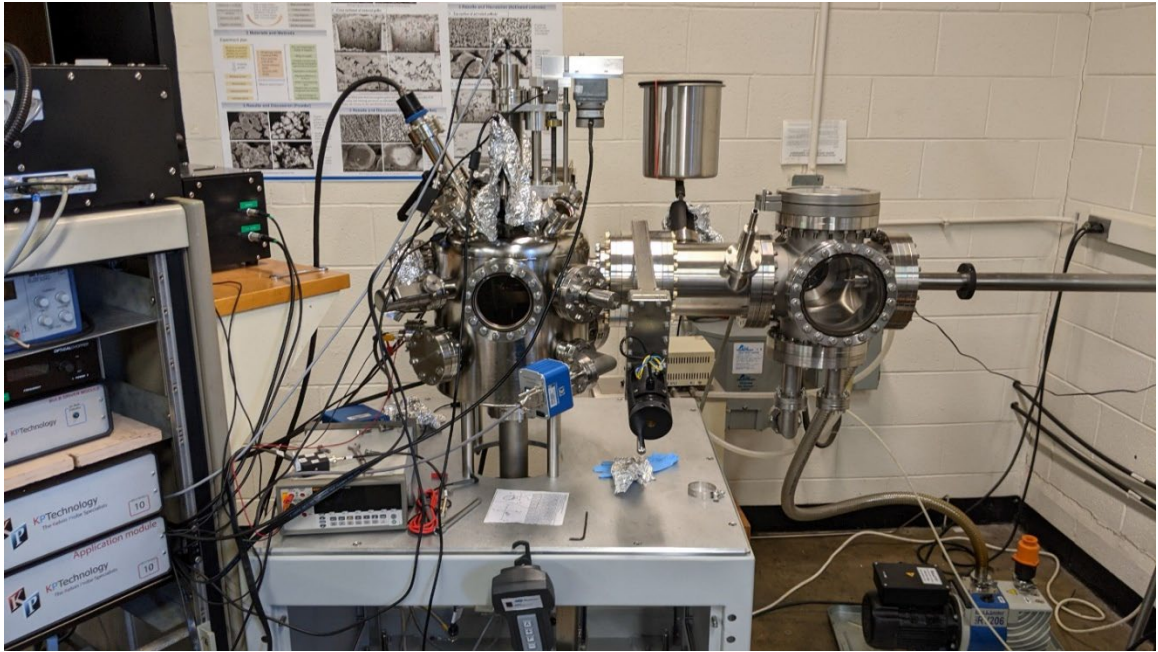


Figure 7. The Cathode Characterization Chamber. A photograph of the CCC assembled at the University of Kentucky, which shows its many different modules and features. A schematic diagram of the CCC is shown in the Figure below:

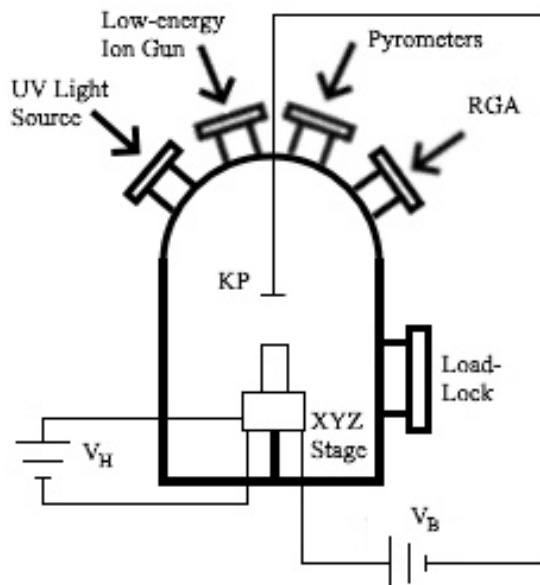


Figure 8. Schematic of the Cathode Characterization Chamber. A diagram which shows a few key features of the CCC of interest to this dissertation, including the Kelvin probe, XYZ stage, and a number of other useful cathode characterization tools.⁶⁹

The components shown in the figure above and many other elements featured on the CCC will be outlined in the following sections in greater detail.

4.1 *Passive Measurement Techniques*

There are three passive systems integrated into the CCC that are relevant to its ability to analyze cathodes. These are systems that are always present and running, regardless of the aims of the experiment within the CCC. They include the Ultra-High Vacuum (UHV) present within the body of the chamber that is capable of reaching pressures in the range of 10^{-10} torr, the Residual Gas Analysis (RGA) system connected to the CCC that can track extant gasses inside the chamber, and the three dimensionally

motorized heating stage with corresponding pyrometry that can heat samples and record the temperature of all internal components.

4.1.1 Ultra-High Vacuum

The UHV environment of the CCC is attained by using a series of pumps. The first is a mechanical pump which is capable of pulling the inner chamber into the < 3 mTorr range. Once this pump has reached its operational limit, a turbomolecular pump is then turned on. This second pump is able to help pull the chamber down into the 10^{-7} torr regime. These two pumps are attached to the load-lock portion of the chamber, or the smaller chamber attached to the main body which allows for easy loading and unloading of samples. The final pump to be activated is the ion pump with accompanying Titanium Sublimation Pump (TSP). This is what finally helps pull the main chamber pressure into the “Ultra-High” regime of 10^{-10} torr. The highest standards are maintained in terms of regular vacuum chamber maintenance as well, including periodic cycling of the TSP, regular baking of the chamber body, care of copper gaskets, helium leak tests, and more. The pressure in the main body of the CCC is monitored by an ion pressure gauge mounted to the side of the chamber.

4.1.2 Residual Gas Analysis

The RGA system incorporated into the CCC is capable of detecting extant gas species within the chamber to partial pressures of 10^{-12} torr. This system is especially useful in the case of atmospheric gasses adsorbed onto the surface of a sample under inspection

being released as a result of heating. This system is also relied upon when conducting helium leak tests in efforts to achieve lower pressures.

4.1.3 Heating Stage and Pyrometry

The heating stage assembly in the CCC is a custom built rig from 3M Technical Ceramics (Lexington, KY). It is designed to be able to hold and heat multiple different types of cathode geometries. The stage itself is attached to a three-dimensional motorized stage, or XYZ stage, which allows for complete control of the sample's location within the chamber. The stage has two leads which exit the main chamber and are connected to an external power supply. It is designed to heat the stage or provide current to a cathode loaded into the rig by applying a voltage across the two exiting leads. This heater voltage is labeled V_H in the schematic figure above and throughout this dissertation.

The pyrometers connected to the CCC are the Optris Xi400 and the Optris PI1M digital pyrometers. These two digital cameras are capable of recording the temperatures of all internal components of the chamber because they are mounted on external viewports, at two different respective angles. Most importantly, these cameras can monitor the temperature of the KP tip and of the sample under inspection (more on this later). Many experiments outlined in this dissertation occurred in sequences of successive temperature steps, so the pyrometers are vital in determining that the temperatures of all involved components have stabilized. Representative images of the KP tip and a hot sample underneath, as seen both through a viewport and by the digital pyrometry, are shown in the figures below.

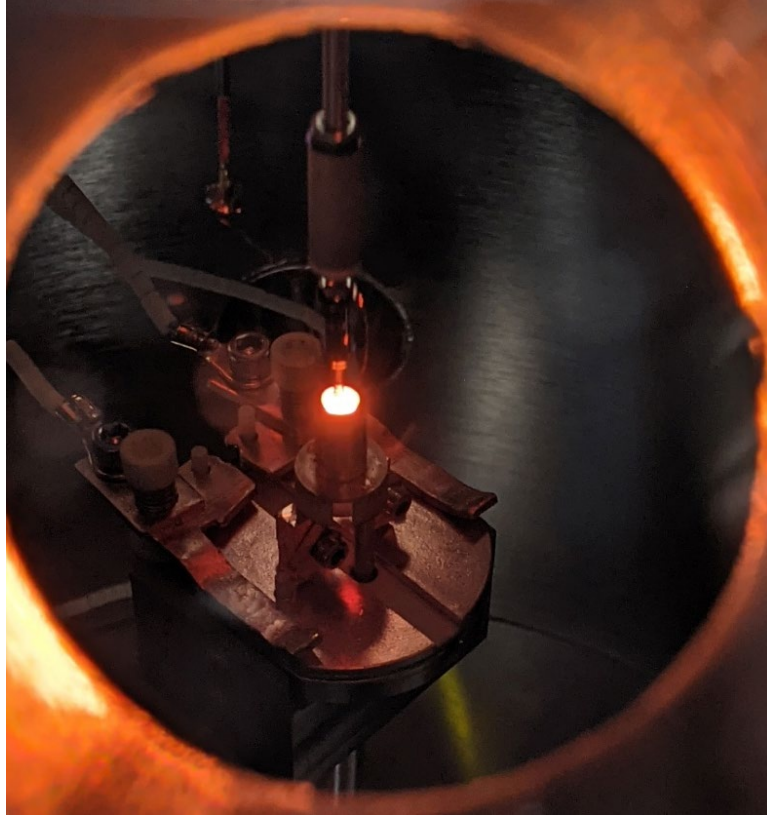


Figure 9. View of a hot cathode in the CCC as seen from an upper viewport undergoing Kelvin probe analysis. The Kelvin probe tip can be seen above the hot, glowing surface of the cathode, which is mounted in the heating stage built by 3M Technical Ceramics.

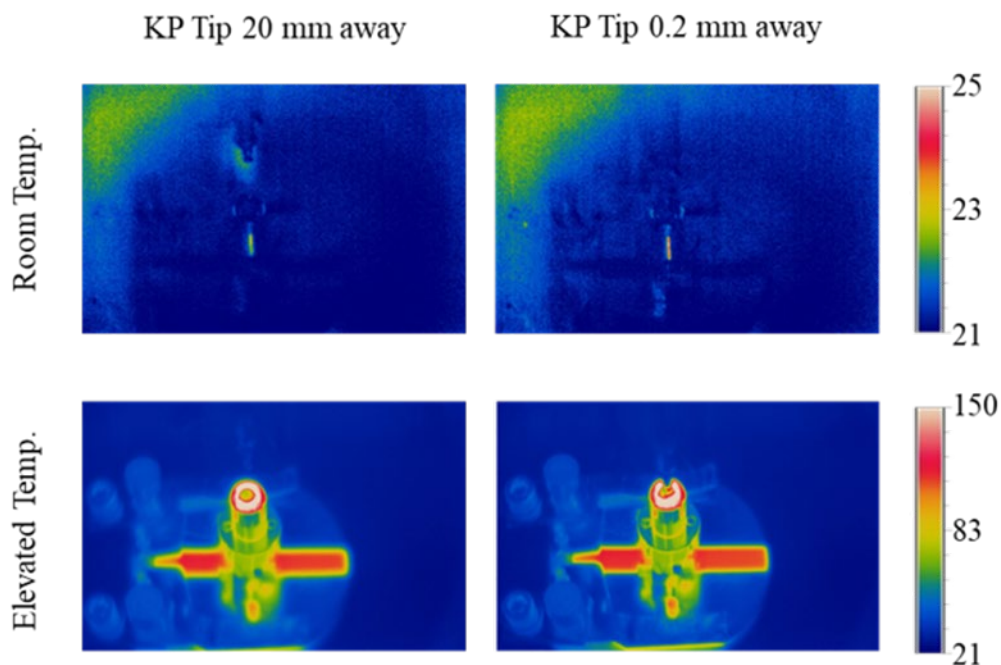


Figure 10. Hot cathode in the CCC as viewed by optical pyrometry. The top row shows the cathode at room temperature. The bottom row shows the cathode at an elevated temperature of about 150 °C. The left column shows the same when the Kelvin probe tip was 20 mm away and the right column shows the KP at 0.2 mm away from the emitting surface.⁴³

These images show a tungsten pellet sitting on top of a heating stage used to heat samples inside of the CCC main vacuum chamber as seen by the Optris Xi400 pyrometer. They show the pellet at room temperature and at 150 °C, respectively, and also show the KP tip far away from the sample surface (2 mm) and at operating distance (200 μm). The temperature color bars are in units of °C. This is just a representative example of how pyrometry is used in the CCC to monitor and record temperature.

4.2 *Active Measurement Techniques*

The techniques that follow are the active measurement techniques of the CCC. These are the modules that have been integrated into the CCC with the goal of providing a unique measurement capability. They include the unsuitably named Ambient Photoemission Spectroscopy (APS) that can detect the absolute work function of a surface via the photoelectric effect, the Kelvin probe that can record the Contact Potential Difference (CPD) between a KP tip and a sample and leads to work function determination, and a Close-Space Diode (CSD) assembly that can collect high currents and yield work function as well. Some additional capabilities are also briefly pointed out which are for other applications than those of interest in this dissertation.

4.2.1 Ambient Photoemission Spectroscopy

APS uses an ultraviolet (UV) light source to subject a sample under inspection to high-energy light. Incident photons with energy greater than the material's work function will liberate photoelectrons from the surface via the photoelectric, which can then be collected by a nearby, positively biased photo-detecting probe. As will be elaborated in a short while, by using an analytical method developed by Fowler²⁸, the work function can be easily obtained from this data.

But first a major caveat: although the name of the technique is “Ambient Photoemission Spectroscopy,” this technique has been carried out in the ultra-high vacuum (UHV) pressure range everywhere reported in this dissertation. APS is a wide-spread, general technique that is often performed in ambient conditions, but recall that one of the

primary objectives of this dissertation is to measure the work function of cathodes in operating conditions, so the vacuum must be present. Because of this, it may be tempting to think the technique can be referred to as simply Photoemission Spectroscopy, or PES, but this name is unfortunately already one well established in materials science as a similar technique that uses X-rays as an ionizing source (incident energy values in the 124 eV to 124 keV range). So, although the technique in question of this section will be referred to as ambient photoemission spectroscopy (APS) throughout this dissertation, please do not forget that here it will always be *in vacuo*.

In this technique, a deuterium light source and attached monochromator allow for a range of high-energy light to strike the surface of a material under inspection in 1 nm increments. In the case of the CCC, the energy range of available light is from 3.0 to 7.0 eV. So long as the incident photons absorbed by the sample material have more energy than the work function of the material, an excited electron at the metal surface has the chance to emit via the photoelectric effect. These emitted photoelectrons can then be collected by the positively biased Kelvin probe tip, and provide a picture of the lowest energy required to eject an electron from the surface, i.e. the work function.

Below the work function potential barrier, no photoemission occurs, so the Kelvin probe tip will only “see” background noise. Above this, however, photoemission current can be collected by the tip and plotted as a function of incident photon energy. R.H. Fowler showed in 1931²⁸ that in metals this photoemission, P , increases with the trend:

$$P \propto (h\nu - \Phi_{\text{Surface}})^{1/2}$$

(Equation 1)

where $h\nu$ is Planck's constant, h , times the frequency of the incident photon, ν . In other words, this value is the incident photon's energy. From this interpretation, called Fowler Analysis, a collected photoemission spectrum can be used to graphically identify the absolute work function (or work functions) present in a material under inspection by identifying where emission occurred significantly above the noise level. A major element of Fowler Analysis to point out, however, is that the square root relationship described by Fowler is only for proper metals – in semiconductors the relationship is a cube root.

The APS technique relies heavily on the phenomenon known as the photoelectric effect. This was laid out theoretically by Einstein⁹ and experimentally verified by R.A. Millikan²⁹ – both of whom would go on to receive the Nobel Prize in Physics for their work on the photoelectric effect.

In solids, electrons are bound to atoms and molecules in distinct energy states. When quanta of light with energy $h\nu$ is absorbed by these atoms, the electrons can enter higher energy states than their binding energy (again, provided that the energy of the absorbed light is greater than the material's work function). These ejected electrons have a kinetic energy, E_k , of

$$E_k = h\nu - E_B$$

(Equation 2)

where E_B is the binding energy of the electron.

The positively biased tip (in the case of the CCC, the tip can receive biases up to +10 V) then attracts the emitted photoelectrons and the plot of photoemission (in units of relative photoemission counts) versus incident photon energy can easily be plotted. An

important note here about the units of photoemission, however, is that the collected photoemission current is in arbitrary units, and it is important to take a photoemission current measurement “in the dark,” or without any incident photons. This establishes a background, or noise, level to set as the zero-photoemission value. This technique, unlike CPD that gives a relative work function value, measures an absolute work function value. In fact, “work function values” may be more appropriate, because APS can even identify multiple work functions present in one surface, although it must be kept in mind that in this technique electrons can be ejected from 1 to 3 μm below the metal surface, depending on the incident light energy, so thin films must be carefully considered when using this technique.³⁰

The importance of the vacuum in replicating the environment of a cathode’s operating conditions already having been stressed, it is now time to turn to APS and sample heating. Recall, the cathode must be heated in order to thermionically emit electrons. Because it has been claimed that CPD must be measured with the tip and sample in thermal equilibrium,³² it might be tempting to think of APS as a valuable tool for determining the work function of heated cathode samples under inspection. A heating stage was built by Ceradyne, Inc., a 3M company, (Lexington, KY) that allows for the application of a known voltage and current to a copper-plated stage and use the following relationship between resistance, R (obtained by applying Ohm’s law), and temperature coefficient of resistance, α , to calculate the stage temperature T :

$$R = R_{\text{ref}} [1 - \alpha(T - T_{\text{ref}})]$$

(Equation 3)

where R_{ref} and T_{ref} represent a reference resistance and a reference temperature for the specific material, respectively. Many cathode assemblies have similar, resistive heating elements built into their systems which heat the cathode proper. Optical pyrometers can then be used congruently to record the temperature of the surface under inspection in either case. An investigation into APS and temperature was performed, nevertheless, and it only highlights the need for something more.

4.2.1.1 The Need for Additional Techniques

APS is an incredibly useful technique for measuring the absolute work function of a surface at room temperature.³⁰ When investigating samples at high temperatures, however, especially at temperatures close to the operating levels of cathodes, APS faces a serious challenge. Most importantly, the difficulty lies in the fact that sufficiently hot samples glow, which means that the photo-collecting probe is going to collect more photons than just the ones emitted via the photoelectric effect and “wash out” anything that might be seen having been released by the photoelectric effect. Consider the following experiment:

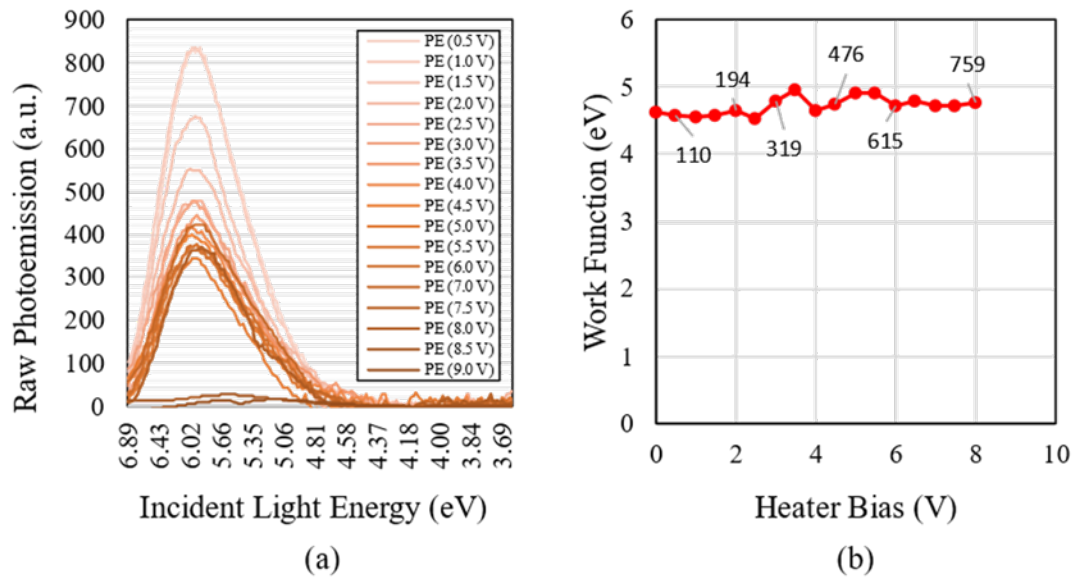


Figure 11. The consequences of APS at high temperatures. (a) shows APS photoemission data collected from a W pellet for a range of heater stage voltages (corresponding proportionally with stage temperature). (b) shows the respective work functions from applying the Fowler analysis to the same.⁴³

These data show an experiment where photoemission (PE) was collected using the APS method on a porous tungsten pellet. The light source used here was a high-intensity deuterium lamp (KP Technology) which was capable of subjugating between 6.9 to 3.5 eV to the sample.

The pellet was on a heating stage whose temperature corresponded linearly with applied voltage. (a) in the figure above shows the PE collected as a function of incident light energy for each successive voltage step. Notice that as the pellet got hotter, the relative collected PE peak got smaller and smaller. This greatly affected attempts to calculate the work function using the Fowler method, where the work function is obtained by identifying the point where the collected PE increases significantly above the noise level.³⁰ Using the APS method with only a pure tungsten pellet, APS could not measure work function beyond a heater voltage of 8 V, or roughly 760 °C. Nowhere near the requirements for

activated cathodes. A different technique, therefore, is required in order to quantify work function for samples at 800 °C and higher.

4.2.2 Kelvin Probe and Contact Potential Difference

For many years, it has been reported that a surface and probe must be in thermal equilibrium in order to obtain accurate values of CPD.^{31,32,33,34} This has even been called one of the most significant challenges facing surface analysis using a Kelvin probe.³⁵ In the following subsections, the traditional application of Kelvin probe to measure CPD is described, as well as why it fails for thermionically emitting samples. The chapter afterward then introduces the non-traditional application employed by the CCC so as to be able to overcome this challenge and successfully make high-temperature CPD measurements.

4.2.2.1 Traditional application of Kelvin probe to measure CPD

As stated previously the CPD is equivalent to the difference of the work functions of the probe tip and sample and is expressed by the following simple equation³⁶

$$\Phi_{\text{sample}} - \Phi_{\text{tip}} = eV_{\text{CPD}}$$

(Equation 4)

where Φ_{sample} is the work function of the sample under inspection, Φ_{tip} is the work function of the Kelvin probe tip, e the elementary charge, and V_{CPD} is the measured value of contact potential difference.³⁷

The traditional application of a Kelvin probe involves bringing the probe and a sample under inspection into a parallel plate configuration. The necessary tip-to-sample spacing is dependent on the diameter of the tip, with 200 μm being typical for a Kelvin probe of 2 mm diameter (the diameter used throughout the work of this dissertation unless otherwise noted). The probe oscillates at a high frequency (typically 70 Hz) at a small amplitude of oscillation (typically 15 μm). This oscillation causes a change in capacitance between the two faces of the metals and induces a measurable current through the probe. In order to find the CPD, a backing bias potential is applied to the tip. This is because the backing bias which cancels out the signal “seen” by the probe will be equivalent to the CPD between the two surfaces. Using this method, CPD can be accurately determined to within several meV.³⁸

Baikie and Estrup developed a highly accurate, computer-integrated method of measuring CPD dubbed the “off-null” method.³⁹ One of the most important features of this technique is that it relies on a symmetric biasing of the Kelvin probe, such as -7 to +7 V, while making a CPD measurement. It does this because it records the signal at both of those points, and then extrapolates the theoretical bias needed to zero out the signal. In this application of Kelvin probe, noise is greatly reduced, and it is capable of accurately measuring work functions within < 0.1 meV.⁴⁰

4.2.2.1.1 *A CAVEAT TO THE KP METHOD*

One important caveat here is that when employing the CPD technique, it is necessary to point out that the Kelvin probe tip “sees” an average of the work functions within the area below it. This is in stark contrast to the APS technique which can identify multiple work functions present on one surface. What follows presently is a short investigation providing evidence for just that (that a KP measures the average of the area beneath it) carried out in a Kelvin Probe System that was built for ambient conditions (a system separate from the *in vacuo* Kelvin probe of the CCC). This system allows for additional sample manipulation and is useful for material samples that can be safely in ambient conditions for extended periods of time. This system features a two dimensional XY stage, but has no heating capabilities, so it is primarily used for studying materials at room temperature.

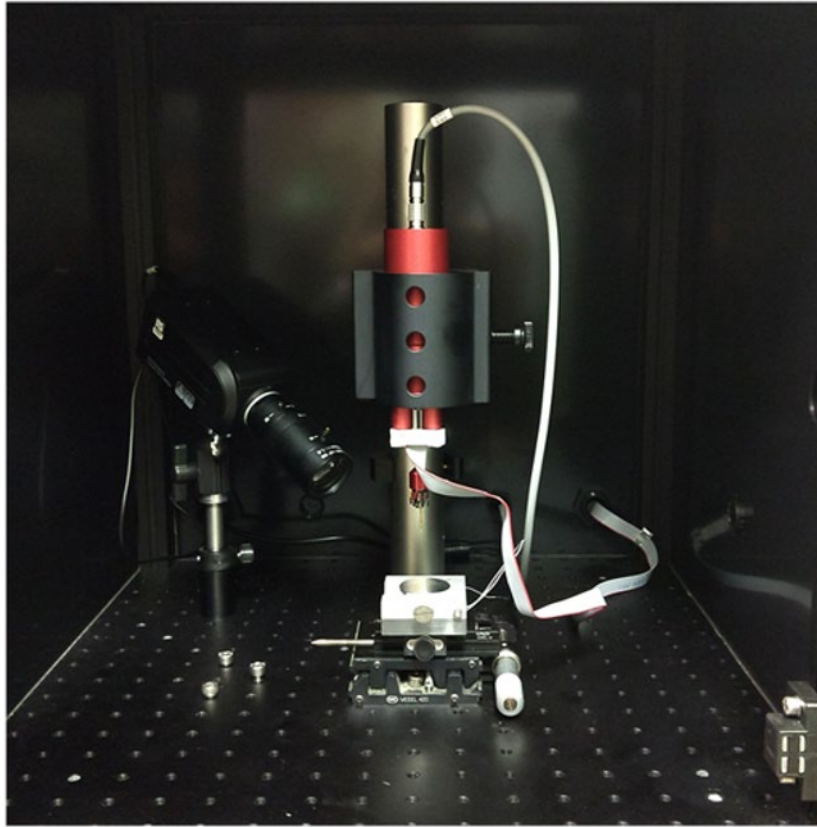


Figure 12. Ambient Kelvin probe system. The Kelvin probe rests above a sample stage. On the left is a camera for monitoring samples while under inspection.

In this particular experiment, 10 nm of tungsten, W, was deposited onto a substrate. Afterward, half of the sample was covered with a protective tape and an additional 10 nm of tantalum, Ta, were deposited onto that. A graphic of the sample is shown in the figure below.

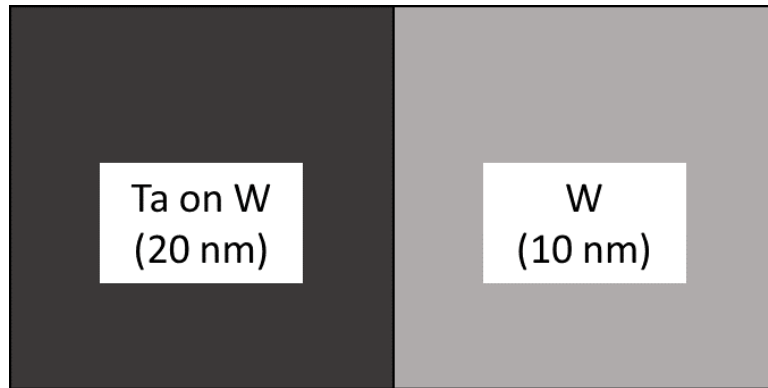


Figure 13. Sample used in “walk across” study. The sample was made to have a high WF material adjacent to a low WF material. In this case, W (~ 4.34 eV) and Ta (~ 4.08 eV) were chosen.

A “walk across” experiment using the Kelvin probe tip in ambient conditions was then performed to record the CPD in small increments, or steps, across the face of the sample; travelling from the higher work function material (W) to the lower work function material (Ta). The tip, not drawn to scale, and its path across the surface are represented in the following figure. If the hypothesis that the tip “sees” an average of what is below it is correct, then the expectation would be to see the highest work function in (a), the lowest at (e), and their average at the 50/50 point (c), with points (b) and (d) having in-between values.

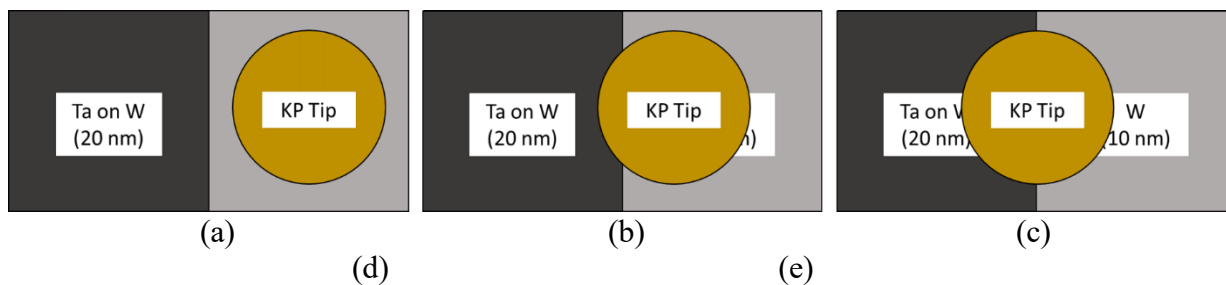
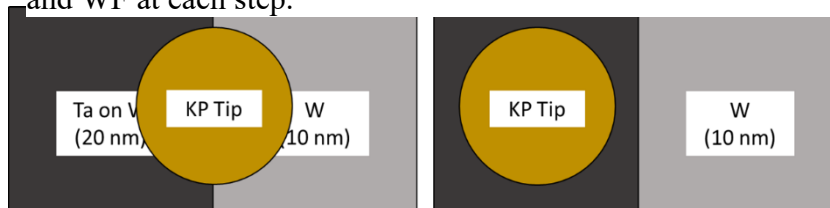


Figure 14. The “walk across” study. The KP tip recorded a CPD measurement on the purely W side of the sample, and then moved across the face of the sample toward the Ta side, recording CPD and WF at each step.



Using a work function of 4.73 eV for the stainless-steel KP tip used in this experiment, a value calibrated by measuring the CPD between the tip and a gold standard sample of known work function, the following corresponding work functions for the sample were obtained during this “walk across” study:

CPD "walk across" Experiment

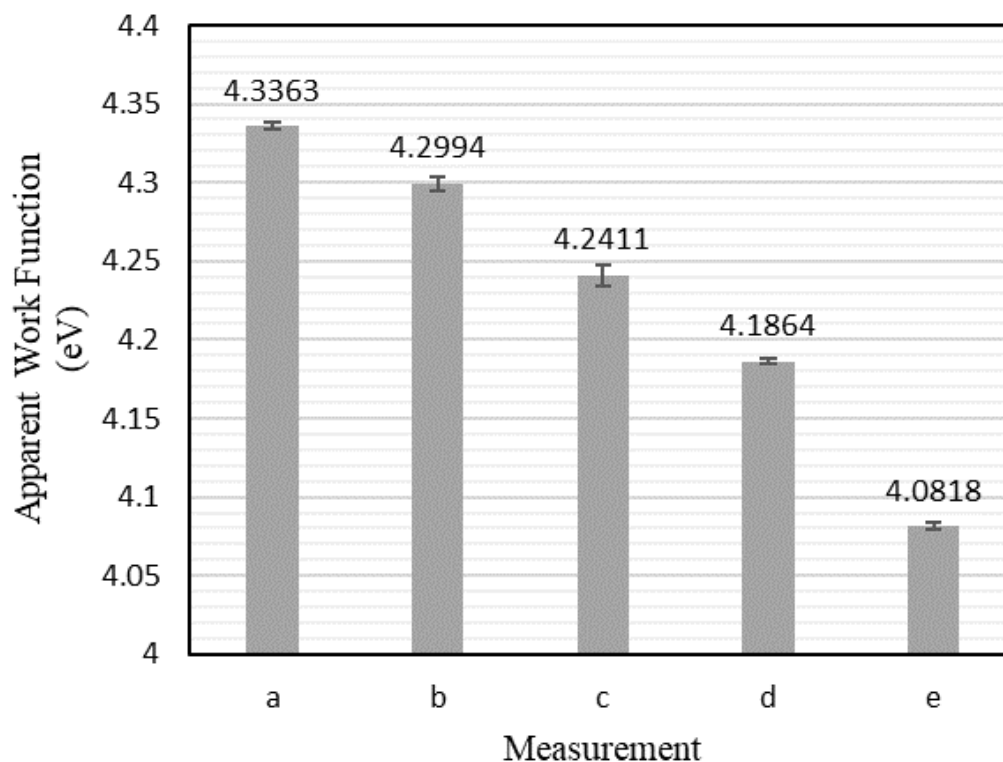


Figure 15. Results of “walk across” study. The WF at the midpoint of the two materials was extremely close to the numerical average of the two on their own, providing the assurance that indeed the KP tip can only “see” an average of the material beneath it.

4.2.2.2 High-Temperature CPD by non-traditional application of Kelvin probe

The issue with applying the traditional CPD measurement technique of a KP is that it involves putting a positively biased metallic probe 200 μm away from a thermionically emitting surface, and the amount of electrons collected by an anode is heavily influenced by its bias.⁴¹ Attempting to make a CPD measurement with a symmetric bias will cause

the received signal to quickly saturate the system’s detection capabilities because it will be collecting so many electrons. It was found, then, that an asymmetrically negative biased probe could avert this issue.

The results in the figure below show what happens when positively biased KP measurements are attempted on an M-type cathode.⁴²

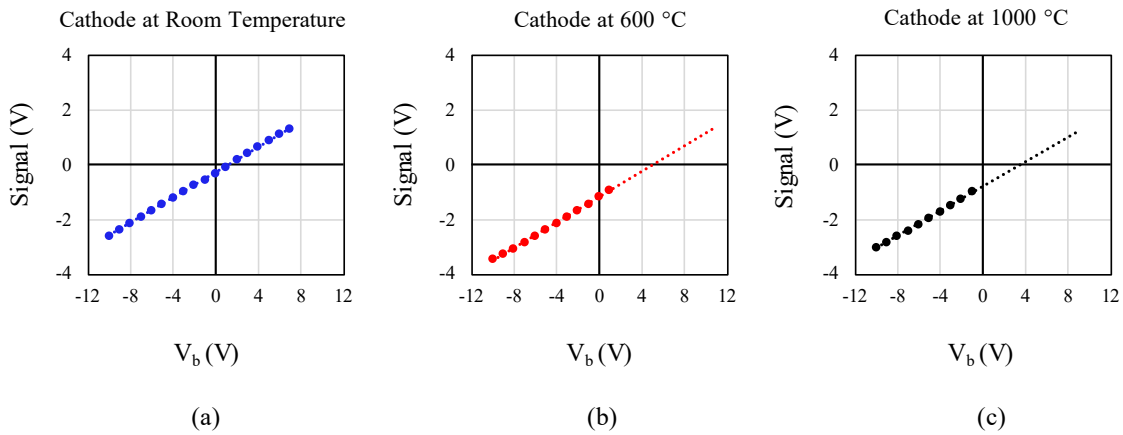


Figure 16. Kelvin probe signal vs. Kelvin probe bias. (a) a room temperature CPD measurement on an M-type cathode; the CPD “null-point” was 1193.0 mV. (b) the same for the cathode at 600 °C; the CPD extrapolated here was 5026.0 mV. (c) same for the cathode at 1000 °C. Note: signal is received by the Kelvin probe as a current, which is passed through an analog-to-digital converter and measured by the system software in volts.⁴³

In (a) the “null-point” was measured to be 1193.0 mV. In (b) it was 5026.0 mV, and in (c) it was 3430.2 mV. Some important things to note here are that a decrease of greater than 2000 mV is expected for M-type cathodes,⁷⁰ and that the signal is listed in units of volts because is received by the KP as a current that is passed through an analog-to-digital converter and recorded by the system software in volts.

These results highlight two important factors in terms of why this asymmetric bias technique is so necessary. The first is that these data show that for sufficiently hot samples,

the traditional application of KP measurement fails and is unable to make CPD measurements. In parts (b) and (c) in the above figure, no signals could be recorded for probe biases greater than +1 V when at 600 °C, and for *any* positive probe bias when at 1000 °C.

The other key takeaway from the figure is that it shows why an asymmetric bias is more desirable, such as using -4 to -10 V, when attempting to make a CPD measurement at high sample temperatures. And especially how the null-point can still be extrapolated, even though it was not contained within the actual window of probe biases used.

4.2.3 Close-Spaced Diode Assembly

Since the 1940s, Close-Spaced Diode testing has been the leading test apparatus for analyzing thermionic emission.^{44,45} A custom CSD assembly was manufactured by eBeam, Incorporated (Beaverton, OR) which could fit into the previously mentioned heating stage. This assembly still allows for the full range of sample temperatures to be reached via the external heating circuit, but its advantage is that it allows for an anode with a significant positive bias to be placed in very close proximity to the cathode.

4.2.3.1 Thermionic Emission

The physics of thermionic emission have been utilized in devices for over 200 years, spanning from Edison's carbon filaments in incandescent lamps, to the high-powered vacuum electron devices (VEDs) used in military radars and space communications today.⁴⁶ As mentioned above, the CSD test has become the industry

standard for evaluating thermionic emission for the past 80 years. This has paved the way for improved understanding of the physics governing thermionic emission and led to better implementations of the devices that make use of the phenomenon.

As shall be detailed later on, more recent advancements have been made at the University of Kentucky in the Cathode Characterization Chamber where a Kelvin probe can be used to collect emission.^{43,47,69} This technique represents a desirable expansion of the capabilities of standard CSD testing because it is highly sensitive, and capable of detecting small levels of emission at temperatures that would not otherwise be possible using standard assemblies and techniques.

O. W. Richardson first presented a relationship between current density thermionically emitted and sample temperature in 1911, as part of a larger body of work that would go on to earn him the Nobel Prize in Physics.⁴⁸ This equation would later receive reinterpretation from S. Dushman and become known as the Richardson-Dushman equation:

$$J = A T^2 e^{-\Phi/kT}$$

(Equation 5)

where J is current density (A/cm^2), Φ is the work function of the emitting surface (eV), T is temperature (K), k is Boltzmann's constant, and A is known as the Richardson constant. The parameter of most interest here, the work function, is in the exponential term. To put it another way, this equation shows just how thermionic emission depends on the work function.

As mentioned previously, the work function can be defined as the energy required to liberate an electron from a material to a point of zero potential energy away from the material's surface.³² The equation above highlights just how the work function can affect the current density emitted by a cathode. In order to extrapolate work function using a technique that measures emitted current density, then, measuring temperature as well and fitting the equation to the data is required. It is an indirect measurement process by which work function is extrapolated from a line of best fit.^{47, 49}

4.2.3.2 Parameters of the Richardson-Dushman Equation

It will be worthwhile here to point out just how current density is dependent on work function and Richardson constant according to the R-D equation. When it was introduced, the Richardson Constant, A , was taken to be a constant $120 \text{ A/cm}^2\text{K}^2$. Later experimentation proved this to not be true, however, and the constant needed to be reevaluated. Experiments have revealed materials that have apparent Richardson constants between 0.2 and 200.⁵⁰ Some have proposed taking A to be equal to $60 \text{ A/cm}^2\text{K}^2$ and applying a unitless material correction factor, b .⁵¹ Assuming a given material had a work function of 2.0 eV, here is how different values of Richardson constant would affect its predicted emission according to the R-D equation:

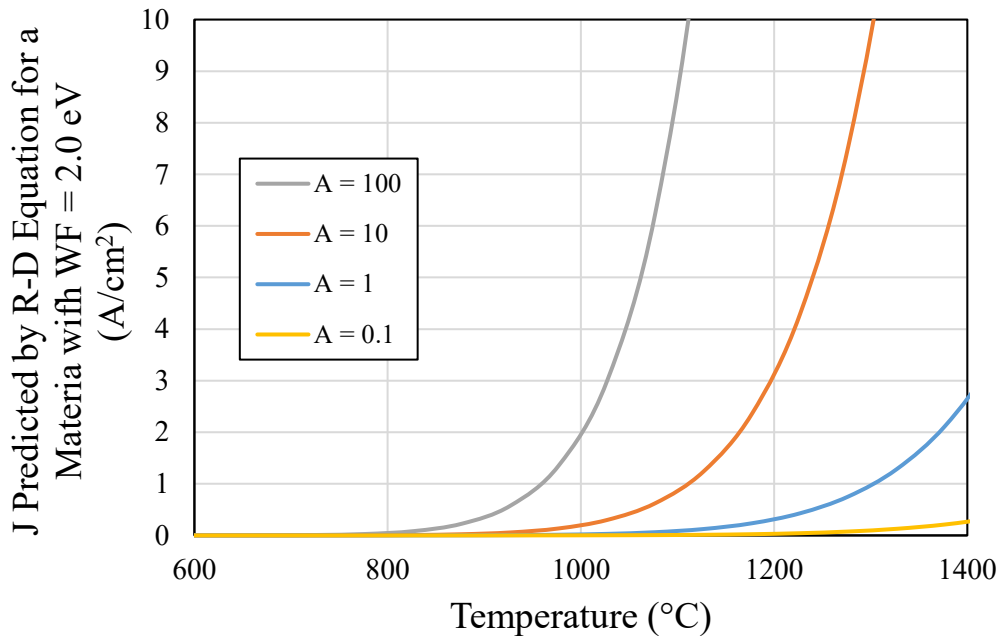


Figure 17. Current density predicted by the Richardson-Dushman equation for a given material with a work function of 2.0 eV. Showing different predicted emission curves with different assumed values for the Richardson constant.

This figure illustrates that a higher Richardson constant corresponds to an increase in emissions for equivalent temperatures. Because the units of the “constant” are A/cm^2K^2 , one way of perhaps mentally picturing the Richardson constant could be by thinking of it as a current density rate change with temperature.

The change in predicted emissions with changing Richardson constant may be considered moderate when looking at an analogous comparison of how work function change affects predicted outcomes of current density for a material with assumed identical Richardson constants. The following figure shows predicted current density from the R-D equation with a fixed $A = 120 A/cm^2K^2$, but with varying values of work function:

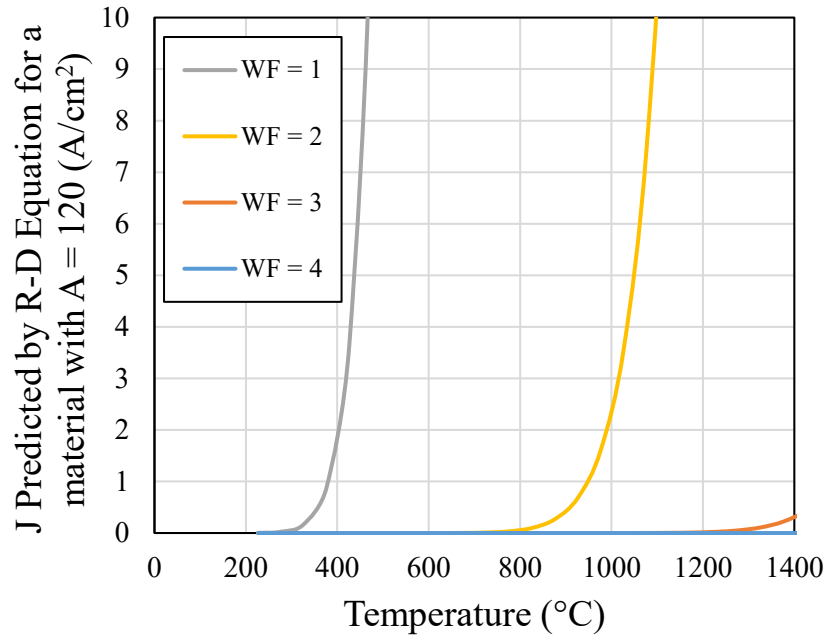


Figure 18. Current density predicted by the Richardson-Dushman equation for a given material with $A = 120 \text{ A/cm}^2\text{K}^2$, showing different predictions for the same material with different assumed work functions.

The change in predicted emission here is much more dramatic, and therefore the work function is one of the most important material parameters to understand when concerning thermionic emission (although the role that Richardson constant plays should not be ignored). Bearing this in mind, consider the real-world example of tungsten, whose work function, as with the majority of materials, is highly dependent on the crystallographic orientation⁵².

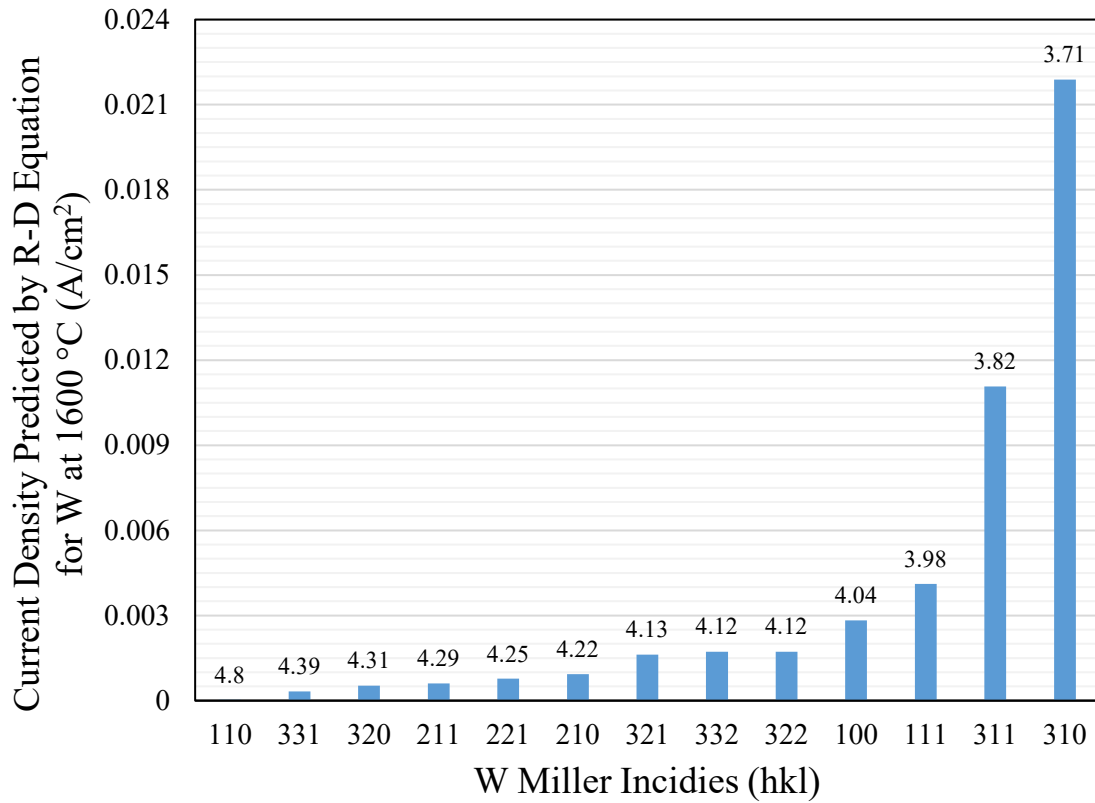


Figure 19. Current density predicted by the Richardson-Dushman equation for different crystallographic orientations of tungsten at 1600 °C.

The figure above provides the example that different crystallographic grain orientations on the same material can have big differences on predicted current emission. In the case above, W (310) crystallographic orientation tungsten is predicted to emit over 800 times that of W (110). This will be very important to keep in mind when comparing experimental results with predictions from the R-D equation.

4.3 *Other Accessories*

There are additional accessories within the CCC that provide more supportive roles, rather than measurement roles, when it comes to the characterization of cathodes. Two which are relevant to point out here are the ion polishing system that cleans the surfaces of materials using high energy incident ions, and the surface photovoltage spectroscopy system that is very useful in the analysis of semiconductors, although it may offer some insights in the present applications.

4.3.1 Ion Polishing

The CCC features an Ag ion gun for the purposes of removing oxide layers adhered onto the surfaces of metals. This gun is capable of subjecting surfaces to incident ions of multiple keVs for sustained periods of time. This is beneficial in the case when there is concern about oxide layers on a sample, but the sample cannot be heated to hot enough temperatures to de-gas the surface (typically around 700 °C).

4.3.2 Surface Photovoltage Spectroscopy

Yet another feature of the CCC is surface photovoltage spectroscopy (SPS). SPS is a powerful and relatively new (first presented in 2002)⁵³ technique that, in some sense, combines the techniques of both CPD and APS, and allows the CCC to assess the optoelectronic response of a surface on the nanometer scale.⁵⁴ SPS involves illuminating a sample under a Kelvin probe and recording the change in CPD of the sample as a function

of illumination wavelength. Unlike in APS, however, the light-source used in SPS is a quartz Tungsten-Halogen lamp with a monochromator attached, allowing for illumination energies in the 1.24 – 3.1 eV range, i.e. in the white light visible spectrum.

4.3.2.1 SPS Justification

Just off the surface of a metal are space charge regions, which create a surface potential, or an electrical potential between the surface and any point just outside that boundary. When a surface is illuminated, this surface potential changes because the incident photons can excite photoelectrons within the material which can then escape the material and therefore change the electrons within the surface charge on their way out. This potential change can be measured directly with the Kelvin probe and the measured potential difference between the illuminated and unilluminated sample is referred to by the surface photovoltage, or SPV. (SPV is merely a change in CPD, but how much harm could one more three-letter acronym do?) In some materials, this difference can be as much as an order of magnitude of change in measured photovoltage.⁵⁵ Nevertheless, an SPV measurement must be made before performing an SPS measurement to ensure that the sample will exhibit a response to illumination.

4.3.2.2 SPS Applications

While widely used in applications for organic semiconductors, study of solar cells, or other light sensitive materials, it had been the author's hope to use SPS to obtain work function information of cathodes. At this point, however, the only meaningful

measurements made using the technique have been SPV measurements on a solar cell for calibration and a low-work function samarium-coated sample as a proof-of-concept, but looking ahead, it is the author's hope that an application to cathode research will be uncovered soon.

CHAPTER 5. HIGH-TEMPERATURE CPD AND WORK FUNCTION

As stated, there is a significant problem when analyzing thermionic emitters using the CPD technique, which is that a stream of electrons is incident upon the probe, which can affect the probe's ability to accurately make measurements. As previously mentioned, cathodes can undergo large changes in work function, sometimes multiple eVs.^{56,57} So the question to answer becomes: how can a Kelvin probe be implemented to make accurate CPD measurements for a thermionically emitting sample? As this chapter will show, a system such as the CCC can be implemented (and indeed has been) to measure CPD of samples at over 1000 °C, but it requires a non-traditional application of the Kelvin probe.

5.1 *Application of the High-Temperature CPD Technique*

The experiment that follows was performed in the CCC using a UHV Kelvin probe system manufactured by KP Technology Ltd.³⁹ This system is capable of making CPD measurements in either the traditional mode or the asymmetric bias mode described previously.

This chapter reports on three different samples using the asymmetric CPD technique: a porous tungsten pellet, and two different M-type cathodes (manufactured by 3M Technical Ceramics (Lexington, KY)). The cathodes were porous tungsten bodies impregnated with different ratios of BaO:CaO:Al₂O₃, a common impregnant material for thermionic emitters.^{58,59} One cathode had an impregnant ratio of 4:1:1 and the other 6:1:2. Being M-type cathodes, these two samples were also coated with a thin film of an osmium-

ruthenium (Os-Ru) alloy (500 nm). The emitting surface for all three samples was 3 mm in diameter, and the Kelvin probe used throughout was made of stainless steel and 2 mm in diameter, and in all cases was centered over the surface under inspection.

Before any heating was done, the work function of the KP tip was first checked against a gold standard. The sample under investigation was then heated using the CCC heating stage built by 3M Technical Ceramics. For the cathodes, they were considered as “fully activated” only after being held at 1200 °C for over 4 hours, as prescribed by the manufacturer.⁶⁰ The same process was done for the tungsten pellet as well for consistency.

For each sample trial, the temperature was lowered in 100 °C increments by decreasing the applied voltage to the cathode (or to the heating stage in the case of the pure metal pellet). For each of these temperature steps, once the temperature of the sample had stabilized, the KP was brought in to 200 μm and a CPD measurement was taken using an asymmetric bias of -4 to -10 V. The tip was then removed to a further distance (enough for the pyrometers to see the sample clearly) and the temperature was lowered to the next target, and the process repeated. It is important to highlight here, too, that the pyrometry could also monitor the temperature of the tip. This is because the work function of the tip could change as a result of these close-proximity heating experiments. But as shall be shown slightly later on, the work function of the tip was monitored before and after every heating trial, and this testing arrangement maintains the integrity of the probe work function very well. In fact, during these experiments the work function of the tip was never observed to deviate too significantly from the expected value of stainless steel (within a standard deviation of 0.18 eV).

5.2 *Results and Discussion*

For all following CPD data points shown, the CPD value was averaged over 200 individual measurements, recorded over a time period of 4.5 minutes, in order to obtain an accurate average and standard deviation of CPD. For example, the room temperature measurement value for the tungsten pellet yielded an average measurement of 248 ± 3 mV using this measurement method.

At this point in time, it is necessary to reiterate that the “off-null” method only measures the signal at two KP tip biases, as illustrated in Figure 16, to determine the CPD. And according to CPD equation, the work function of the KP tip must be known in order to determine the work function of the sample from the value of CPD. Therefore, the tip work function is calibrated to a known sample, such as a sputtered thin film of gold, heavily decorated with the Au (111) crystallographic orientation and having a well-established, known work function.⁶¹ It is important to check on the tip before and after any heating experiment, but especially so in the case of M-type cathodes, which are known to evaporate barium from the impregnant material into the environment.^{62, 63}

5.2.1 Work Function of the Kelvin Probe

In the case of M-type cathodes especially, the work function of the Kelvin probe must be calibrated before and after heating experiments because of the impregnant material dispensing from the emitting surface.³⁶ Bearing in mind that the work function of the Ba (100) surface has been experimentally measured to be 2.70 eV, what follows is a table

showing the work function values of the KP tip before and after all heating experiments discussed in this chapter.⁶⁴ The lack of serious change in work function indicates that the tip is not seriously being affected by its proximity to the hot surface, although the small variations may indicate some degassing is occurring, but the fact that the tip's work function is not even close to 2.7 eV is an indication that it is not being coated in barium.

Table 1. Work function of the stainless-steel KP tip⁴³

State of Kelvin Probe Tip	W Pellet Trial	M-Type 4:1:1 Trial	M-Type 6:1:2 Trial
Pre-Heating KP Tip WF (eV)	4.58	4.80	4.79
Post-Heating KP Tip WF (eV)	4.81	4.35	4.63

These data show an average tip work function of 4.66 ± 0.18 eV, which is a reasonable work function of stainless steel.

5.2.2 Work Function and KP Temperature

As stated before, in order to make accurate work function measurements using the CPD technique, the KP tip face must be very close to the surface. Therefore, an investigation into the dangers of tip heating was carried out to ensure the safety of the

system. The tip was brought to the CPD working distance and the backed away by 10.16 mm. An increase of 0.5 volts was then applied to the sample heating stage every 5 minutes, while sample and KP tip temperatures were monitored using the Optris Xi400 pyrometer. The results are shown in the figure below.

The most important takeaway from this figure is that significant heating of the sample does not severely heat the KP tip head. Two caveats to the figure are firstly, that emissivity correction was made to the W-pellet sample measurements based on disappearing filament pyrometer measurements, but that emissivity correction was not applied to the measurements of the KP tip. And secondly, that the apparent dip in temperature observed in the graph is due to the measurement being at the limits of the camera's settings at the time.^c

^c Author's note: the Optris Xi400 pyrometer has three "modes" of operation, respectively covering the ranges of -20 – 150 °C, 0 – 250 °C, and 150 - 900 °C. That point where there is a "dip" in temperature was made with the camera switched to the second mode, at the limit of its capabilities there. At the time when this data was recorded, the sample was assumed to have the same emissivity correction across the three measurement modes, which has been observed to not always be the case. As such, the right hand side data are likely to be in error by a constant scaling factor, which was not recorded at the time of collection.

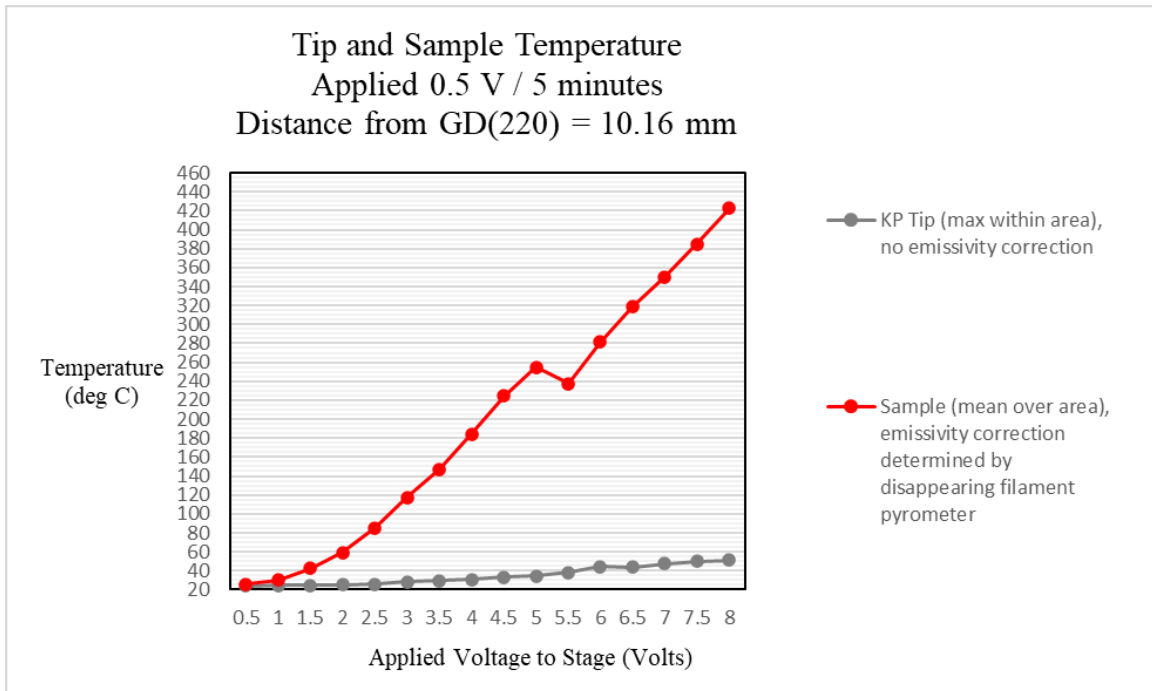


Figure 20. Sample and KP Tip Temperature. Shows the relationship between sample surface temperature and Kelvin probe tip temperature, for when the tip was stationed roughly 10 mm away from the surface.

It should be noted, however, that the tip work function does indeed change. This is influenced by a number of environmental properties, including the KP tip being exposed to atmosphere, sitting in the vacuum chamber, being held close to hot surfaces, but also can be affected by things like the humidity or the presence of specific gasses inside the chamber walls. Confidence in the KP work function is essential, though, and toward that end, consider the following:

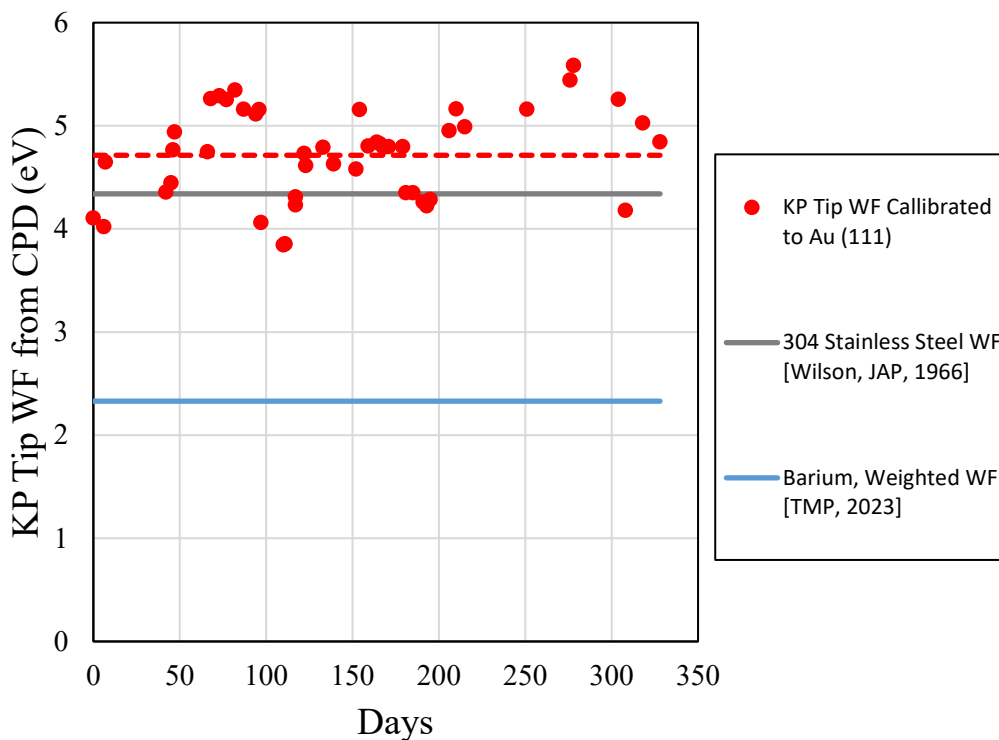


Figure 21. Work function of the stainless steel Kelvin probe tip over the period of 1 year. The tip WF was calibrated to a reference sample of Au (111) crystallographic gold. The red dashed line represents the average of the KP WF values, 4.71 eV. The grey line is a literature reference value of an acceptable WF for stainless steel and the blue line is a reference value for a WF of barium.

This plot shows the WF of a stainless steel KP tip calibrated to a gold reference sample over 1 year of measurements made primarily on dispenser cathodes. During all of that time, the WF of the tip maintained an average WF of 4.71 ± 0.46 eV. Two additional lines highlight a reference value for the work function of stainless steel⁶⁵ and for barium.⁶⁶ This provides strong evidence that any emitted barium from the dispenser cathode was not deposited on the surface of the KP tip.

5.2.3 Work Function and Sample Temperature

The experimental procedure outlined above was carried out on the three samples mentioned: the tungsten pellet and the two M-type cathodes with different impregnant material. The results are shown in Figure 22.

The first thing that can be noted in the figure is that the pure metal, tungsten, does not appear to change work function seriously with temperature. In fact, work function was once assumed to be constant with temperature for pure metals.⁶⁷ However modern studies have shown that many refractory metals, including tungsten, do indeed experience a slight decrease in work function at temperatures of cathode operation.⁶⁸ This is both due to the fact that residual gasses, especially oxygen, on the surface can be released with temperature, and due to the fact that work function is dependent on changes in surface state with temperature. The data for tungsten in the figure show a decrease of only 0.04 eV between room temperature and 1000 °C.

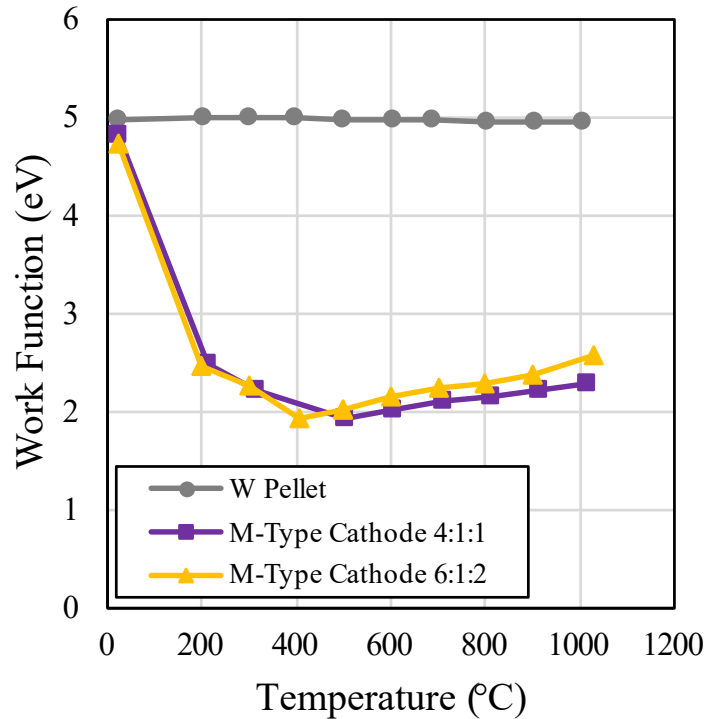


Figure 22. Work function and temperature from the asymmetric bias technique. Data for a W pellet and two M-type cathodes are shown. The two M-type cathodes were identical in body matrix but had different BaO:CaO:Al₂O₃ impregnant ratios, in particular 4:1:1 and 6:1:2, respectively ⁶⁹

This plot shows the work function from CPD for a tungsten (W) pellet in grey circles, an M-type cathode with 4:1:1 impregnant in purple squares, and an M-type cathode with 6:1:2 impregnant in yellow triangles.

On the other hand, the M-type cathodes exhibited very different behavior. Both showed an apparent minimum in work function in the 400 to 500 °C range, which may, in part, be explained by barium adsorption on the surface. Recall that these measurements were taken from high temperature to low temperature, so the dip and then raise seen in the moderate-to-low temperature measurements is theorized to be indicative of the breakup of barium on the surface and the subsequent reabsorption of gasses, a phenomenon known to

occur on barium-impregnated dispenser cathodes.⁸⁰ At their highest temperature measurement, 1000 °C, it is curious to note that the cathode with the BaO:CaO:Al₂O₃ impregnant ratio of 6:1:2 showed a work function of 2.57 eV, while the cathode with a ratio of 4:1:1, i.e. with a lower proportional amount of barium, exhibited a lower work function of 2.28 eV. Both values were very close to that of Ba (100) as reported in the literature.⁶⁸

The other noticeable feature of the data is the difference between the room temperature and the activation temperature work functions in the M-type cathodes. From prior emissions studies, M-type cathodes are known to experience a decrease in > 2.0 eV.⁷⁰ As stated before, this particular phenomenon is exactly what makes M-type cathodes so desirable as thermionic emitters.⁷¹

This figure ultimately summarizes how useful the asymmetric CPD technique is. It provides a meaningful way to measure the work function of thermionic emitters at a range of temperatures, something that traditional techniques could not do. Once these values are compared to work function values from theory or from emissions testing, this will only further reveal itself to be an exceptional testing technique.

5.3 *Work Function and Other Material Properties*

This dissertation is chiefly interested in the relationship between work function and thermionic emission. It is worth mentioning, however, that some studies have investigated the work function as being a predictor of a number of different material properties. Some have even so far as to propose models for these behaviors, such as Hua and Li who proposed the following relationship between work function and Young's modulus⁷²:

$$E = 0.02233 \Phi^6$$

(Equation 6)

Where E is the Young's Modulus (how easily a material can stretch and deform), and Φ is the work function. In an attempt to verify this claim, the work function of a number of bulk material samples were measured using an ambient Kelvin probe system. The corresponding Young's Moduli were taken from an online database and the following resulted:

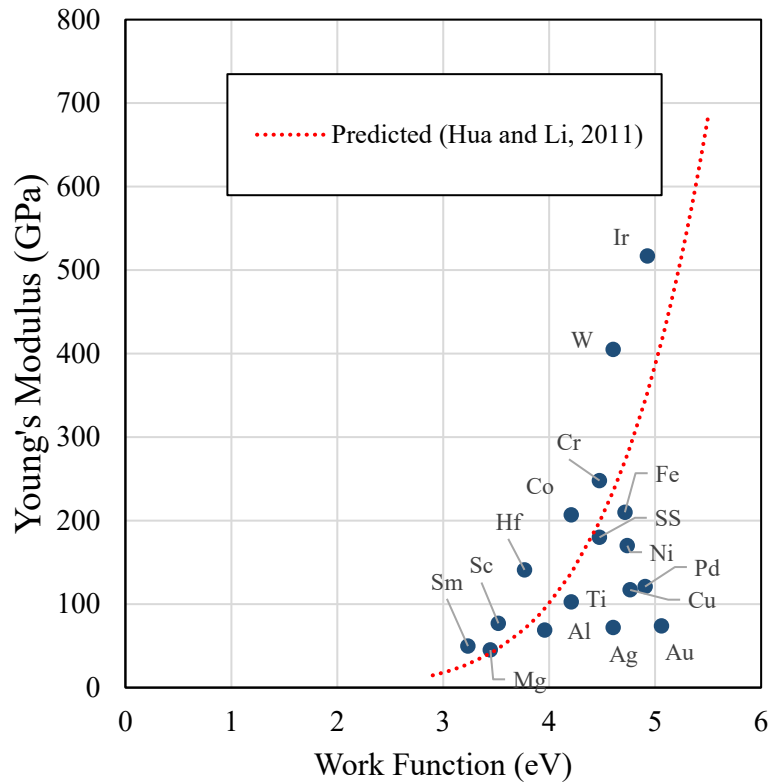


Figure 23. Young's Modulus vs. Work Function. Work function measured on bulk samples using ambient Kelvin probe system and Young's Modulus from online reference.⁷³ The red dashed line shows the prediction from Hua and Li, 2011.

So there may be some agreement from bulk Kelvin probe measurements, although further analysis into the extent to which the data demonstrate sufficient correlation to claim the proposed relationship should be conducted. Another material property that has been claimed to be predicted by work function is the plane-strain fracture toughness, or a material's resistance to crack under linear-elastic conditions.⁷⁴ Using this same data of work function measured under ambient conditions on bulk material, the following was produced:

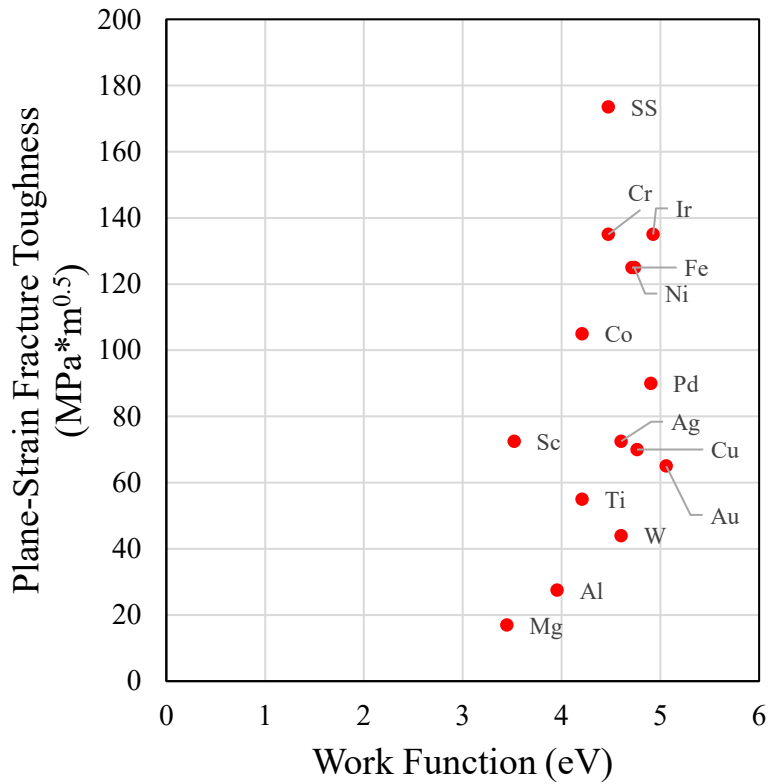


Figure 24. Plane-Strain Fracture Toughness vs. Work Function. Work function values were measured on bulk material samples and values of fracture toughness were taken from an online database.⁷⁵

Again, this plot indicates that there may be more to the relationship between work function and other material properties than what meets the eye at first, but additional studies should be carried out to that end. Ultimately, this is an avenue of investigation that will be relegated to either additional work or another's study altogether, since this dissertation is principally concerned with the properties of thermionic emission.

5.4 *Conclusions*

This chapter built off of earlier sections exploring the limitations of the traditional CPD technique for thermionic emitters and showed that the asymmetric CPD technique is accurate and effective and a viable alternative for cathode studies. Where APS could not determine work function above 800 °C, and where traditional Kelvin probe methods could not determine work function above 600 °C, the asymmetric bias technique revealed itself to function successfully at cathode operating temperatures (> 1000 °C), addressing the biggest problem facing the traditional applications of cathode analysis in the extreme environment of high temperature and high vacuum. This achievement was only possibly by using an asymmetric, negative bias on the probe using the “off-null” method, thereby circumventing the saturation problem presented by putting a positively biased probe so close to a surface emitting a high density of electrons.

This chapter also highlighted that the Kelvin probe itself was relatively unaffected by the extreme environments that it was subjected to as a result of these tests. That is, despite being in such close proximity to a hot surface, and despite being so close to a material known to be emitting barium, the probe work function never deviated dramatically

from what was expected for stainless steel. These findings reaffirm the technique's suitability for many applications in thermionic emissions studies.

CHAPTER 6. THERMIONIC EMISSION COLLECTION AND WORK FUNCTION

6.1 The Richardson-Dushman Equation

In addition to work function measurements using the asymmetric bias CPD technique, the CCC is also capable of using the KP tip to measure the emitted current density of hot cathodes, using the exact same hardware within the UHV chamber as described previously. As stated before, the collected current density can then be fitted to the Richardson-Dushman equation:

$$J = A T^2 e^{-\Phi/kT}$$

(Equation 5)

where J is current density (A/cm^2), Φ is the work function of the emitting surface (eV), T is temperature (K), k is Boltzmann's constant, and A is known as the Richardson constant. Historically, A has often been reported $120 \text{ A}/\text{cm}^2\text{K}^2$ – experimentally, however, a material-specific correction factor to this term is virtually always needed.^{76,77,46,78} According to the Richardson-Dushman equation, metals that have high work functions, such as 4 to 5 eV, require very high temperatures ($> 2000 \text{ }^\circ\text{C}$) just to achieve current densities greater than $1 \text{ A}/\text{cm}^2$.⁷⁰ On the other hand, M-type cathodes can produce much higher current densities at significantly lower operating temperatures – with some cathodes even being able to emit $1 \text{ A}/\text{cm}^2$ at less than $800 \text{ }^\circ\text{C}$ (as shall be demonstrated later). But no matter the level of emission, so long as the cathode is operating in the “temperature limited (TL) regime,” which is to say the region where emission changes with temperature,

then the R-D equation is held to be valid. By measuring temperature and emitted current density together, then, and fitting the R-D equation to a line of best-fit, the work function and Richardson constant can be extracted.

6.2 *Collecting Current Density with KP*

Recall that when using a KP tip to measure CPD above an emitting surface, a positive probe bias was a hinderance because it effectively turned the probe into a current collector and saturated the collection capabilities. But if the aim is to collect current, then this is an ability that should be taken advantage of! In the sets of experiments that follow in this chapter, three separate samples were investigated. The testing procedure was the same for all three. First, the sample was heated to the point of activation, which for the specific samples described here was 1200 °C for at least 4 hours according to the manufacturer. A positive probe bias and tip-to-sample spacing were then decided upon (both parameters were modulated and the results are shown below) to use as the collection parameters. Current density was recorded and then the sample was cooled in successive steps, where at each step, once the temperature had stabilized, the current density was measured again. This process repeated all the way down until thermionic emission could no longer be detected above noise levels. The fixed tip-to-sample spacings include 2, 1, and 0.5 cm, and the KP tip biases cover +1, +5, and +10 V. As will be shown, tuning these parameters can lead to the detection of current density from cathodes at emission levels and at temperatures significantly lower than more traditional tests.

The Kelvin probe system of the CCC is ideal for this application because it was configured to explicitly measure tiny currents due to the rapid KP tip oscillation associated

with measuring CPD. This allows for detection of current density at temperatures as low as 500 °C and emissions levels that are so low, they would likely be undetectable by any other method.

Once again, the spacing and probe bias can have significant impact on the measured current, and it is important to investigate how those parameters will change the data collected (and possibly the resulting WF and Richardson constant that come from R-D analysis). This is relevant because it is possible to saturate the detection capabilities of this sensitive system, by either using a too-small spacing or a too-high bias. This will cause the delicate system hardware to measure unrealistic, saturated current densities, and therefore if R-D analysis is applied in those regions, inaccurate and impractical values of work function and Richardson constant can be obtained. The observation that corresponds to this is a “flatlining” of collected current density, which was seen to occur at the same voltage in all measurement sets (leading to the conclusion that this was a firm saturation limit imposed by the hardware of the KP system).

As before, the temperatures of the CCC internal components, i.e. the sample surface and the probe tip, were monitored with digital pyrometry and the data for sample surface temperature were then used to fit the R-D equation. Values for work function and Richardson constant were then extrapolated from lines of best fit and are presented in tables accompanying the results.

6.3 *KP Parameters and Current Density*

In order to extrapolate work function more easily, as well as the Richardson constant, indirectly from current density and temperature data, it is more convenient to

rewrite the Richardson-Dushman equation in the following form:

$$\ln\left(\frac{J}{T^2}\right) = -\frac{\Phi}{kT} + \ln(A)$$

(Equation 7)

Such that a plot of $\ln(J/T^2)$ vs. $1/T$ should yield a linear trend, wherein the slope multiplied by $-k$ would yield the work function, and $e^{\text{y-intercept}}$ would yield the Richardson constant.

The figures that follow are plotted to fit this equation, and they indicate the effects of the various parameter changes on collected current density when using the KP in the current collection mode. The first figure shows how changes in the KP tip bias effect emission collection when the probe is fixed at 2 cm away from the surface. The two samples shown are two identical M-type cathodes save for different the BaO:CaO:Al₂O₃ impregnant ratios (4:1:1 and 6:1:2, respectively).

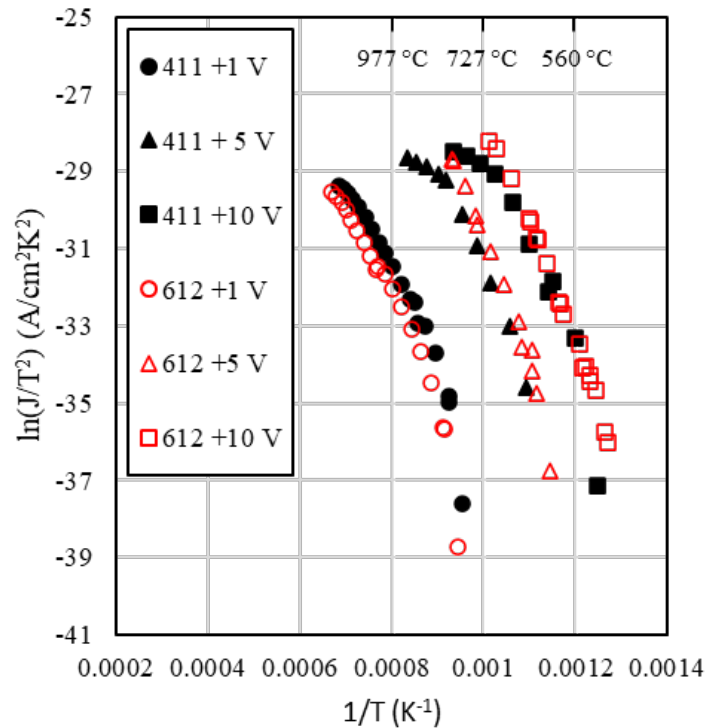


Figure 25. Modulated KP Bias, Fixed Spacing. Current density collected by the Kelvin probe from a fixed distance of 2 cm away from the emitting surface for an M-type cathode with 6:1:2 impregnant (open red), and an M-type cathode with 4:1:1 impregnant (closed black). The shapes correspond to the tip biases of +1 V (circle), +5 V (triangle), and +10 V (square).⁶⁹

The data in the above figure show that increasing the magnitude of the positive bias of the tip leads to more current collection from a given sample, and it allows the system to access different temperature ranges of emission that might have been otherwise inaccessible. The small, non-linearities in current density observable at the “top end” of each measurement, that is to say at the higher temperatures of each set, are suspected to be relating to that functional detection limit of the system hardware mentioned previously. This is because, as will be demonstrated further on, when fitting the R-D equation to these areas it does not produce reasonable work function values or Richardson constants that are

in agreement with expected values at those temperatures. As discussion will clarify after looking at other samples and parameter modulation, this is why striking a delicate balance of spacing and bias must be achieved when using this technique to obtain accurate values of work function.

The next figure shows data collected on one M-type cathode and also a bare tungsten (W) pellet, meant to simulate an unimpregnated and uncoated cathode. In this dataset, the KP probe bias was fixed to +1 V and this time the tip-to-sample spacing was modulated, using distances of 0.5, 1.0, and 2 cm, respectively.

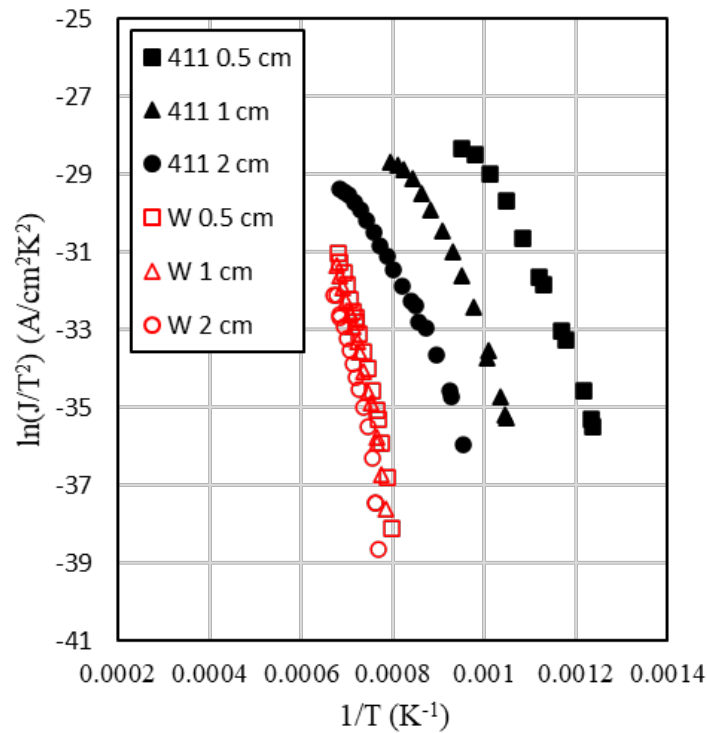


Figure 26. Fixed KP Bias, Modulated Spacing. Current density collected by the Kelvin probe at a fixed bias of +1 V for a porous tungsten pellet (open red) and an M-type cathode with 4:1:1 impregnant (closed black). Measurements at tip-to-sample distances of 0.5 cm (square), 1 cm (triangle) and 2 cm (circle).⁶⁹

In this trial, as was similarly observed in the preceding one, different current densities and temperature ranges could be accessed by adjusting the parameters. This set showed that higher current densities could be recorded by backing the probe further away from the emitting surface, and that higher temperatures could be accessed by bringing the tip closer in. These data also highlight the striking difference between emission collected from an M-type cathode and a pure metal. The W data, it turns out, reveals the exact importance of balancing these parameters, because it reveals two consequences about this technique. Firstly, that as spacing decreases and as bias increases, the emission collection reaches an asymptote. This limit, as shall be seen, might be the key to this technique. Because secondly, this asymptote will reveal that this process is capable of recording values that are in great agreement with values reported across literature when the W data is scrutinized in greater detail in just a bit.

A more focused dataset on the W pellet appears in the following figure:

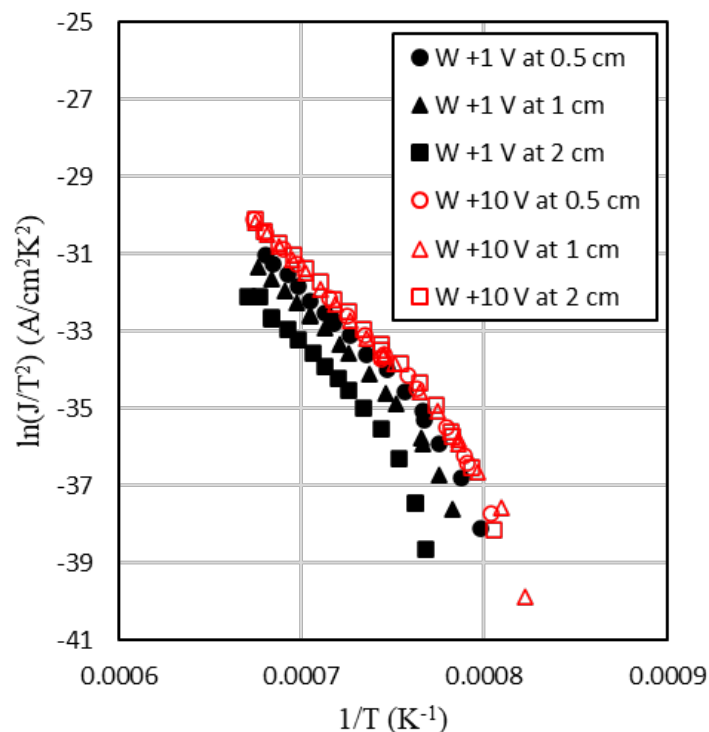


Figure 27. W Pellet, Modulated KP Bias and Spacing. Current density collected by Kelvin probe from a porous tungsten pellet, with probe bias of +1 V (closed black) and +10 V (open red); tip-to-sample spacings of 0.5 cm (circle), 1 cm (triangle), and 2 cm (square).⁶⁹

These data show that with an increase in probe bias and a decrease in tip-to-sample spacing, the collected current density converges toward a common trend. This will be shown explicitly in the next figure, but it turns out that this data yields values of work function and Richardson constant that agree strongly with literature expectations.⁷⁹ This provides evidence that this system can indeed obtain accurate values from collected current density. Of critical importance to note, however, is that for a material with a relatively high work function like the porous tungsten pellet, the current density emitted was well within the detection capabilities of the instrumentation. For other samples, however, such as low work function M-types, they can emit much larger current densities and saturate the system

for similar positions and tip biases. This was observed to be the case for the two M-types shown above, and as will be demonstrated further on, R-D analysis should not be done in these regions.

6.4 *Work Function, Thermionic Emission, and R-D Analysis*

By fitting the R-D equation to the current density data, both work function and Richardson constant can be derived. The work function can then be compared to CPD data obtained from the same KP system in order to obtain a more full picture of the emitting sample surface. This, in effect, provides congruent measurements of direct work function from measurement and indirect work function from mathematical analysis.

The following figure shows how R-D analysis is performed using current density and temperature when fitted to the modified R-D equation shown previously. The first step involves identifying a temperature region where emission current is within the linear response range appropriate for measuring current, that is to say within the TL regime where the R-D equation is valid. For higher emitters when using this technique this is more of a concern, because, as can be seen by the figure, for the lower emitting W pellet, the data are not saturated even at its highest temperatures.

After the appropriate TL regime is identified, the slope and y-intercept are found by fitting a linear fit of the modified R-D equation, such that the work function can be obtained by the slope and the Richardson constant from the y-intercept.

In the case of the figure below, which shows data collected on a W pellet when the KP tip was biased at +10 V and 0.5 cm away, it can be seen that when the parameters of bias and spacing are tuned just right, values of work function and Richardson constant can

be obtained that are in excellent agreement with literature values.⁷⁹ The challenge of using this technique, therefore, becomes how to balance this geometry to yield accurate values, because even when it is off slightly, the system can become quickly saturated.

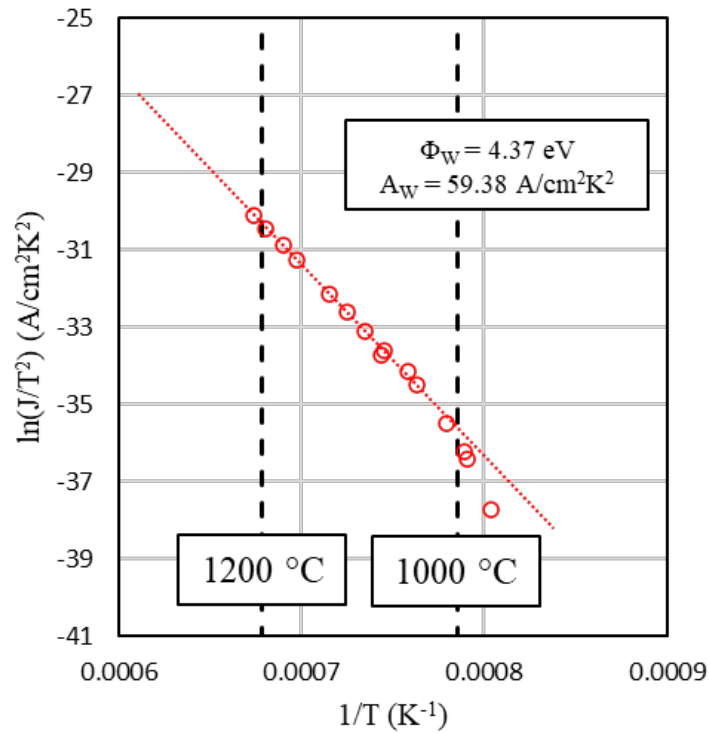


Figure 28. R-D Analysis, W Pellet. Emission data collected from a tungsten pellet with a Kelvin probe tip bias of +10 V and a tip-to-sample spacing of 0.5 cm. These data were presented previously, but here the relevant elements of Richardson-Dushman analysis are highlighted as an example of how work function and Richardson constant can be derived from the data.⁶⁹

In order to illustrate how the saturated regimes can influence apparent work function and Richardson constant, consider the following figure, which shows current emission data from the 4:1:1 impregnated M-type cathode with fixed KP bias and modulated tip-to-sample spacing. Multiple linear regions of interest have been marked and

labeled, from which respective work functions and Richardson constants were extrapolated and are listed in the accompanying table below.

This presents an interesting picture, where higher temperature regions produce work function values that are within expected limits for activated M-type cathodes (< 2.0 eV), but which have apparent Richardson constants that are quite small.⁵⁷ Conversely, the moderate temperature regions produce work functions that would be slightly higher than anticipated for an activated M-type cathode (~ 3.5 eV), but the Richardson constants are within ranges typically reported for emitting surfaces (between $0.02 - 200 \text{ A}^1\text{cm}^{-2}\text{K}^{-2}$).⁷⁸ These very low values of Richardson constant seen here are theorized to be representative of the very low densities of emission being collected by the KP tip, lower than 10^{-6} A/cm^2 in all cases, when using this setup. They may also indicate just how tremendously sensitive this system is with respect to detecting patchy emission from the cathode surface. This could explain Richardson constants that are significantly different from other emissions studies that use anodes with significantly higher biases and much smaller sample spacings that collect much more current density.

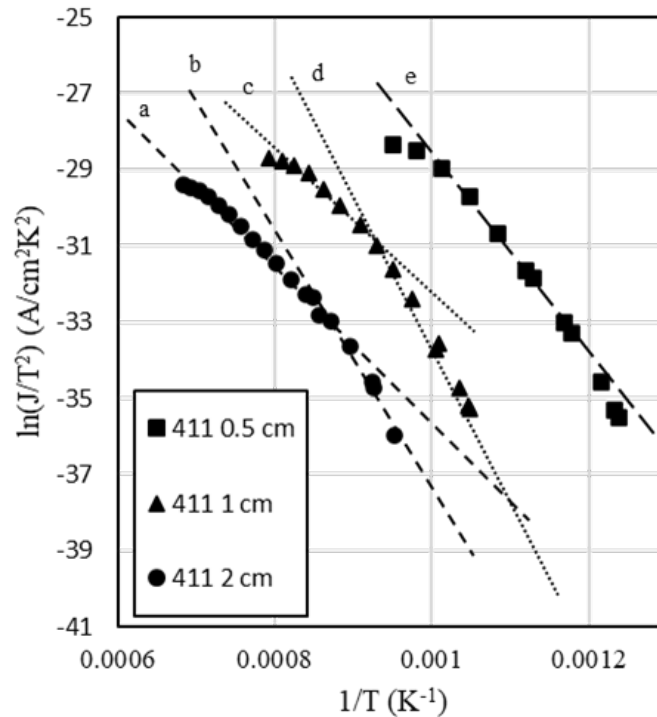


Figure 29. Regions of Interest for R-D Analysis, Modulated Spacing. Effects of varying the tip-to-sample distance for an M-type cathode with 4:1:1 impregnant material, as before, but now with the addition of lines highlighting distinct linear regions from which to extrapolate work function and Richardson constant. The respective values for these parameters are shown in the table below.⁶⁹

Table 2. Work Function and Richardson Constant from Figure 29

Plot Region	Temperature Range (°C)	Work Function (eV)	Richardson Constant (A/cm ² K ²)
a	1200 – 900	1.86	7.0 * 10 ⁻⁷
b	900 – 700	3.57	32
c	1000 – 800	1.88	2.1 * 10 ⁻⁵
d	800 – 700	3.53	72
e	800 – 500	2.64	12

The takeaway from these results is that the KP can access higher temperature ranges when further away from the emitting surface and that fitting the R-D equation to different regimes can yield a range of work functions and Richardson constants. On its own,

however, the above figure and table do not fully illustrate the consequences of saturating the system. What follows will exemplify the dangers even more thoroughly.

As shown for the W pellet previously, it is more desirable to have a higher positive bias closer to the emitting surface in order to collect more amounts of current density. For higher emitters, however, the collected current density was observed to flatten out at high temperature measurements. The consequences of applying R-D analysis to these regions are shown below in data that were collected on the same M-type sample but this time with fixed tip-to-sample spacing and modulated bias. Linear regions of interest have been marked and labeled, and the accompanying table shows the extrapolated WF and Richardson constant values.

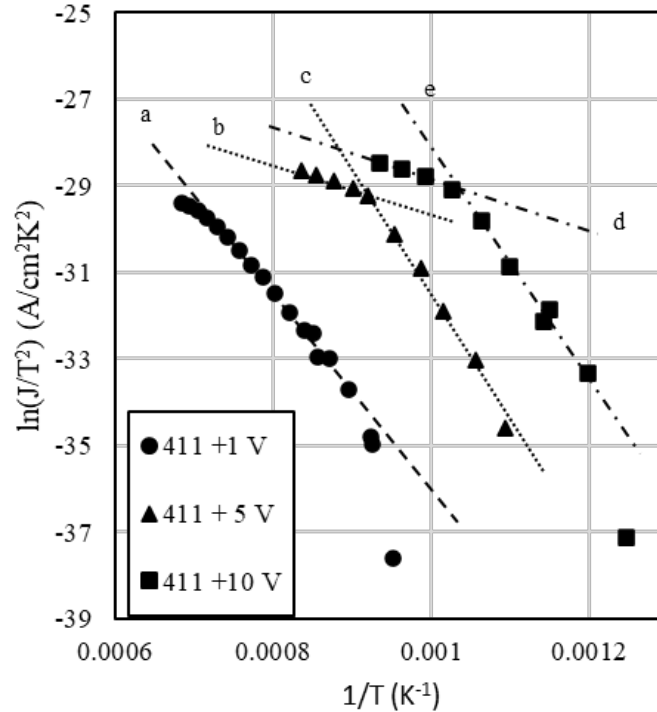


Figure 30. Regions of Interest for R-D Analysis, Modulated Bias. Kelvin probe data for an M-type cathode with 4:1:1 impregnant material, where tip bias has been varied as before, but now with the addition of lines highlighting distinct linear regions from which to extrapolate work function and Richardson constant. The respective values for these parameters are shown in the table below.⁶⁹

Table 3. Work Function and Richardson Constant from Figure 30

Plot Region	Temperature Range (°C)	Work Function (eV)	Richardson Constant (A/cm ² K ²)
a	1200 – 850	1.80	3.8 * 10 ⁻⁷
b	950 – 800	0.58	0.9 * 10 ⁻¹⁰
c	800 – 600	2.50	0.1
d	800 – 700	0.57	2.1 * 10 ⁻¹⁰
e	800 – 500	2.43	0.1

Finally the results of saturating the system become apparent, as evidenced by regions b and d in the preceding figure where the current density flattens out. The apparent work functions and Richardson constants that come out of R-D analysis in these regions

are unexpectedly small for any known material. Hence, these regions are speculated to be artifacts that result from the geometry of the system, and the justification for the claim that R-D analysis should not be performed in these regions. Evidence for this was also provided because the saturation limit was observed to be at the same value in all test conditions. So the conclusion is that the parameters must be delicately tuned such that the system avoids these regions. These parameters are not the same for pure tungsten as they are for M-type cathodes, so they must be tuned for each specific emitting surface under inspection.

For the regions where the system is not saturated, however, expected values of work function can be obtained for the M-type cathodes, albeit with relatively small values of Richardson constant. As mentioned previously, this is interpreted to reflect the very small amount of current being collected by the probe ($< 10^{-6}$ A/cm²), although it is plausible that it is the result of the probe collecting different current density rates from different patches of the emitting area below. Future investigations, either relying on experiment or theory and computer simulations, should explore the complicated dynamics of this unique geometry. Such work might even probe the need for yet another reinterpretation of the Richardson constant.

CHAPTER 7. MATERIALS CHARACTERIZATION OF CATHODE SURFACES

7.1 SEM

Scanning electron microscopy is a well-established form of microscopy that is capable of generating images at very high magnifications using electrons. It has been in development for nearly 100 years, although really only being commercially available since the mid-1960s. It is useful to the understanding of cathodes because it can help reveal things about the surfaces of cathodes before and after testing – and remember, this dissertation is very concerned with the relationship between work function and surface. In order to better understand the behavior of surface morphologies of thermionic emitters, therefore, both before and after activation, scanning electron microscopy (SEM) was carried out to image the surfaces of the M-type cathodes reported on previously. Specifically, the following images were made using a FEI Helios Nanolab 660 scanning electron microscope at the University of Kentucky's Electron Microscopy Center. The findings of this widespread characterization technique applied to an M-type cathode with 4:1:1 impregnant are shown below

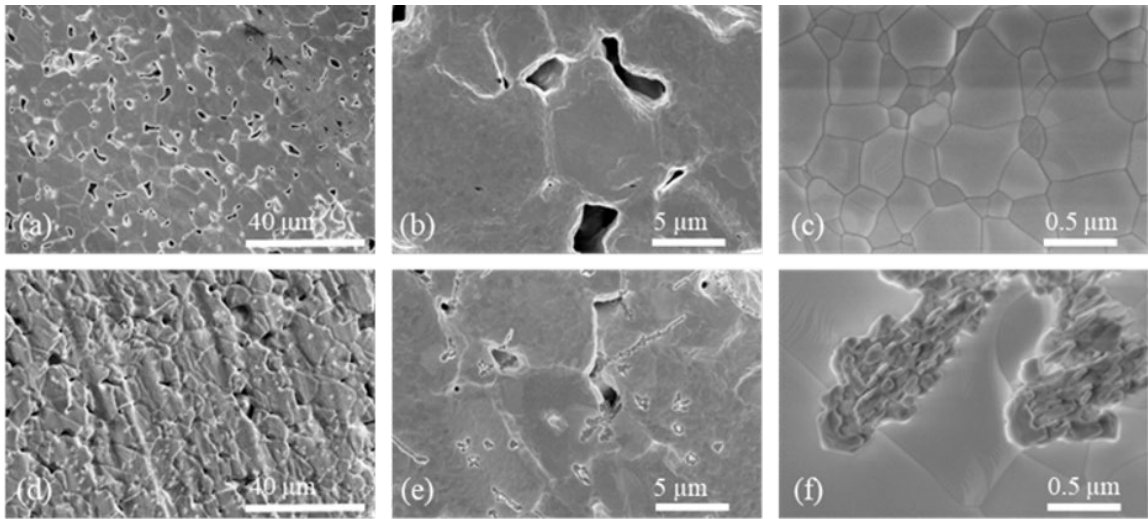


Figure 31. SEM of an M-type cathode before and after activation. (a-c) SEM micrographs of an as-received M-type cathode with 4:1:1 impregnant, before any heating. (d-f) Micrographs of the same M-type cathode after the full set of heating experiments described in this paper were carried out. Scale bars: (a) 40 μm , (b) 5 μm , (c) 500 nm, (d) 40 μm , (e) 5 μm , (f) 500 nm. Complementary EDS analysis for this same sample is shown in Figure 33.⁶⁹

In the figure above, (a)-(c) are of the cathode surface before activation, i.e. as received from the manufacturer, and (d)-(f) are corresponding images of the surface after activation and testing in the CCC. These representative images correspond to similar behaviors seen on before/after images taken on other impregnated M-type dispenser cathode studied in this system as well.

The most notable feature is the appearance of impregnant material, emanating out of the pores and onto the cathode surface. To confirm the identity of these tendrils, however, another technique was applied. And this shall be elaborated upon in a following subchapter, but before moving on from SEM, another interesting result should be noted.

These tendrils were not noted on every cathode. What follows are SEM images of a scandate cathode (eBeam Incorporated) before and after heating.

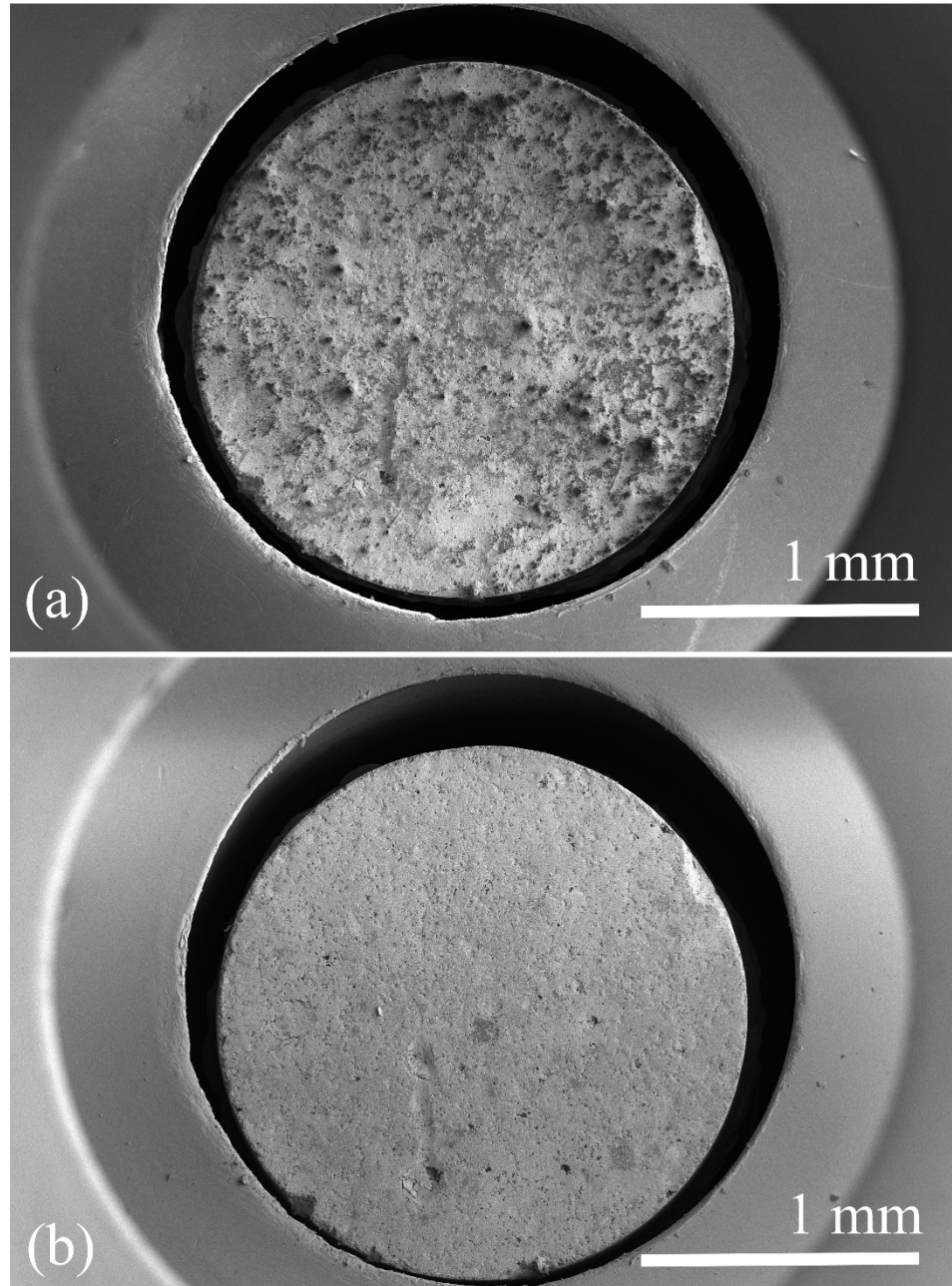


Figure 32. Scandate cathode surface (a) as received from the manufacturer and prior to heating, (b) after undergoing the activation heating schedule outlined by the manufacturer.

In the figure above, it is interesting to note the homogenizing that occurred across the surface as a result of undergoing the manufacturer's activation heating schedule. In the

before image, as received by the manufacturer, there is much more texture. In the activated surface, much smoother. Additional surface characterization studies using SEM must be carried out in order to obtain a fuller picture of how these surface features and changes affect work function.

7.2 EDS

X-ray energy-dispersive spectroscopy (EDS) is a useful technique for elemental analysis wherein a sample is excited by incident electrons and the characteristic X-rays released by the “relaxing” atoms are recorded as a spectrum. EDS was performed using an FEI Quanta 250 EDS microscope (also at the Electron Microscopy Center) in order to analyze the elemental composition of the tendrils shown on the previous cathode surface.

The figure below shows the results of performing EDS analysis on the tendrils observed to be coming out of the body pores post-activation. They were seen to be high in Ba and O, both present in the impregnant material, leading to the conclusion that these tendrils had spread out on to the surface as a result of the heating and emissions testing.

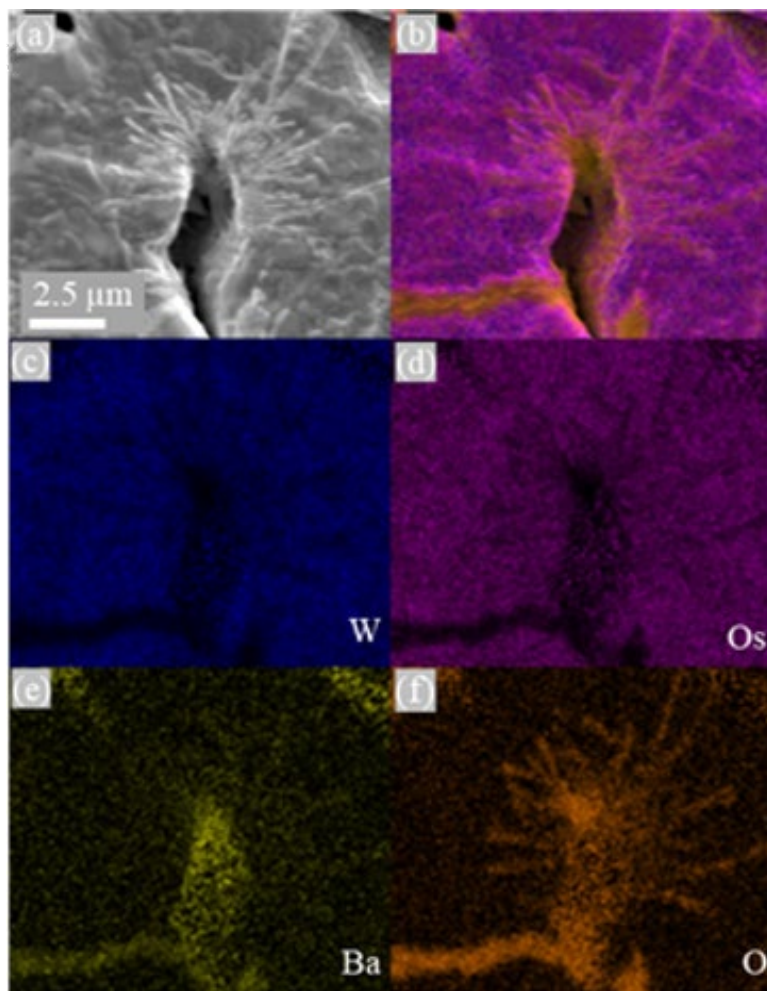


Figure 33. EDS of an M-type cathode post-activation. Specifically, the analysis of the tendrils growing out of the pores on the same M-type cathode surface shown in Figure 17. (a) SEM image with scale bar of 2.5 μm , (b) Composite EDS elemental map, (c) Tungsten (W), (d) Osmium (Os), (e) Barium (Ba), (f) Oxygen (O).⁶⁹

7.3 *XRF*

X-ray fluorescence spectroscopy (XRF) is also a technique that is useful for characterizing the elemental composition of surfaces. XRF was used in this work to analyze a test sample made for an investigation into M-type cathode coating candidates, and the corresponding results will appear later on in Chapter 9 accompanying a description of the experiment done using it.

7.4 *Results and Discussion*

Diverse materials characterization techniques are important for understanding the behavior of the surfaces of thermionic emitters. Clearly, cathode surfaces can undergo serious changes before and after experiencing activation and testing, so studying them is incredibly informative. Investigations into how these changes affect emission performance must also be carried out so that a complete picture can be painted of how they relate to one another. Finally, because a cathode's ability to emit is so closely tied to its surface state, the integration of multiple materials characterization techniques and the understanding of work function presented in this dissertation will be needed if a truly improved cathode surface is ever to be found.

CHAPTER 8. CSD AND THE KP EMISSION METHOD

8.1 *CSD in the CCC*

As stated previously, CSD testing is a standard, useful method of quantifying thermionic emission as a function of temperature for cathodes. A custom CSD testing assembly was provided by eBeam, Incorporated (Beaverton, OR), designed to fit within the XYZ motor stage of the CCC. A photograph of this unique system is shown in the figure below:



Figure 34. Custom UHV CSD assembly. Built by eBeam Incorporated. The ~2 mm diameter cathode face can be seen, as the anode plate is swiveled downward in an open position.

This assembly was specifically designed to heat ~2 mm diameter thermionic emitters to temperatures of 1200 °C, which, as stated previously, is a typical activation temperature for cathodes used in industry.⁵⁷ In typical fashion for a CSD test, this rig was structured with an anode plate roughly 1 mm away. For the tests reported below, an anode bias of +700 V was used, pulsed at 60 Hz with 2% symmetry. This configuration was recommended by the manufacturer and allowed for current collection on the order of 10 A/cm². This is representative of the demands put on dispenser cathodes used in industrial applications today.^{57,80}

The primary objective of incorporating such a CSD assembly into the UHV chamber of the CCC was to establish a baseline, or a standard test, to which the KP emissions tests could be compared. CSD testing already having established itself as the leading technique to evaluate thermionic emission, the question remained of how data from the innovative and novel techniques of KP emissions collection and high temperature CPD compared.

8.1.1 On CSD Testing and Temperature

Of course, with the anode plate closed over the emitting face, it is difficult to observe the surface temperature of the cathode using optical pyrometry. In order to solve this problem, the previously mentioned pyrometers attached to the CCC (Optris Xi400 and Optris PI1M) were used to monitor applied heater power and temperature, measured while the anode plate was opened. Therefore, an accurate picture of temperature could be known, even when the anode was covering the surface of the thermionic emitter.

8.2 Work Function from CSD

The figure below shows the results of an experiment where current density was collected from a scandate cathode provided by eBeam, Incorporated designed to fit inside of the CSD assembly previously described. The data were collected following a 24-hour activation schedule that was outlined by the manufacturer.

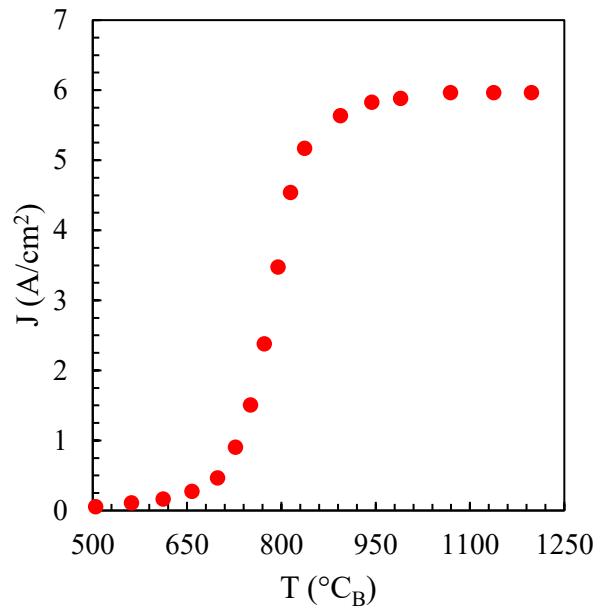


Figure 35. Current Density from CSD Testing, collected on a dispenser cathode using the custom CSD assembly built by eBeam, Incorporated.

Such a plot is called a “knee curve” and is typical for a plot of current density vs. temperature for modern cathodes. The “knee” in question is the point of the rightmost bend where the emission transfers from the temperature-limited regime (i.e. where emission changes with temperature) to the space-charge limited (SCL) regime (i.e. where change in temperature no longer changes emission). The knee temperature is regularly used as an

indicator of how successful a cathode is – the main idea being that the lower the knee temperature then the lower temperature needed to get the cathode’s emission to stabilize.

In the figure above, the knee temperature is 843 °C, revealing that this is a well-performing cathode when compared to those that are used in industry today.⁸⁰ By fitting the Richardson-Dushman equation to the temperature (TL) regime, which is to say the range where the R-D equation is held to be accurate, the figure yields an apparent work function for this cathode of 1.63 eV. This is also indicative that this cathode is a good emitter.

8.2.1 Knee Temperature and Activation Schedule

The importance of using the correct activation heating schedule should be stressed here, because the process implemented to heat a cathode can have a serious effect on the cathode’s performance and lifetime. Consider the following: a scandate cathode was received by a manufacturer and heated to 1200 °C in the CSD testing rig of the CCC and an activity curve was collected. Afterward, the manufacturer revealed that their recommended activation schedule was to cycle the cathode between 1000 and 1150 °C per hour each for 24 hours, prior to collecting an activity curve. This was then performed on the same cathode and the results are shown in the figure below:

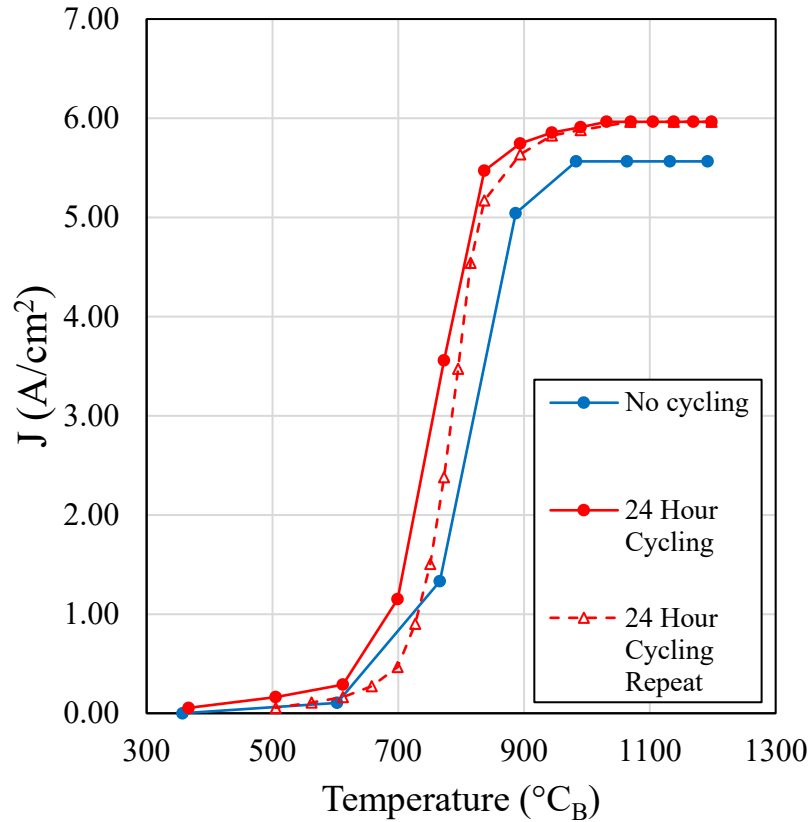


Figure 36. CSD activity curves for a scandate cathode, showing different trials where different heating schedules were used. Collected using the eBeam Incorporated custom CSD assembly, using a pulsed anode bias of +700 V.

Here the importance of an activation schedule is stressed. When the cathode was just heated and the curve collected, the cathode emitted only at 5.56 A/cm² and the knee temperature was at a relatively high 902 °C. When the recommended heating schedule was followed, the cathode then emitted at 5.96 A/cm² under the same conditions and exhibited a knee temperature at 837 °C on the first cycling trial, and 843 °C upon a repeat trial. This leads to another important aspect of testing cathodes: their ability to emit is also known to decay over time.

8.2.2 Emission Decay and Recovery

Modern dispenser cathodes can operate on the order of 50,000 hours when pulsed, but when operating at 1200 °C continuously their lifetime of usefulness plummets to about 1,000 hours (or the difference between over 5 and a half years versus 1 month and a half).⁵⁷ It is the case, however, that a bit of recovery can occur when using the right activation procedure. In the following study, a scandate cathode was heated to 1000 °C for 100 hours and then an activity curve was collected. There was a slight decrease in emission magnitude noticed following this data collection, but there was a significant increase observed in the knee temperature. That is to say, moving forward, the cathode would require much more energy before emitting at stable level again. Naturally, the question then arose of would it be possible to recover the cathode to a lower knee temperature and/or higher emission? Just such a recovery attempt was made by doing a 2 hour hold at 1200 °C – a “jumpstart” of sorts. The hypothesis here being that this brief high temperature hold would introduce more barium from the impregnant material to the surface, lowering its work function and improving emission performance. See the figure below for details:

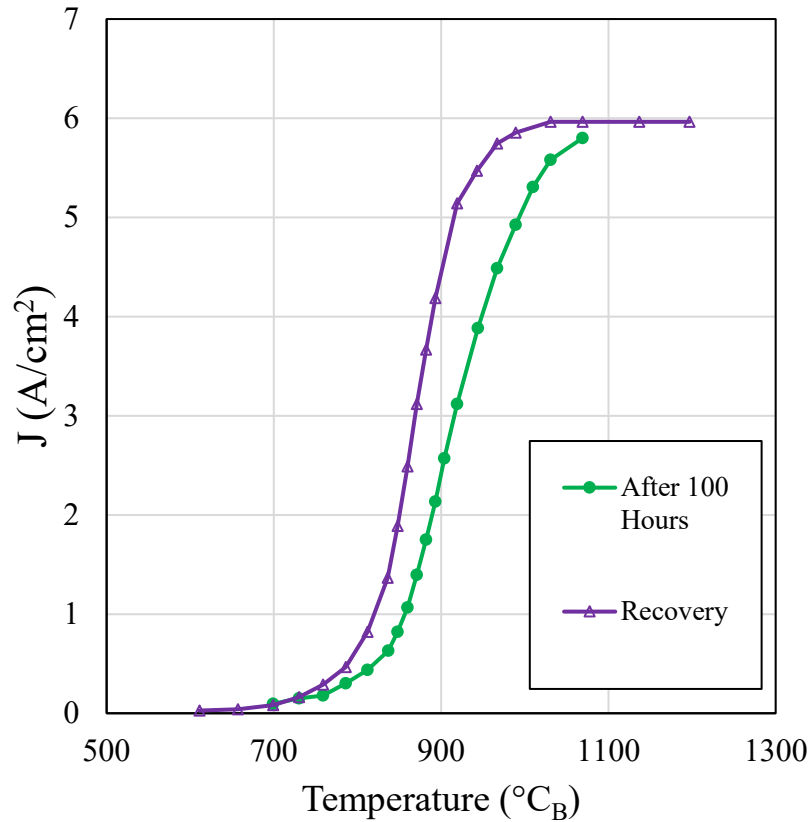


Figure 37. CSD test results following a 100 hour test and subsequent attempt at recovery. Collected using the eBeam Incorporated custom CSD assembly, using a pulsed anode bias of +700 V.

Following the hundred hour hold test, the cathode exhibited a knee temperature of 1006 °C and emitted at 5.80 A/cm² – roughly 170 °C higher than the scandate cathode measured after following the manufacturer’s activation schedule, and having values that are more on par with the types of activity curves seen on the older, un-coated dispenser cathodes. Following the 2 hour hold at 1200 °C recovery procedure, however, the emission crept back up to 5.96 A/cm² and the knee temperature was lowered to 924 °C. This is important because it shows that at least a little bit of recovery can be made in cathodes after long periods of operation.

8.3 *Work Function from KP Method*

The question now becomes “How does the KP emissions collection method compare to the standard CSD test?” As a reminder, the Kelvin probe system in the CCC is capable of evaluating thermionic emission at very low emission levels and at relatively low temperatures.^{47, 69} This is because of its significantly increased tip-to-sample spacing of 2 cm and because of its greatly reduced positive anode bias of only +10 V. This technique has shown itself already to access areas inaccessible by the standard CSD method, but how do the results of the two techniques compare?

The following figure was collected on the same sample as the previous one in Figure 35, but instead this time using the KP emissions collection method. Also the same as before was the cathode heating schedule, wherein the cathode was brought to a temperature of 1200 °C and then decreased in successive temperature steps. At each step, the probe was brought in to a tip-to-sample spacing of 2 cm and biased at +10 V and a current density measurement was made.

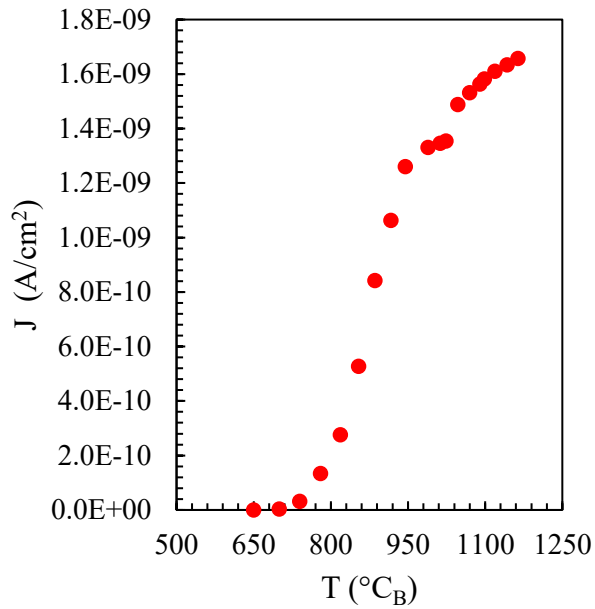


Figure 38. Current Density vs temperature for the same cathode as previous, but from the KP Method introduced in this dissertation.

Recall that from the CSD test, a work function of 1.63 eV was recorded. Fitting the TL regime of the above figure to the R-D equation yields an apparent work function of 1.65 eV – remarkably only a 1.2% difference with the work function measurement from the CSD test. The most significant aspect of this measurement technique, then, is that it yields accurate values achievable using traditional methods, while collecting *ten times less* current density. The fact that these two results, one from the novel KP emissions collection method and one from the traditional CSD method, correlate so well with each other is promising, because it expands the possible parameter space of testing available for thermionic emitters.

8.4 *Work Function from High-Temperature CPD*

The point then remains of how the preceding results compare to data taken using the innovative, high-temperature CPD method developed using this testing chamber.^{43,47} For the purposes of having a complete set of data comparing all of these techniques, the same sample was then once more heated to 1200 °C, i.e. to activation, and then cooled in successive steps. This time, however, the KP was brought in to the necessary tip-to-sample working distance for CPD measurement (200 μm for a 2 mm diameter KP). As another reminder, this was done using an asymmetrically, negatively biased KP tip of -4 to -10 V in order to not act as a current collector and saturate the probe's collection capabilities.

The data in the following figure show the results of carrying out high-temperature CPD measurements over the same scandate cathode as previously described, using an asymmetric bias of -4 to -10 V. Some important notes are that the data were recorded from high temperature to low temperature and that the final room temperature measurement was made after the sample sat, cooling in the vacuum chamber for a period of 24 hours.

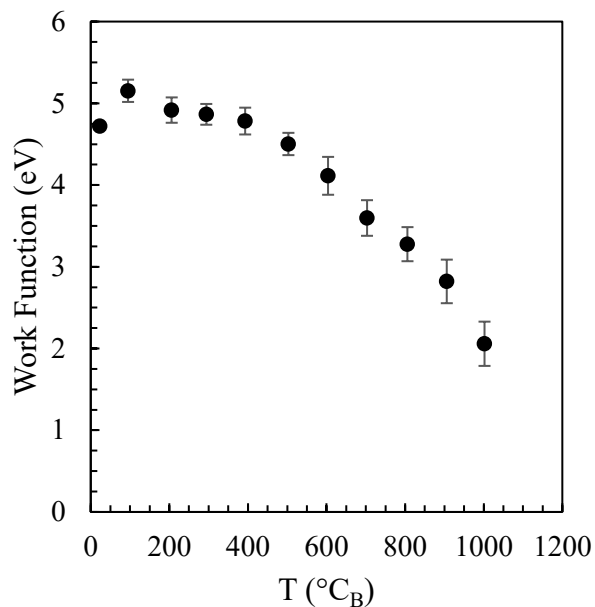


Figure 39. Results from applying the high-temperature, asymmetric bias CPD method to the same cathode as previous.

At the highest temperature where a measurement was recorded here, 1000 °C, the work function of the cathode as recorded to be 2.06 ± 0.27 eV. While it is interesting to note that this value is close to the values reported from the previous R-D analysis on the same sample, it is perhaps more important to note the behavior of CPD-derived work function within the same temperature regions of current collection where the R-D analysis was performed. For both the CSD testing and KP emission collection method, the work function was extrapolated from applying a best fit of the R-D equation within the TL regime, which was between 700 and 850 °C in each case. In both situations, a work function of ~ 1.6 eV was recorded. On the other hand, the high-temperature CPD technique measured higher work function values within that same temperature range, ~ 3.2 eV throughout.

Rather than being an indicator of a failure of the experiment, or disagreement between the techniques, this is proposed to be a result of the effects of defining a single value of “work function” to a polycrystalline multi-face surface. That is to say that the former technique relies on calculating work function via collected emissions, where low work function areas of the surface might be preferentially represented, and where the latter technique relies on measuring an electric potential between an area of two facing surfaces. This perhaps begs for more precise definitions for the difference between things like “electronic work function” or “material work function,” but no widely accepted consensus exists in the current body of studies.

The most likely explanation to describe the behavior of the increasing work function with decreasing temperature is the adsorption of surface gasses as the sample cooled. The final, slight decrease in work function observed on the final room temperature measurement is curious too. It is worthwhile to note again that this measurement was made 24 hours after power to the heating element was turned off and the lower work function may be related to the sample having remained under vacuum for such a long period of time afterward.

8.5 *Conclusion.*

The KP emissions collection method reveals itself to be able to access emissions significantly smaller than traditional testing and can still yield similar, if not near-identical, work function values to the traditional testing technique. When comparing the work function results from these experiments to the high-temperature CPD method, however, a slightly more intricate picture of the nature of work function presents itself. Specifically,

the behavior of work function with temperature, which has a more nuanced expression than may have been previously expected. This was observed as different values of apparent work function in similar temperature regions across two different techniques. Earlier parts of this dissertation have addressed the confusion surround defining “work function,” but perhaps these results provide experimental evidence that even modern definitions of “work function” do not quite grasp the full picture, or at least that “work function” might be being used to describe more than one nuanced material property. Future research should explore the refinement of understanding of the nature of the work function as a material property. To summarize, the KP emissions collection method has demonstrated the ability to access regions of emission inaccessible using traditional techniques, while still yielding comparable work function values, and when compared to the novel asymmetric CPD technique also outlined in this dissertation, insight into the nature of work function as a material property can be seen and the need for further understanding of it is highlighted.

9.1 *Processing and Design*

In this penultimate chapter, the goal now turns to being able to use these tools to help develop the next generation of dispenser cathodes. As mentioned before, the M-type cathode has been the industry standard for decades.⁵⁷ And scandate cathodes, despite showing promise as high-emitters and receiving more scientific study recently, have failed to gain significant integration into industrial use because of poor understanding of the relationship between emission physics and underlying microstructure.^{80, 81, 82} So rather than start from scratch, perhaps the existing infrastructure can be improved upon.

Recall that the feature that makes the M-type cathode desirable is the “anomalous effect” that they exhibit high work functions at room temperature (> 5.0 eV), but low work functions when heated to activation (< 2.0 eV).^{83, 71} This behavior is observed across dispenser cathodes with a variety of different refractory metal coatings, however osmium-ruthenium (Os-Ru) alloys a few hundred nanometers thick have been established as industry standard.^{56, 84} In attempt to expand upon previous studies on dispenser cathode coatings and work function⁸³, this chapter seeks to use a Kelvin probe system to identify candidates for next-generation M-type cathode coatings. But where the aforementioned study looked at Os-Ru-W ternary alloys and work function, as a means of identifying the ideal mixture, this dissertation seeks to look at the same alloys but containing two additional refractory elements, iridium and rhenium, as a means of identifying a new alloy for M-type cathode coatings.

9.1.1 Cathode Coatings

When M-type cathodes are heated to activation temperatures ($> 1200\text{ }^{\circ}\text{C}$), W from the porous matrix body of the cathode will diffuse into the Os-Ru coating on top.^{56, 85, 86, 87} Therefore any study into the work function of M-type cathode coatings should consider this ternary alloy. Two other metals that have been considered as dispenser cathode coatings are iridium (Ir) and rhenium (Re).⁸⁸ That work, however, was concerned with W-Ir and W-Re alloys, but ultimately lead to some interesting conclusions about cathode coatings. Firstly, that the Os-Ru-W alloy, not the Os-Ru coating alone, was responsible for the emissions enhancement. And secondly, and more importantly for this study, that a high work function coating results in an activated cathode surface with low work functions. (Critically, it must be noted, this is not true of all metals, as gold and platinum do not produce low work function cathodes.⁸⁹)

9.2 *Sample Design*

In order to study how these five elements alloy together to produce multi-element candidates for the next generation of M-type cathode coatings, a thin film (150 nm) alloy was made in a magnetron sputtering system (AJA Orion) on a silicon substrate. This was made using four sputtering source targets arranged in a crossed 'X' pattern. Four targets were used because Os is regularly alloyed with Ru in order to mitigate its otherwise harmful risks to human health, so the four targets were W, Re, Ir, and Os-Ru.

9.2.1 XRF

As mentioned earlier, XRF was performed on this sample. This was so that a compositional map of the relative percentages of the elements in the alloy on the surface of the substrate could be understood. Because the W-Os-Ru alloy had already shown itself to be the leading M-type cathode coating, the goal was to have smaller ratios of Ir and Re, to act as “dopants” of sorts in the next-generation candidates. The results are shown in the figure below:

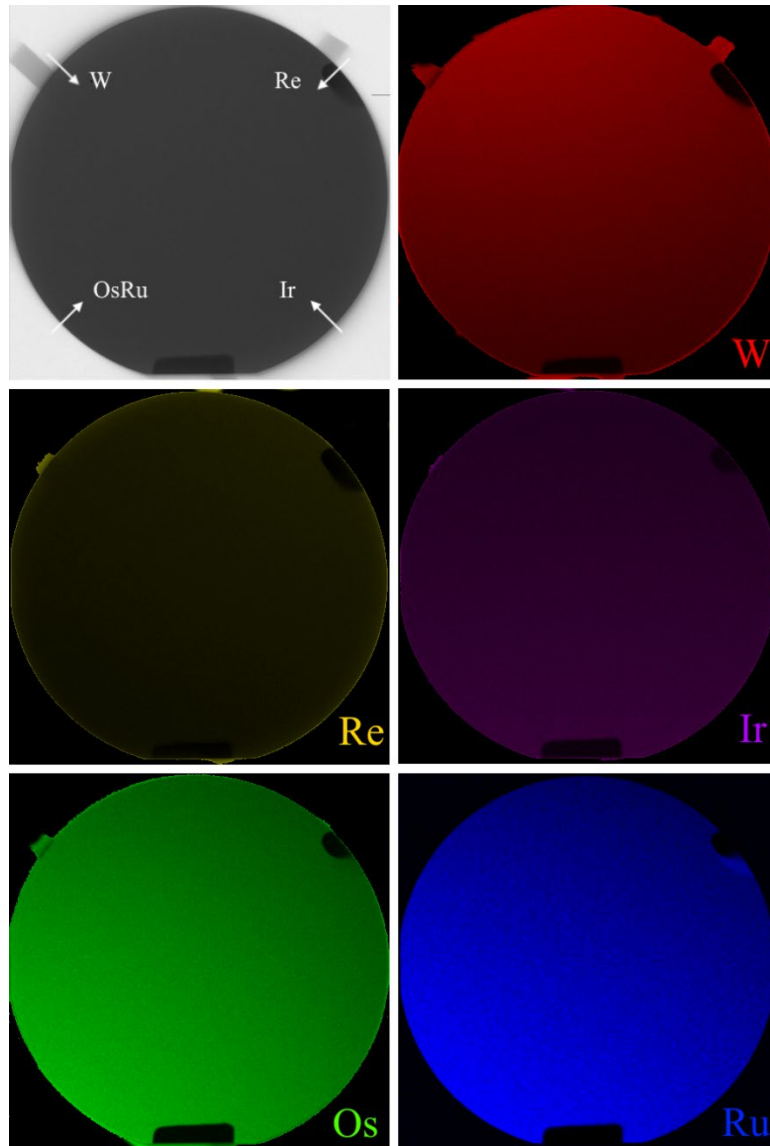


Figure 40. XRF results for the sample made to identify M-type cathode coating candidates. Showing quantities of W, Re, Ir, Os, and Ru.

At the center of the substrate, the following wt.% were measured:

Os: 37.9 %

Ru: 20.4 %

W: 31.4 %

Re: 8.9%

Ir: 1.4 %.

9.3 *KP and Cathode Coating*

The next step in this study was to use a Kelvin probe system to make a series of CPD measurements across the face of the sample. This was done in order to produce a work function map, which could help identify high work function compositions, or regions of interest, that might make successful candidates for M-type cathode coatings. This was also done using the ambient Kelvin probe system (A-KPS) introduced much earlier, a separate system to the one in the CCC which is useful for projects such as this, where replicating the cathode's UHV environment is not critical. The main idea was to measure enough points so as to have an understanding of how the various elemental gradients affected or in some instances did not affect work function. The analysis was performed using the following points:

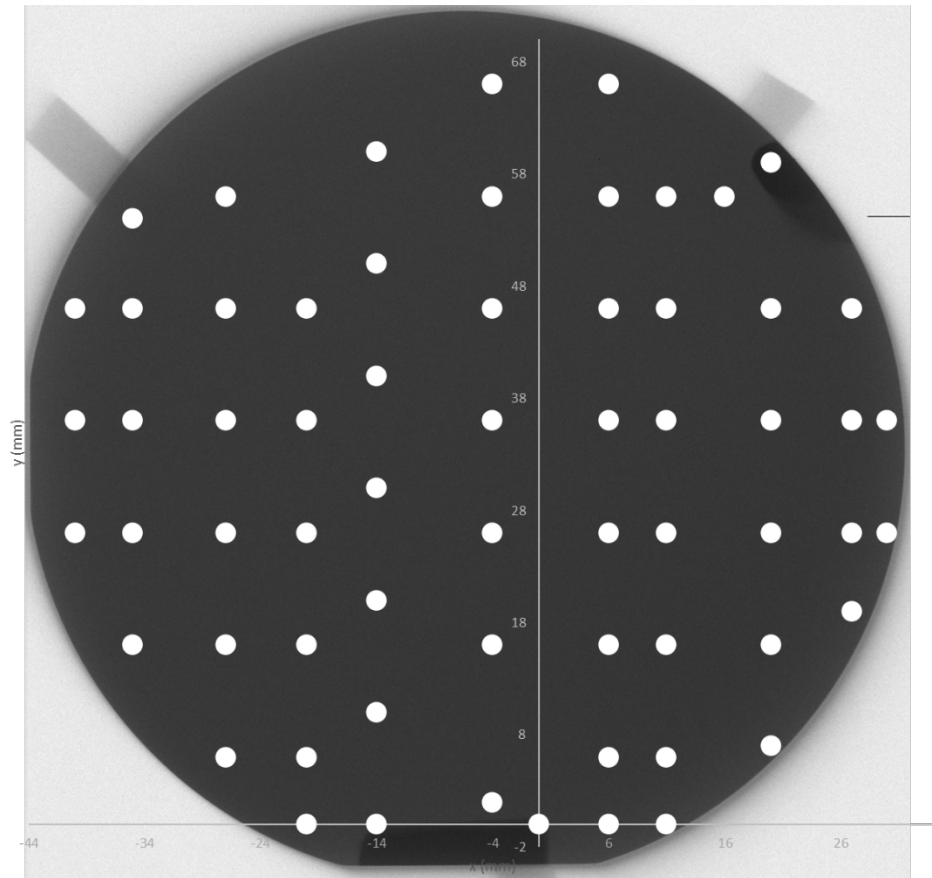


Figure 41. CPD measurement array overlaid on an image of the M-type cathode coating candidate sample, showing the locations of points where CPD was measured.^d

The work function values measured at each point were then plotted in a heat map, and the work functions of the areas not measured were interpolated between nearest neighbor points using the code provided in the appendix. This interpolated heat map is as follows:

^d Author's note: prior to publication, this data will be recollected using an array of measurement points in a more regular, square pattern. The irregularity in the measurement spacing geometry here is indicative of the exploratory nature and curiosity of the experimenter (which is to say I picked regions of interest and filled in the gaps).

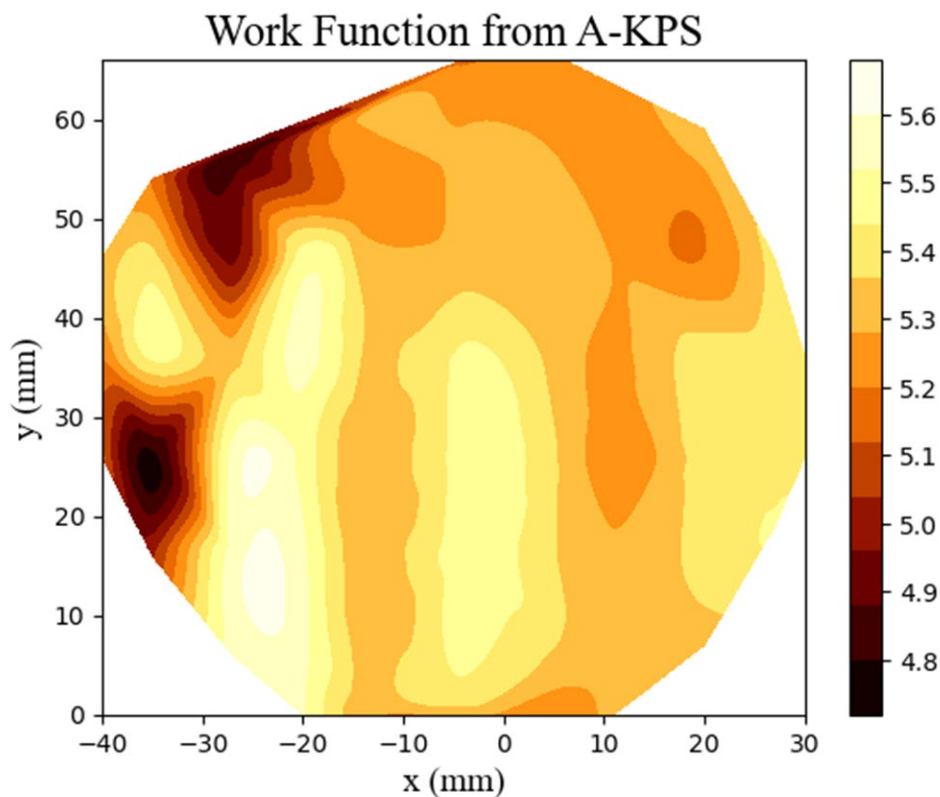


Figure 42. Interpolated WF heat map from the WFs obtained by measuring CPD across the face of the M-type cathode coating candidate sample. The code used to generate this plot is given in the appendix.

9.4 Results and Discussion

There are a number of interesting behaviors to note here. Firstly, that the Os-Ru heavy area (bottom left) seems to maintain a high work function with limited amounts of impurities in it. This has, in fact, been observed before, where the ternary alloy W-Os-Ru had high WF for heavy Os-Ru, low WF for heavy W, and a peak WF of 5.3 eV at ~30 % W.⁸³ But this is interesting to point out because there are regions there that are observed to maintain a high work function, despite increasing diffusion of W. Secondly, Ir heavy areas

appear to yield higher WFs than the Re heavy areas, although this may come as no surprise given Ir's naturally higher work function than Re. But it is interesting to note that, similar to W, the region that has heavy Os-Ru and Ir also maintains a high WF area, regardless of quantities expressed therein.

Perhaps the most interesting result, however, is identifying regions where increased W content does not severely lower work function. This is because tungsten diffusion is known to be a major killer of cathodes. In the figure above, where the angle of W deposition is oriented to be roughly in the top left of the image, regions where increased W composition can be seen where the WF remains high. Understanding these regions can lead to cathodes that are more resistant to W diffusion and ultimately be able to be used for longer.

9.4.1 Correlation with Previous Work and Next Steps

As mentioned, the W-Os-Ru system seems to be in close agreement with what has been measured by other studies of cathode coating alloys. The W-Os-Ru-Ir alloy presents itself as an interesting candidate for further investigation. In order to test this hypothesis, therefore, a cathode manufacturer would need to provide an M-type cathode with a Os-Ru-Ir coating with only a small amount of Ir, corresponding to the regions of the test sample that maintained a high work function despite increasing quantity of W. Once this sample was made, it would to be shipped to the University of Kentucky for the CCC to fully test and characterize the cathode's performance in comparison to a traditional M-type.

CHAPTER 10. CONCLUSION

10.1 *Summary and Conclusions*

This concludes the presentation of the work comprising this dissertation. It opened with a historical perspective on cathodes, thermionic emission, and work function, and gave an overview of the samples used throughout this work along with a brief introduction to the method of the Kelvin probe. It then gave a comprehensive overview of the Cathode Characterization Chamber, the unique testing system capable of testing and evaluating cathodes in the extreme environments that are necessary for their myriad industrial applications (> 1000 °C and in the Ultra-High Vacuum regime). Its many features were shown and arguments for why certain standard techniques needed to be expanded upon, such as APS and traditional Kelvin probe, were given.

The first technique developed using the CCC outlined in this dissertation was that of high-temperature contact potential difference measurement, or the asymmetric bias technique. This technique allows for work function determination of hot samples, even up to activation temperature. Overcoming a barrier that some had even said was the greatest challenge facing CPD measurements. Specifically, it was found that with increased emission, a more negatively offset bias was needed. Ultimately landing on -4 to -10 V for the cathodes studied here, different ranges are likely to be more useful for emitters of different strengths. This technique could reliably provide work function measurements for samples > 1000 °C.

The second new technique developed using the CCC that was described in this dissertation was using a Kelvin probe system to measure electron emission. This technique

revealed itself to be very useful because it could measure emissions at lower temperatures than traditional methods, and it could collect *significantly* less current and still produce equivalent work functions from the same samples when measured using traditional methods. That is to say, it could measure emission below 500 °C and collect ten times less current density than leading techniques like CSD, and still provide work function values that agreed with literature.

These two techniques represent major advancements in the characterization of thermionic emission, a field which still largely relies on decades old testing methods – many of which are ill suited to the unique environment of cathodes. Both these techniques are able to accurately and effectively characterize thermionic emitters at high temperatures and in ultra-high vacuum environments.

Thirdly, this dissertation described a traditional cathode testing method, close-spaced diode testing, which was integrated into the CCC and proven to be useful in confirming the accuracy of the two previously mentioned techniques. This same system was used to show the importance of how an activation heating schedule can affect a cathode's performance, as well as how a cathode might be able to be recovered after extended hours of operation. It was demonstrated that a 24 hour cycling procedure produces higher emission and a lower knee temperature than that of merely heating a cathode to activation, which was also found to be repeatable. The CSD system was also used to show that after degradation of a long lifetime test, a cathode's activity curve can be slightly recovered.

Lastly, using this knowledge, candidates were put forward for a new M-type cathode coating for the next generation of cathodes. In this proposal, instead of the standard

W-Os-Ru alloy, an alloy of W-Os-Ru-Ir-Re was considered. Critically, compositions were identified where increased W content did not significantly reduce work function. This could lead to the extension of cathode lifetimes, as M-type cathodes with these coatings would be more resistant to W diffusion over time.

In summation, one unique testing system was established to be a very useful apparatus for the evaluation of dispenser cathodes and other thermionic emitters. This system was shown to be able to use known techniques for cathode testing, but also pioneer new techniques, which revealed themselves to be very useful for studying cathodes in their activated environment (in the Ultra-High Vacuum regime and at activation temperatures > 1000 °C). Using this newfound understanding of surfaces unveiled by the CCC, an investigation into a novel candidate of M-type cathode coating was performed, which found possible candidates for the next generation of M-type dispenser cathodes.

In addition to uncovering new modes of cathode analysis, the CCC has also unveiled new questions about the behavior of cathodes: primarily, the rectification of the unexpectedly small Richardson constants when using the KP emissions collection method in Chapter 6. Since its introduction, the Richardson constant has been needed to be reevaluated on more than one occasion (recall this is partly why it is now called the Richardson-Dushman equation and not just the Richardson equation). Are the unexpectedly low values obtained in this system geometry indicative of the sensitivity of the technique? Or is there more to be understood about this parameter that can help broaden the current understanding of thermionic emission?

10.2 *Future Work*

The most pressing experiment would be to have a cathode manufacturer produce an M-type cathode with a coating proposed in the cathode coating study (Chapter 9). And then for this cathode to be tested using the techniques of the CCC. These results would need to be then compared to a complementary M-type cathode with a more traditional composition. Activity curves over lifetimes of usage would need to be collected, as the hypothesis proposed here is that these cathodes are more resistant to W diffusion and therefore able to have longer lifetimes than traditional cathodes.

Another study of interest would be an investigation into the effects of impregnant ratios using this system. Two M-type cathodes were shown with two different impregnate ratios already. Recall that at 1000 °C the cathode with the BaO:CaO:Al₂O₃ impregnant ratio of 6:1:2 showed a work function of 2.57 eV when applying the asymmetric CPD technique, while the cathode with a ratio of 4:1:1 (a lower proportional amount of barium and aluminum) exhibited a lower work function of 2.28 eV (Chapter 5). What was the specific cause of that discrepancy? If provided with sufficient identically bodied cathodes with different impregnant recipes, the CCC would be an excellent system for studying the changes therein.

Generally speaking, the CCC can be a very useful tool for screening cathodes before going into long-term operation as well, because it can provide manufactures with the ability to understand the behavior of their product at a breadth and depth unavailable by more common testing facilities.

The CCC must be used to study other next-generation cathode candidates as well. Scandate cathodes were mentioned, but 3D-printed cathodes are only just beginning to be

studied and have already shown themselves to be good candidates for thermionic emissions applications. These cathodes present an interesting opportunity, since some 3D printing facilities are even able to print precise grain orientations, allowing for printing a surface with a specifically desired work function. One initial set of results using the KP emissions collection method on a 3D printed cathode in comparison to scandate cathode with the same impregnant, and another example showing asymmetric CPD results on the same samples are both shown below. These are provided not to provide in depth discussion at this time, but rather to introduce the reader to the idea that exciting new dispenser cathodes are being developed even to this day.

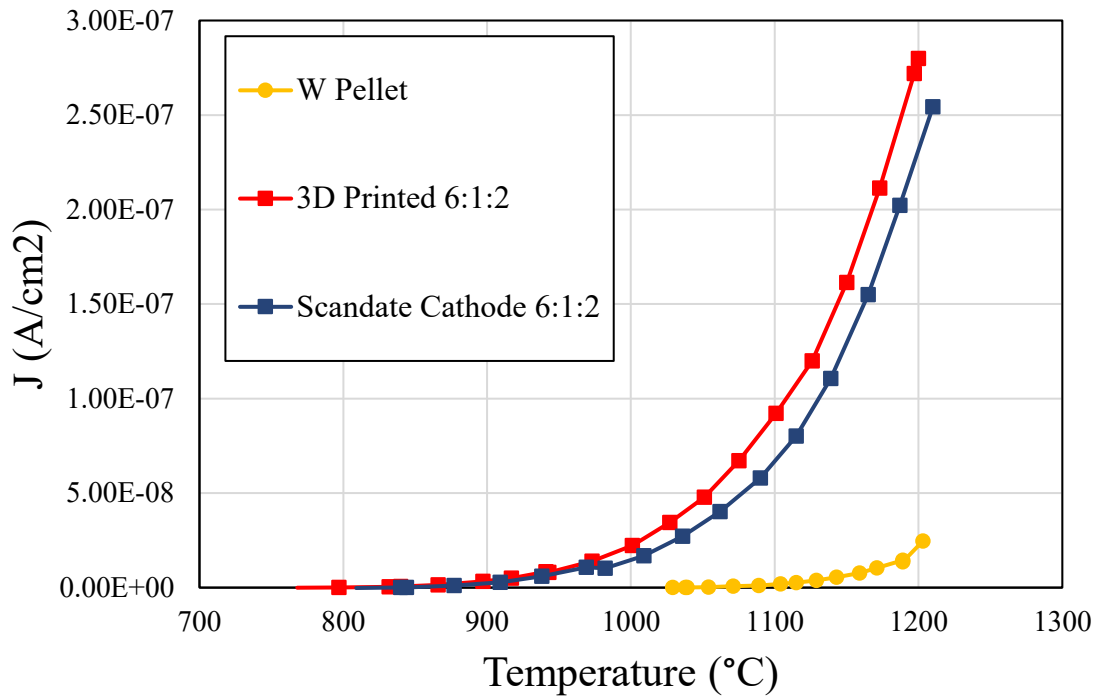


Figure 43. Current density from the KP emissions collection method for a 3D printed cathode and a scandate cathode with the same impregnant ratios. A W pellet is also shown for comparison.

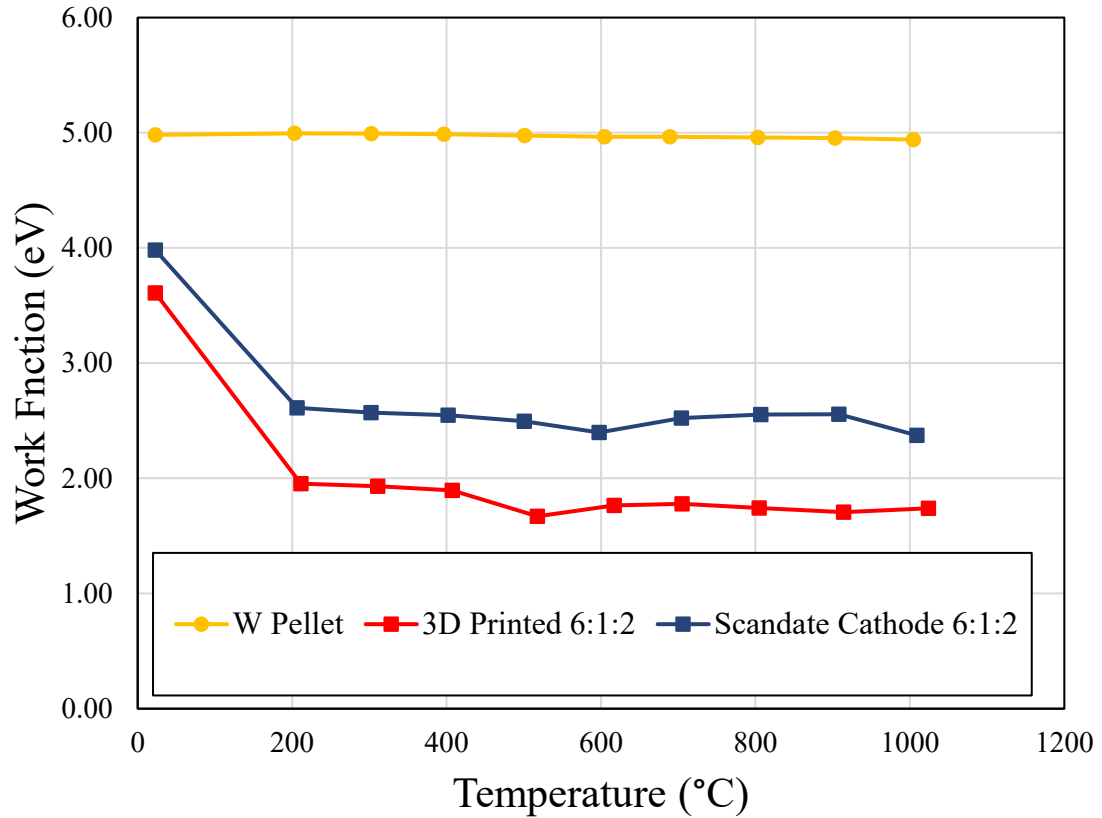


Figure 44. Asymmetric CPD method results for a 3D printed and scandate cathode with the same impregnant ratio. A W pellet is included for comparison.

It is the author’s sincere hope that the CCC will continue to be used to study many different kinds of cathodes, of many different designs. It will be extremely useful to the cathode community as a whole, but especially to those manufacturers who want to properly evaluate a cathode prior to deployment – this is especially relevant for space applications, where the logistics of replacing a burnt out cathode are, to put it mildly, challenging. All in all, the CCC and this work made using it open up the door to a greater understanding of the physics and materials science of the relationships of material properties, work function, and thermionic emission of dispenser cathodes.

APPENDIX

A.1 Code Used for Interpolated Heat Map

```
“””
```

Thanks must be given to the following stack overflow thread which inspired this code <https://stackoverflow.com/questions/2369492/generate-a-heatmap-using-a-scatter-data-set>. As well as to Dr. Zachary Vealey and Dr. Eric Suter, whose expertise in programming was a wellspring of helpful advice.

```
“””
```

```
import matplotlib.pyplot as plt
import numpy as np

from scipy.interpolate import griddata

data = np.array([
    [XX, YY, WF], ...
    ...])

x, y, vals = data[:,0], data[:,1], data[:,2]

X, Y = np.meshgrid(
    np.linspace(np.min(x), np.max(x), 1000),
    np.linspace(np.min(y), np.max(y), 1000)
)

interpolated_vals = griddata((x, y), vals, (X, Y), method='cubic')

ticks = np.linspace(4.5,5.7,13,endpoint=True)

plt.contourf(X, Y, interpolated_vals, cmap="afmhot", levels=13)
plt.xlabel("x (mm)", font="Times New Roman", fontsize=14)
plt.ylabel("y (mm)", font="Times New Roman", fontsize=14)
plt.title("Work Function from A-KPS", font="Times New Roman", fontsize=18)
plt.colorbar(ticks=ticks)
plt.show()
```

A.2 Data Used for Interpolated Heat Map

x	y	WF
0	0	5.2583
-4	2	5.4142
-4	16	5.479
-4	26	5.4712
-4	36	5.4512
-4	46	5.3127
-4	56	5.2957
-4	66	5.1889
6	66	5.2006
6	56	5.2757
16	56	5.2455
20	59	5.3459
11	56	5.2401
11	46	5.2756
11	36	5.2609
11	26	5.2226
11	16	5.3008
11	6	5.3259
11	0	5.321
-14	0	5.2976
-14	10	5.311
-14	20	5.2945
-14	30	5.3157
-14	40	5.3607
-14	50	5.2432
-14	60	5.2886
6	46	5.3082
6	36	5.3139
6	26	5.3398
6	16	5.3461
6	6	5.3399
6	0	5.2079
20	7	5.3326
20	16	5.3882
20	26	5.3967
20	36	5.4013
20	46	5.2007
27	46	5.398
27	36	5.4084
27	26	5.415

A.2 Data Used for Interpolated Heat Map (Continued)

x	y	WF
27	19	5.4488
30	26	5.4257
30	36	5.4365
-20	36	5.5446
-20	46	5.4786
-20	26	5.4874
-20	16	5.534
-20	6	5.539
-20	0	5.5318
-27	6	5.5458
-27	16	5.5529
-27	26	5.5422
-27	36	5.3307
-27	46	4.9444
-27	56	4.8251
-35	54	5.1805
-35	46	5.3802
-35	36	5.45
-35	26	4.7748
-35	16	5.0197
-40	26	5.1401
-40	36	5.1861
-40	46	5.283

REFERENCES

- 1 E. Becquerel, Diss. Pres. Acad. of Sci., (1853, July).
- 2 I. Falconer, Phys. Education, 32(4), 226 (1997).
- 3 F. Guthrie, The London, Edinburgh, and Dublin Phil. Mag. and J. of Sci., 46(306),
257-266, (1873).
- 4 E. Goldstein, Annalen der Physik, 300(1), 38-48, (1898).
- 5 G. Shiers, Sci. American, 230(3), 92-101 (1974).
- 6 T. A. Edison, Electrical Indicator. Specification Forming Part of Letters Patent No.
307,031 (1884, October).
- 7 D. K. Simonton, Psy. Aesthetics, Creativity, and the Arts, 9(1), 2 (2015).
- 8 A. Einstein, Ann. Physik, 17, 132 (1905).
- 9 A. Einstein, Am. J. Phys., 33(5), 367, (1965).
- 10 J. K. Jensen, *Introduction to the Physics of Electron Emission*, John Wiley & Sons.
(2017).
- 11 A. Kahn, Mat. Horizons, 3(1), 7-10 (2016).
- 12 P. A. Thiel and J. M. Dubois, Nature, 406(6796), 571-573 (2000).
- 13 A. E. Kramida, and J. Reader, Atomic Data and Nuclear Data Tables, 92(4), 457-
479. (2006).
- 14 S. Yamamoto, Reports on Progress in Physics, 69(1), 181. (2005).
- 15 J. H. Glenn, Retrieved August 31, 2020, from
<https://www.techbriefs.com/component/content/article/tb/pub/techbriefs/electronics-and-computers/19551> (2014, May 1).

- 16 J. W. Gibson, G. A. Haas, and R. E. Thomas, *IEEE Trans. Elec. Devices*, 36(1),
209-214 (1989).
- 17 J. Li, S. Yan, W. Shao, Q. Chen, and M. Zhu, *App. Surf. Sci.* 215(1-4), 49-53.
(2003).
- 18 G. Gaertner and Y. Wang, *Mod. Dev. Vac. Elect. Sources*, 83-172 (2020).
- 19 M. Mroz, S. Tenney, and M. E. Kordesch, in *2018 IEEE International Vacuum
Electronics Conference (IVEC)*, 327-328, IEEE. (2018, April).
- 20 W. B. Nottingham, *et al.* in *Thermionic emission*, Springer Berlin Heidelberg
(1956).
- 21 R. A. Millikan, and C. F. Eyring, *Physical Review*, 27(1), 51 (1926).
- 22 K. Hirose, and M. Tsukada, *Physical Review B*, 51(8), 5278. (1995).
- 23 B. Coaker and T. Challis, *Microwave Journal*, 51(10), 32-43 (2008).
- 24 X. Liu, in *Characterization of Nanostructure, Materials, and Electron Emission
Performance of Next-generation Thermionic Scandate Cathodes*, (2019).
- 25 J. Y. Gao, Y. F. Yang, X. K. Zhang, S. L. Li, P. Hu, J. S. Wang, *Tungsten*, 2, 289-
300 (2020).
- 26 L. Kelvin, *Phil. Mag.* 5(46), 278, 82-120 (1898).
- 27 P.W. Pridgman, in *Thermodynamics of Electrical Phenomena in Metals*, Dover
Publications, (1961).
- 28 R. H. Fowler, *Physical review*, 38(1), 45. (1931).
- 29 R. A. Millikan, *Physical Review*, 7(3), 355. (1916).
- 30 I. D. Baikie, A. C. Grain, J. Sutherland, and J. Law, *Eng. Proc.* 60, 48-56 (2014).

- 31 V. A. Tyagai, Y. M. Shirshov, O. V. Snitko, and V. D. Yarinovskii, *Physica status
solidi (b)*, 33(1), 469-475 (1969).
- 32 N. A. Surplice, and R. J. D'arcy, *J. Phys. E: Sci. Insts.* 3(7), 477 (1970).
- 33 O. M. Ottinger, C. Melzer, and H. J. von Seggern, *Appl. Phys.* 106(2), 023704
(2009).
- 34 J. W. Kim, and A. Kim, *Curr. Appl. Phys.* 31, 52-59 (2021).
- 35 P. D. Swartzentruber, M. J. Detisch, and T. J. Balk, In *2016 IEEE International
Vacuum Electronics Conference (IVEC)* (pp. 1-2). IEEE (2016, April).
- 36 I. D. Baikie, A. C. Grain, J. Sutherland, and J. Law, *Appl. Surf. Sci.* 323, 45-53
(2014).
- 37 A. M. Mántica, and T. J. Balk, In *2020 IEEE 21st International Conference on
Vacuum Electronics (IVEC)*, 391-392, IEEE (2020, October).
- 38 W. A. Zisman, *Rev. Sci. Insts.* 3(7), 367-370 (1932).
- 39 I. D. Baikie, and P. J. Estrup, *Rev. Sci. Insts.* 69(11), 3902-3907 (1998).
- 40 I. D. Baikie, S. Mackenzie, P. J. Z. Estrup, and J. A. Meyer, *Rev. Sci. Insts.* 62(5),
1326-1332 (1991).
- 41 J. Bao, B. Wan, and P. Wang, *Vacuum*, 81(9) (2007).
- 42 P. Swartzentruber, T. J. Balk, J. O. Tarter, and D. Busbaher, In *IEEE International
Vacuum Electronics Conference (IVEC)*, 135-136, IEEE (2014, April).
- 43 A. M. Mántica, M. J. Detisch, T. J. Balk, *Vacuum*, 215, 112169, (2023).
- 44 C. Herring and M. H. Nichols, *Rev. Mod. Phys.* 21(2), 185, (1949).
- 45 J. B. Scott, *IEEE Trans. Electron Devices*, 28(5), 593-595, (1981).
- 46 S. Dushman, *Rev. Mod. Phys.* 2(4), 381, (1930).

- 47 A. M. Mantica, M. J. Detisch, and T. J. Balk, in *2022 IEEE 23rd International Vacuum Electronics Conference (IVEC)*, IEEE (forthcoming, accepted 2022 April).
- 48 O. W. Richardson, *Phys. Rev.*, 23(2), 153, (1924).
- 49 A. L. Smith and R. Breitwieser, *J. App. Phys*, 41, 436 (1970).
- 50 V. S. Fomenko, in *Handbook of thermionic properties: electronic work functions and Richardson constants of elements and compounds*, Springer Science & Business Media (2012).
- 51 F. L. Yost, in *A Study of Thermionic Emission from a Tungsten Filament*, (1931).
- 52 N. D. Lang and W. Kohn, *Phys. Rev. B*, 1 (12), 4555, (1970).
- 53 S. Saraf, R. Shikler, J. Yang, and Y. Rosenwaks, *Applied physics letters*, 80(14), 2586-2588. (2002).
- 54 F. Streicher, S. Sadewasser, and M. C. Lux-Steiner, *Review of Scientific Instruments*, 80(1), 013907, (2009).
- 55 S. Kwon, M. H. Kwon, J. Song, E. Kim, Y. Kim, B. R. Kim, ... and D. W. Kim, *Scientific reports*, 9(1), 1-6. (2019).
- 56 J. L. Cronin, In *IEEE Proc*, 128(1), 19-32, (1981, February).
- 57 D. M. Kirkwood, S. J. Gross, T. J. Balk, M. J. Beck, J. Booske, D. Busbahr, ... and J. E. Yater, *IEEE Trans. Electron Devices*. 65(6), 2061-2071 (2018).
- 58 J. M. Roquais, F. Poret, R. Le Doze, J. L. Ricaud, A. Monterrin, and A Steinbrunn, *App. Surf. Sci.*, 215(1-4), 5-17 (2003).
- 59 S. Yin, Z. Zhang, Z. Peng, Q. Zheng, and Y. Wang, *IEEE Trans. Elec. Devices*, 60(12), 4258-4262 (2013).

60 D. E. Bugaris, C. Goggin, K. Baker, J. Balk, D. Busbahr, and J. Tucek, In *2020 IEEE 21st International Conference on Vacuum Electronics (IVEC)*, pp. 79-80, IEEE (2020, October).

61 G. N. Derry, M. E. Kern, and E. H. Worth, *J. Vac. Sci. Technol. A: Vac. Surf. Films.* 33(6), 060801 (2015).

62 P. D. Swartzentruber, M. J. Detisch, and T. J. Balk, *J. Vac. Sci. Technol. A: Vac. Surf. Films.* 33(2), 021405 (2015).

63 X. Chen, H. Liu, Y. Cai, W. Zhou, S. Chen, J. Peng, Y. Yang, and J. Wang, *Vacuum*, 200, 111016 (2022).

64 K.C. Mishra, R. Garner, and P. C. Schmidt, *J. Appl. Phys.* 95(6), 3069-3074 (2004).

65 R. G. Wilson, *J. App. Phys.*, 37(6), 2261-2267, (1966).

66 The Materials Project at <https://materialsproject.org/materials/mp-122>

67 S. Dushman, *Phys. Rev.* 21(6), 623 (1923).

68 H. Kawano, T. Takahashi, Y. Tagashira, H. Mine, and M. Moriyama, *Appl. Surf. Sci.* 146(1-4), 105-108 (1999).

69 A. M. Mantica, M. J. Detisch, and T. J. Balk, *IEEE Trans. Electron Devices.* 70(6), 2864-2871, (2023).

70 E. L. Murphy and R. H. Good, Jr., *Phys. Rev.* 102(6), 1464-1473 (1956).

71 P. Zalm and A. J. A. van Stratum, *Philips Tech. Rev.* 27(4), 69-75 (1966).

72 G. Hua and D. Li, *Appl. Phys. Lett.*, 99, 041907 (2011).

73 <https://periodictable.com/Properties/A/YoungModulus.al.html>

74 G. Hua and D. Li, *Phys. Chem. Chem. Phys.*, 18, 4753, (2016).

75 AZO Materials <https://www.azom.com>

- 76 O. W. Richardson, Nobel Lecture, (1929).
- 77 O. W. Richardson, in *Monographs on Physics, vol. 8*, Longmans, Green and Co.,
Paternoster Row, London, 29-59, (1921).
- 78 C. R. Crowell, *Solid-State Electronics*, 8(4), 395-399, (1965).
- 79 R. Iiyoshi, H. Shimoyama and S. Maruse, *Microscopy*, 45(6), 514-517, (1996).
- 80 X. Liu, Q. Zhou, T. L. Maxwell, B. K. Vancil, M. J. Beck, and T. J. Balk, *Mat.*
Char. 148, 188-200 (2019).
- 81 B. Vancil, I. Brodie, J. Lorr, V. Schmidt, and *IEEE Trans. Electron Devices*, 61(6),
1754-1759 (2014).
- 82 X. Liu, B. K. Vancil, M. J. Beck, and T. J. Balk, *Materials*, 12, 636 (2019).
- 83 P. D. Swartzentruber, M. J. Detisch, T. J. Balk, *J. Vac. Sci. Technol. A*, 33(2),
021405, (2015).
- 84 P. D. Swartzentruber and T. J. Balk, *J. Vac. Sci. Technol. A* 32(4), 040601, (2014).
- 85 M. C. Green, H. B. Skinner, and R. A. Tuck, *Appl. Surf. Sci.*, 8(1-2), 13-35,
(1981).
- 86 D. Jones, D. McNeely, and L. W. Swanson, *Appl. Surf. Sci.*, 2(2), 232-257, (1979).
- 87 A. J. A. van Stratum, *J. Appl. Phys.*, 42(11), 4436-7, (1971).
- 88 R. E. Thomas and J. W. Gibson, *Appl. Surf. Sci.*, 29(1), 49-66 (1987).
- 89 R. A. Tuck, *Platinum Met. Rev.*, 26(4), 167-173, (1982).

VITA

Antonio Mántica was born in Lafayette, Indiana and raised moving back and forth between Indiana and Georgia. He graduated from Oglethorpe University (Atlanta, GA) with a B.S. in physics in 2011 and from the University of Georgia (Athens, GA) with an M.S. in physics in 2019. In that same year, he joined Dr. John Balk's group at the University of Kentucky (Lexington, KY) to pursue a Ph.D. in materials science and engineering.

Education

University of Kentucky – Candidate for Ph.D. in Materials Science and Engineering

University of Georgia – M.S. in Physics

Oglethorpe University – B.S. in Physics

Research Positions

Cathode Characterization Research Assistant – University of Kentucky

Quantum Nano-Optics Research Assistant – University of Georgia

Gravitational Physics Research Assistant – University of Georgia

Magnetic Resonance Imaging Research Assistant – University of Georgia

Teaching Positions

Materials Engineering Teaching Assistant – University of Kentucky

Head Teaching Assistant – University of Georgia

Physics Tutor – University of Georgia

Graduate Teaching Assistant – University of Georgia

Student Lab Teacher – Oglethorpe University

Tutor and Note Taker – Oglethorpe University Disability Services

Honors and Awards

Completed University of Kentucky’s Certificate in Materials Characterization Program

Lyman T. Johnson Diversity Fellowship Recipient

Graduate School Teaching Seminar Assistantship Recipient

Robert M. Wood Award for Outstanding Achievement in Lab Teaching

Outstanding Teaching Assistant Award

Listed in the 2017 edition of Who’s Who Among Students in American Universities and Colleges

James Edward Oglethorpe Award for Excellence in Scholarship and Service

Sigma Pi Sigma Award for Excellence in Physics

Joseph LeConte Award for Most Outstanding Student in the Natural Sciences

Omicron Delta Kappa Leadership Recognition Award

Alpha Psi Omega Wendell Brown Award for Excellence in Performing Arts

Georgia Shakespeare Scholarship Recipient

Completed Oglethorpe University’s Certificate Honors Program

Publications

Mantica, Antonio M., Detisch, Michael J., Balk, T. John. “High-Temperature Contact Potential Difference Measurement of Surface Work Function using in vacuo Kelvin Probe,” *Vacuum*, 215, 2023.

- Mantica, Antonio M.**, Detisch, Michael J., Balk, T. John. "Thermionic Emission Characterization of M-type Cathodes using Kelvin Probe in an Ultra-High Vacuum Environment," *IEEE Transactions on Electron Devices*, 70(6), 2023.
- Mantica, Antonio M.**, Detisch, Michael J., Balk, T. John. "M-Type Cathode Characterization Using a Kelvin Probe System Vacuum Chamber," *2022 IEEE 23rd International Vacuum Electronics Conference (IVEC)*, IEEE 2023.
- Mantica, Antonio M.**, Detisch, Michael J., Balk, T. John. "High-Temperature Contact Potential Difference and Thermionic Emission Analysis Using Kelvin Probe Systems," *2022 IEEE 23rd International Vacuum Electronics Conference (IVEC)*, IEEE 2023.
- Bugaris, Daniel E., Goggin, Claudia, **Mantica, Antonio M.**, Balk, T. John, Chubaruk, Ruslan, Busbaher, Daniel. "Evaluation of Work Function for Scandate Cathodes Produced from Nano-Scandia/Tungsten Composite," *2022 IEEE 23rd International Vacuum Electronics Conference (IVEC)*, IEEE 2023.
- Mantica, Antonio M.**, and Balk, T. John. "Quantifying Work Function Using Kelvin Probe Systems," *2020 IEEE 21st International Vacuum Electronics Conference (IVEC)*, IEEE 2020.
- Mantica, Antonio M.** "Models of Time Travel and their Consequences," *Oglethorpe Journal of Undergraduate Research*, 5.2 (2015): 1.